EFFECTS OF MOLECULAR STRUCTURE ON THE RHEOLOGY AND PROCESSABILITY OF HIGH DENSITY POLYETHYLENE BLOW MOLDING RESINS

by

ALFONSIUS BUDI ARIAWAN

B.A.Sc., The University of British Columbia, 1996

A THESIS SUBMITTED IN PARTIAL FULFILLMENT OF THE REQUIREMENTS FOR THE DEGREE OF MASTER OF APPLIED SCIENCE

in

THE FACULTY OF GRADUATE STUDIES
Department of Chemical Engineering

We accept this thesis as conforming to the required standard

THE UNIVERSITY OF BRITISH COLUMBIA

June 1998

In presenting this thesis in partial fulfilment of the requirements for an advanced degree at the University of British Columbia, I agree that the Library shall make it freely available for reference and study. I further agree that permission for extensive copying of this thesis for scholarly purposes may be granted by the head of my department or by his or her representatives. It is understood that copying or publication of this thesis for financial gain shall not be allowed without my written permission.

Department of Chemical ENGINEERING

The University of British Columbia
Vancouver, Canada

Date July 6 '98

DE-6 (2/88)

ABSTRACT

Resin processability depends heavily on its rheological properties. The molecular structure of the resin, in turn, influences its rheological behavior. In this work, experiments were conducted using capillary and extensional rheometers, a melt indexer and a blow molder unit to determine the rheological properties and processability of high density polyethylene blow molding resins. Twenty four commercial resins were analyzed in terms of their shear flow properties, extensional flow properties, extrudate swell characteristics, and melt strength. The studied samples had varying molecular weight characteristics and were produced using a variety of technologies. Using the experimental results, correlations between rheological properties and molecular structures were determined. Furthermore, to assess resin processability, pillow mold (blow molding) experiments were performed. The implications of rheology on processability (parison sag and weight swell) were then discussed. Additional experiments were also conducted to assess the usefulness of melt index *(MI)*, stress exponent *(S.Ex.)* and melt flow ratio *(MFR)* in characterizing rheological properties.

It was found that shear viscosity is technology dependent and that it is influenced by the weight average molecular weight (M_w) and polydispersity index *(PI)*. Increasing M_w was found to increase the shear viscosity, while increasing *PI* by increasing the concentration of smaller molecules increases the tendency of the resin to shear thin. The extensional viscosity was also affected by M_w in the same manner. The influence of *PI* on extensional viscosity, however, was not apparent. In order to relate the melt strength and temperature sensitivity of shear viscosity to molecular parameters, resins had to be

grouped according to the polydispersity index ranges of $PI<8$, $8<PI<10$, and $PI>10$. Moreover, it was possible to relate melt strength to the Hencky strain obtained from creep experiments. With regard to extrudate swell, it was found that the Z-average molecular weight (M_z) and *PI* are useful for determining the sensitivity of the swell to changes in shear rate. Extrudate swell behavior and melt strength are important parameters to be considered during parison formation, as observed during blow molding experiments. Finally, *MI*, *S.Ex.*, and *MFR* were found to be technology dependent and are useful only for resin comparisons.

TABLE OF CONTENTS

LIST OF FIGURES

LIST OF TABLES

ACKNOWLEDGEMENTS

I would like to express my sincere gratitude to my supervisor Dr. Savvas G. Hatzikiriakos, and Dr. Shivendra K. Goyal for their guidance throughout the course of this work, and to NOVA Chemicals for the sponsorship of this thesis project.

I also wish to thank Dr. Phil Edwards, Dr. Charles Russell, Dr. Tim Bremner, and Henry Hay of NOVA Chemicals, and the members of NOVA Chemicals' rheology group, headed by Dr. Joo Teh, for their support, encouragement, and assistance with the rheological equipment at NOVA Research and Technology Center. My gratitude also goes to the members of the rheology team of the University of British Columbia (Rheolab) for their academic guidance.

Finally, I would like to extend a special note of thanks to Natural Sciences and Engineering Research Council of Canada for its financial support, and to others who have in one way or other helped me with the completion of this project.

To *B, C, D, E, and F*

This is not the end. This is not even the beginning of the end.
This is the end of the beginning

Winston Churchill

1 INTRODUCTION

1.1 INTRODUCTION

The characteristics of most engineering materials are widely known, owing to their vast usage and development over the course of many years. There has also been much experience with their applications. However, the same cannot be said about plastics. Even though plastics are becoming increasingly important as building materials, there is still not enough accumulated information and experience, making it hard to truly appreciate the application of plastics as engineering materials. Studies are continuously being performed in order to gain a better understanding of plastic behavior. Numerous researches are also being conducted in search of improvements to the characteristics of plastics as a relatively new class of engineering materials.

Blow molding is one type of conversion process that is used to produce plastic products with hollow parts. The process of blow molding is principally governed by the rheological behavior of the resin used. The molecular structure of the resin, in turn, influences its rheological properties. High density polyethylene is one of the most common types of resin used in blow molding.

The purpose of this chapter is to provide a general introduction to polymeric materials and their processing behavior. Background information on polymers and, particularly, high density polyethylene is provided in the next section of the chapter, followed by a general discussion on polymer rheology. In addition, the process of blow molding and the applicability of polymer rheology to this process are discussed. Finally, the objectives of this thesis project are described in the last section.

1.2 BACKGROUND

1.2.1 Polymers

Over the last fifty years, there has been a particularly great interest in materials made up of high molecular weight molecules, also known as 'macromolecules'. Polymers are macromolecules consisting of a large number of repeating units called 'monomers' being joined together to form a pattern, in much the same way as links make up a chain. A 'homopolymer' is a type of polymer in which only one kind of monomer is used to make up the macromolecular chain. If two or three different kinds of monomers are used, the products are called 'co-polymers' and 'terpolymers', respectively. In order to have a technological significance, however, the molecular weight of a polymer has to be high enough. Polymers with very high molecular weights are also called 'high polymers'.

The chains that make up a polymer are usually not of equal length. Instead, there is a distribution of chain lengths or molecular weights. There are various factors that affect the exact shape of the distribution, such as the mechanism of polymerization and the subsequent treatment carried out on the polymer. For example, treating the polymer with solvent may selectively remove low molecular weight fractions. Higher molecular weight components may preferentially be removed by shear induced degradation. Also, either crosslinking or chain scission may be caused by chemical reactions such as oxidation. Since the average molecular weight and the molecular weight distribution of polymeric chains affect the physical properties of the bulk polymer, it is therefore important to have some quantitative measures of these parameters. Several molecular weight averages are normally determined for this purpose.

The weight average molecular weight can be defined by considering the weight fraction $w_i(M_i)$ of a polymer having molecular weight M_i. The weight average molecular weight, M_w, is then

$$M_w = \frac{\Sigma M_i \cdot w_i(M_i)}{\Sigma w_i(M_i)} \qquad (1.1).$$

Often, the distribution $w_i(M_i)$ is expressed as a continuous function $w(M)dM$. Under these circumstances, the summation in Equation 1.1 is replaced by an integral. Experimentally, M_w may be determined by Gel Permeation Chromatography (GPC) [Dealy and Wissbrun (1995)].

The number average molecular weight is also defined similarly by considering the number fraction $n_i(M_i)$ and summing it over M_i. However, $n_i(M_i)$ may be related to $w_i(M_i)$ by the expression $n_i(M_i) = w_i(M_i)/M_i$ and, hence, the number average molecular weight, M_n, can be defined in terms of weight fraction distribution as

$$M_n = \frac{\Sigma w_i(M_i)}{\Sigma\left(w_i(M_i)/M_i\right)} \qquad (1.2).$$

M_n may be measured experimentally by chemical or spectroscopic end group determinations or by GPC [Dealy and Wissbrun (1995)].

There are also other molecular weight averages which can be defined similarly. Two that are important are also called the Z and $Z+1$ molecular weight averages. These are defined as:

$$M_z = \frac{\Sigma M_i^2 \cdot w_i(M_i)}{\Sigma M_i \cdot w_i(M_i)} \tag{1.3}$$

and

$$M_{z+1} = \frac{\Sigma M_i^3 \cdot w_i(M_i)}{\Sigma M_i^2 \cdot w_i(M_i)} \tag{1.4}.$$

Figure 1.1 shows two typical molecular weight distribution curves. As shown in this figure, M_z is weighted heavily towards the high end of the molecular weight distribution, while M_n is weighted towards the low end. The type of distribution curve depends on the chemistry of the polymerization reaction and any subsequent treatment. The 'most probable' distribution is described by the equation

$$w(M) = \left(\frac{M}{M_n^2}\right) \cdot \exp\left(-\frac{M}{M_n}\right) \tag{1.5}$$

and is usually true for polymers produced by condensation reactions, such as Nylon 6-6 and polyethyleneterephthalate (PET). The more complicated 'log-normal' distribution curve is described following the Gaussian normal error curve having the form

$$w(M) = \frac{1}{\beta\pi^{\frac{1}{2}}M} \cdot \exp\left\{\frac{-\left(\ln\left(\frac{M}{M_o}\right)\right)^2}{\beta^2}\right\} \tag{1.6}.$$

The two parameters M_o and β in Equation 1.6 describe the location of the distribution and its breadth, respectively. This distribution usually holds for polymers produced by polymerization with a heterogeneous catalyst, such as high density polyethylene (HDPE). There are also other types of distribution curves, some even having more than one peak. The latter are called multi-nodal distributions.

The molecular weight distribution of a polymer can be described quantitatively by introducing a parameter called the polydispersity index (*PI*) which is defined as the ratio of M_w to M_n. A *PI* value of unity indicates monodispersity and larger *PI* values indicate broader molecular weight distributions.

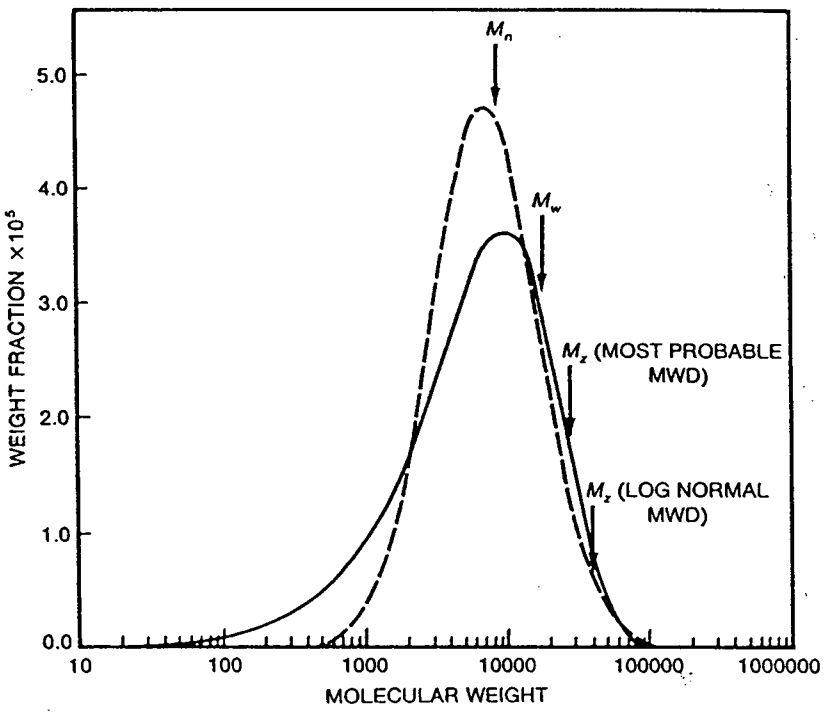

Figure 1.1 Differential molecular weight distribution for most probable (solid) and log normal (dashed) molecular weight distribution, both with M_w/M_n=2.

Chemically, there are three basic types of polymerization reactions, namely addition reactions, condensation reactions and a combination of the two. An addition reaction may occur simply by external chemical activation of molecules, resulting in the combination of these molecules in a chain type reaction. Rearrangement of atoms within two reacting molecules, or the opening up of molecules containing any ring atoms may also cause the addition type of polymerization to occur. This type of polymerization does not result in the formation of any by-product, unlike the condensation type of polymerization. In a condensation reaction, chemical union of two molecules is achieved by splitting out a molecule (a by-product) which is usually small. Normally, this by-product is immediately removed since it may inhibit further polymerization, or appear as an undesirable impurity in the final product. Nylon, phenolics, amino resins and polyester pre-polymers are examples of products formed through condensation polymerization. The third method of polymerization involves the combination of both addition and condensation reactions. Normally, the condensation reaction takes place first to form a relatively small polymer, which is then capable of undergoing addition polymerization. This type of polymerization reaction is used in the formation of polyesters and polyurethanes.

In actual practice, there are many different ways of carrying out these polymerization reactions. However, most involve one of the following four general methods of polymerization, i.e. the polymerization of monomer in bulk, in solution, in suspension, or in emulsion form. Bulk and solution polymerization techniques are usually used for the formation of both addition and condensation type polymers, whereas suspension and emulsion techniques are used widely for addition polymerization. Different

polymerization techniques can result in polymers with different molecular characteristics. The number and size of the resulting polymer molecules may be significantly affected by the rate of polymerization, the solvent and the extraneous media involved in each technique, causing this difference in the molecular characteristics. This causes the properties of the polymer to be affected accordingly.

Some polymers may be used as they are, i.e. directly from the polymerization process, but most of them require mixing with additives before they can be made into useful products. Some typical additives are plasticizers, pigments, fillers, lubricants, extenders, antioxidants, and heat and light stabilizers. These physical mixtures of polymer and additives are called plastics. Therefore, it is important to distinguish between the words polymer and plastic, since they refer to essentially different materials although they are often used as if they were synonymous.

In this work, the rheology and relevant processability of high density polyethylene (HDPE) blow molding resins were studied. Polyethylene is one type of polymer which has found usage in many applications. It is characterized by its toughness, near-zero chemical absorption, excellent chemical resistance, excellent electrical insulating properties, low coefficient of friction, and ease of processing. Different types of polyethylene are classified according to their density. HDPE, for example, has a density range between 0.941 to 0.965 g/cm^3 at 25°C. Polyethylene having different densities differ in their rigidity, heat resistance, chemical resistance, and ability to sustain load. Generally, as density increases, hardness, heat resistance and stiffness increase, while permeability decreases. Figure 1.2 shows schematically the molecular structures of the

different types of polyethylene. Low density polyethylene is characterized by its large number of side branches, which may also be relatively long. Linear low density polyethylene has less branching, while high density polyethylene has very few side branches.

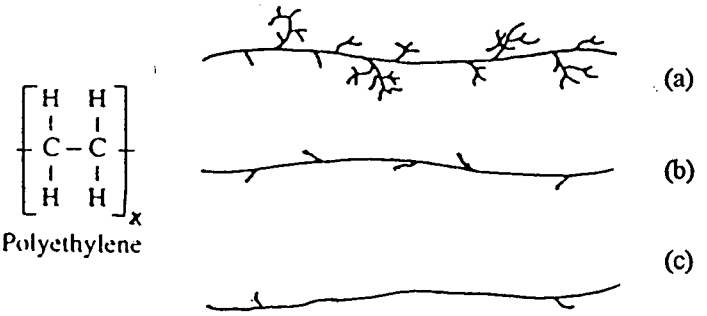

Figure 1.2 Chemical and molecular structures of (a) Low Density Polyethylene (LDPE), (b) Linear Low Density Polyethylene (LLDPE), and (c) High Density Polyethylene (HDPE).

HDPE polymers are highly crystalline and tough materials. Applications for HDPE include blow molded containers for household and industrial chemicals, injection molded items such as crates, housewares, pails, and dunnage containers, and extruded items such as pipes, tubes, and wire insulators. HDPE is also blown into film for packaging and rotationally molded into containers, toys, and sporting goods. Within the density range of HDPE, stiffness, tensile strength, melting point and chemical resistance improve at the high end. However, materials with the highest densities have lower stress crack resistance and lower impact strength at low temperatures.

1.2.2 Polymer Rheology

Rheology is defined as the science of material behavior under deformation, due to the presence of external forces. It attempts to understand why a material behaves in a certain way when a force is applied. The response of a deformed material is related to the

deforming force by what is known as a constitutive equation. To many design engineers, rheology is an important science. For example, in order to optimize the design of an extruder, a plastics engineer must know the relationship between the rate of deformation (shear rate) and the response of the polymer, so that the viscosity of the polymer may be determined. In injection molding, the same information is needed for the design of the mold so that the polymer melt will completely fill it with each injection. In blow molding, the processes of parison sag and swell are governed entirely by the rheological properties of the melt.

The rheology of polymer melt is made interesting by the fact that polymers are viscoelastic materials, i.e. they exhibit both viscous and elastic properties. The viscous part of the polymer tends to dissipate energy as heat when a force is applied during deformation. The elastic nature of the polymer, however, tends to store this energy and use it to bring the polymer back to its original undeformed state when the force is removed. Due to this elastic response, polymeric materials are said to have 'memory'. This memory can be understood by considering the molecular structure of a polymer. The long chain molecules that make up a polymer cause entanglements to occur at the molecular level, forming a temporary network. The network is only temporary because of Brownian motion, which has a greater effect at higher temperatures. However, in an equilibrium state, there is a most probable molecular configuration. Deforming the polymer melt will alter this molecular configuration, but when the deformation is stopped, the Brownian motion will tend to return the polymer molecules to the equilibrium configuration.

The rheological response of a polymer may be represented by a model consisting of a combination of springs and dashpots. The spring may be thought of as the elastic component of the material, while the dashpot represents the viscous component. The two simplest models of viscoelasticity are known as the Voigt and Maxwell models and are shown in Figure 1.3. The force in the spring is assumed to be proportional to its elongation and the force in the dashpot is assumed to be proportional to its rate of elongation, reflecting the time dependency of the response of the material. The Voigt model can be used to explain viscoelastic behavior in the presence of a constant force, also called creep behavior. Upon the application of a constant force, the assembly in the Voigt model will not respond immediately due to the presence of the dashpot. The ratio of the proportionality constants of the spring and the dashpot governs this time dependency. Such a response is also called a 'retarded' elastic response. The Maxwell assembly, on the other hand, attempts to explain the stress relaxation phenomena in a viscoelastic material. When the assembly is subjected to a sudden elongation, a stress is

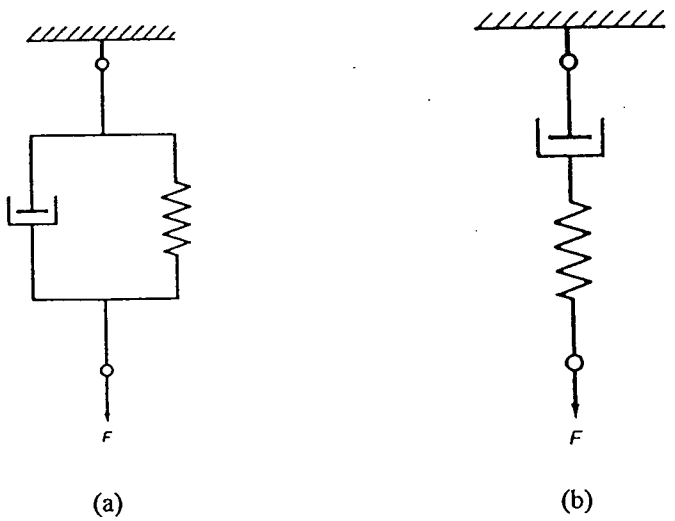

Figure 1.3 Analogs of viscoelastic materials: (a) Voigt model, (b) Maxwell model.

created. The magnitude of this stress, however, decreases with time as the assembly 'relaxes'. An equation that includes an exponentially decaying term can be written to show this behavior. In a real polymeric system, a more complex combination of springs and dashpots is needed to represent its rheological behavior.

The simplest type of viscoelastic behavior is called linear viscoelasticity and can be observed at very small and slow deformations. With small deformations, molecules are disturbed from their equilibrium configuration to only a negligible extent, and when the deformations are slow, there is time for the molecules to be brought back to the equilibrium configuration by Brownian motion. Under these conditions, the response of the material is independent of the rate, size and kinetics of the deformation. Linear viscoelasticity, however, is not particularly useful in polymer processing, since, in polymer processing, large and fast deformations are involved. It is nonetheless useful for equilibrium molecular characterizations and resin comparisons (quality control).

In a simple shear experiment, material is placed between two parallel plates separated by a distance h, as shown in Figure 1.4. One of the plates is kept stationary, while the other is moved at a constant velocity V. Assuming that no material slippage occurs at the material-plate boundary, the shear strain, γ_o, can defined as

$$\gamma_o = \frac{\Delta X}{h} \tag{1.7}$$

The shear rate can then be defined as

$$\dot{\gamma}_o = \frac{V}{h} \tag{1.8}$$

In the simple extensional experiment shown in Figure 1.5, a rod - shaped material is subjected to an elongational force at one end. The resulting extensional strain is defined as

$$\varepsilon_o = \ln\left(\frac{L}{L_o}\right) \tag{1.9}.$$

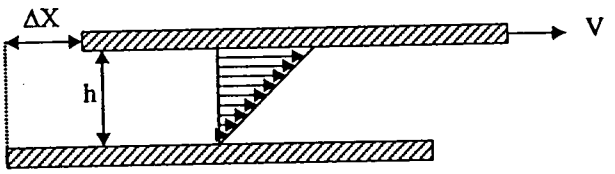

Figure 1.4 A schematic diagram of simple shear experiment

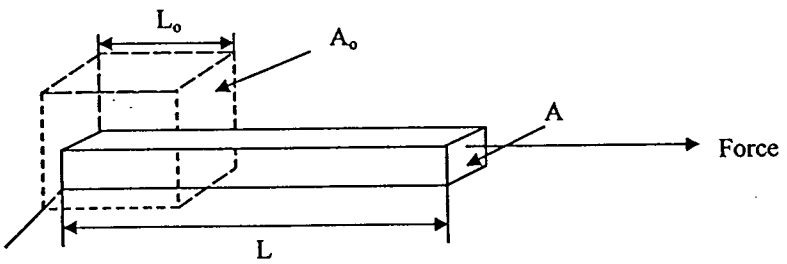

Figure 1.5 A schematic diagram of simple (uniaxial) extensional experiment

Knowing the shear and elongational strain magnitudes, the shear and tensile relaxation moduli can then be defined as

$$G(t,\gamma_o) \equiv \sigma(t)/\gamma_o \tag{1.10}$$

$$E(t,\varepsilon_o) \equiv \sigma_E(t)/\varepsilon_o \tag{1.11}$$

where $\sigma(t)$ and $\sigma_E(t)$ are the shear and extensional stresses, respectively.

In the linear viscoelastic regime, G and E are independent of deformation size and hence, for a shear type of deformation, the following equation can be written:

$$\sigma(t) = G(t)\cdot\gamma_o \tag{1.12}.$$

The modulus can be separated into the elastic (storage) and viscous (loss) moduli, G' and G'', respectively, i.e.

$$G = |G^*| = \sqrt{G'^2 + G''^2} \tag{1.13}$$

where G^* is the complex modulus.

In an oscillatory shear experiment, these moduli can be obtained as functions of frequency, ω. The viscosity of the material can then be approximated as the complex viscosity using the Cox-Merz rule [Dealy and Wissbrun (1995)]:

$$|\eta^*| = \sigma_o/\dot{\gamma}_o = \sqrt{\left(\frac{G'(\omega)}{\omega}\right)^2 + \left(\frac{G''(\omega)}{\omega}\right)^2} \tag{1.14}.$$

Also, using the generalized Maxwell model, the following equations can be derived:

$$G'(\omega) = \sum_{i=1}^{n} \frac{G_i(\omega \cdot \lambda_i)^2}{\left[1+(\omega \cdot \lambda_i)^2\right]} \tag{1.15}$$

$$G''(\omega) = \sum_{i=1}^{n} \frac{G_i(\omega \cdot \lambda_i)}{\left[1+(\omega \cdot \lambda_i)^2\right]} \tag{1.16}$$

where G_i and λ_i are the discrete relaxation modulus and time, respectively. These parameters indicate the relaxation behavior of the molecules. Therefore, by fitting Equations 1.15 and 1.16 to the data obtained from oscillatory shear experiments, the relaxation behavior of the molecules can be determined as a discrete set of data consisting of G_i and λ_i values.

For large and fast deformations, the theory of linear viscoelasticity is no longer valid. This regime is also called the non-linear viscoelastic regime. There is no general theory that can be used to predict non-linear viscoelastic material behavior, i.e. in this regime, information gained from one type of deformation cannot be used to predict behavior in a different type of deformation. Material functions such as the damping function are often defined to indicate deviation from viscoelastic behavior.

Rheological properties are usually temperature dependent and hence, to obtain a complete picture of material behavior, experiments must be carried out at many temperatures. Fortunately, it is often found that data taken at several temperatures can be brought together on a single master curve by means of 'time-temperature superposition'. This makes it possible to display on a single curve, corresponding to a particular reference temperature, T_o, the material behavior covering a much larger range of

deformation. According to the time-temperature superposition theory, quantities that contain the unit of time need to be shifted by a shift factor, a_T, such that the unit of time is eliminated. Thus, if one makes a plot of the complex viscosity, η^* (Pa.s) versus the frequency of shear (s^{-1}), the resulting master curve can be accomplished by plotting η^*/a_T versus $\omega.a_T$. The shift factor can then be related to temperature by either the Arrhenius type equation

$$a_T = \exp\left[\frac{E_a}{R}\cdot\left(\frac{1}{T}-\frac{1}{T_o}\right)\right] \tag{1.17}$$

or the WLF *(Williams, Landel, and Ferry)* equation

$$\log(a_T) = \frac{-C_1^{\,o}\cdot(T-T_o)}{\left[C_2^{\,o}+(T-T_o)\right]} \tag{1.18}$$

Equation 1.17 is valid for temperatures that are at least 100 K above the glass transition temperature, T_g. The term E_a in this equation is the flow activation energy, which gives an indication of the sensitivity of material flow to temperature change. For temperatures closer to T_g, Equation 1.18 is found to be more useful, where the constants $C_1^{\,o}$ and $C_2^{\,o}$ can be determined using any optimization technique. Knowing E_a, or $C_1^{\,o}$ and $C_2^{\,o}$, a_T at any other temperature can be calculated, and, referring back to the master curve, the rheological property at the desired temperature can then be obtained [Dealy and Wissbrun (1995)]. Figure 1.6 illustrates the time-temperature superposition principle. The complex viscosity obtained from oscillatory experiments is plotted as functions of frequency at different temperatures in Figure 1.6(a). Selecting the temperature of 150°C

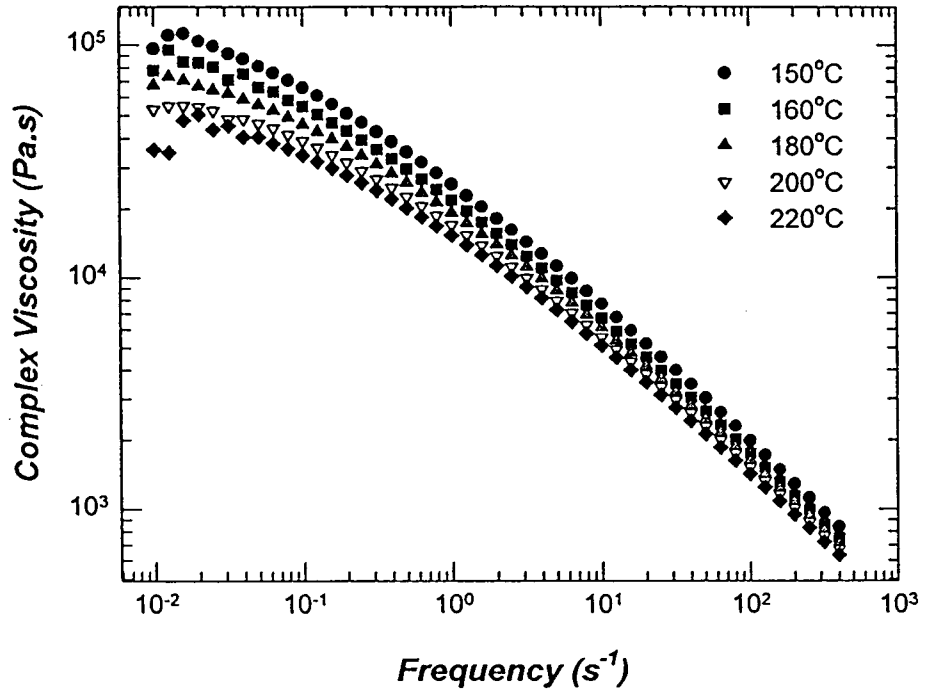
Complex Viscosity (Pa.s)
Frequency (s^{-1})
150°C
160°C
180°C
200°C
220°C

(a)

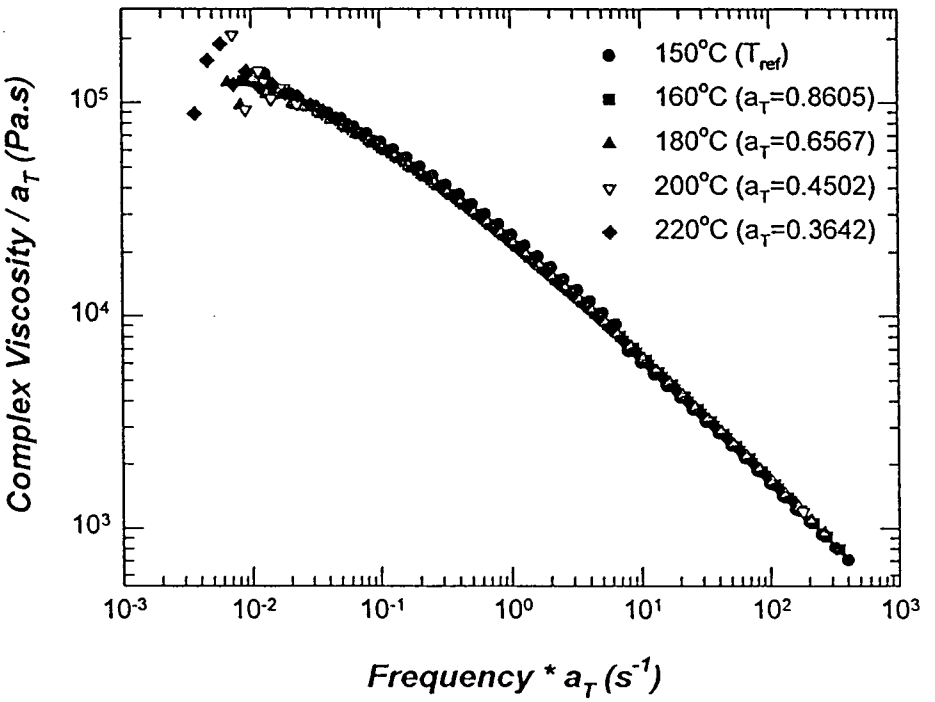
Complex Viscosity / a_T (Pa.s)
Frequency * a_T (s^{-1})
150°C (T_{ref})
160°C (a_T=0.8605)
180°C (a_T=0.6567)
200°C (a_T=0.4502)
220°C (a_T=0.3642)

(b)

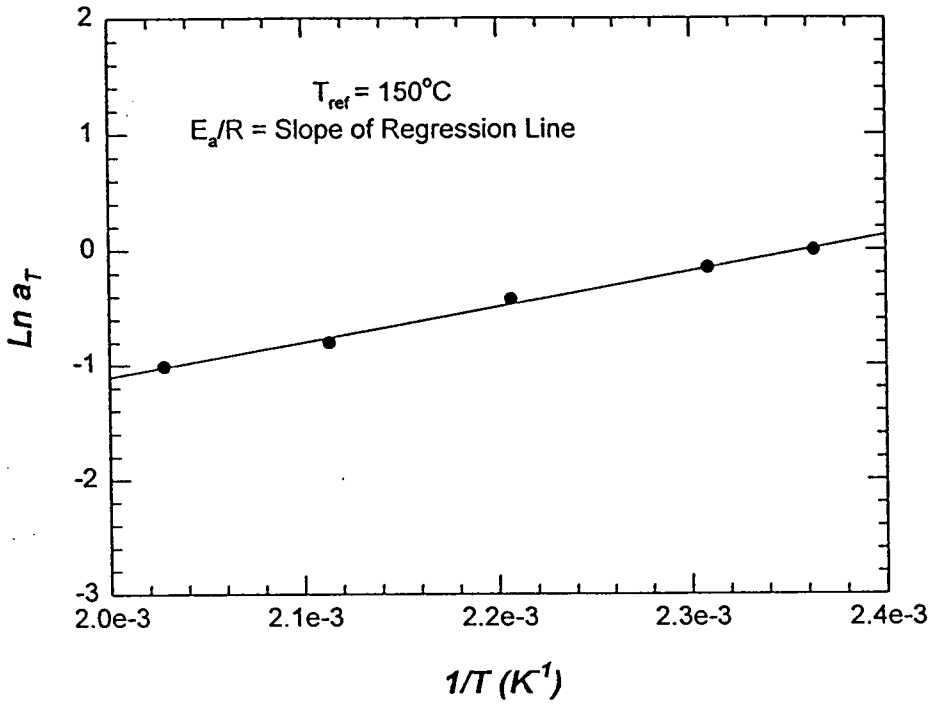

(c)

Figure 1.6 Time temperature superposition of complex viscosity curves obtained at different temperatures: (a) before superposition, (b) after superposition, (c) the fit of shift factors to the Arrhenius equation

as the reference temperature and performing both horizontal and vertical shifts to these data yield the master curve shown in Figure 1.6(b). The scatter observed in the plot at low frequency is due to the experimental difficulties at very low deformation rates. In Figure 1.6(c), the natural logarithmic values of the shift factors are plotted versus the inverse of temperature according to Equation 1.17. The activation energy of the polymer can then be determined by calculating the slope of the straight line obtained in Figure 1.6(c).

1.2.3 The Process of Blow Molding

In blow molding, the polymer is first softened by electrical and mechanical heating in an extrusion barrel. The resulting melt is then extruded through a die head to form a hollow tube called a parison. The thickness of the blow molded part is determined by the thickness of the parison, which is in turn determined by the shape of the die opening and the extrusion speed. Several seconds after the parison is fully extruded, the two halves of the mold close and pinch off the extruded parison which surrounds the blow pin. The blow pin provides the opening for compressed air to enter the parison and inflate the polymer melt so it forms to the contours of the mold. An overview of this process is depicted in Figure 1.7. Figure 1.8 illustrates the molding process, and in Figure 1.9, the method of controlling the wall thickness is shown schematically. The control of wall thickness is a critical part of the process and may be achieved partially by controlling the position of the mandrel in the die head. Lowering the position of the mandrel increases the parison wall thickness and vice versa.

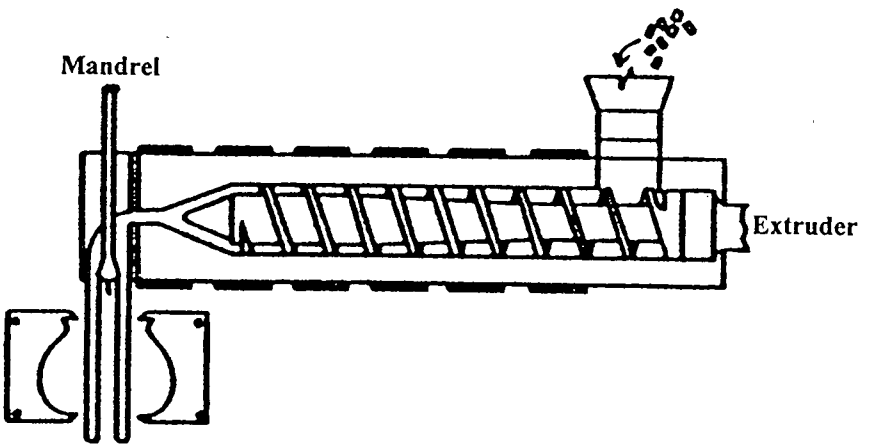

Figure 1.7 Overview of blow molding process.

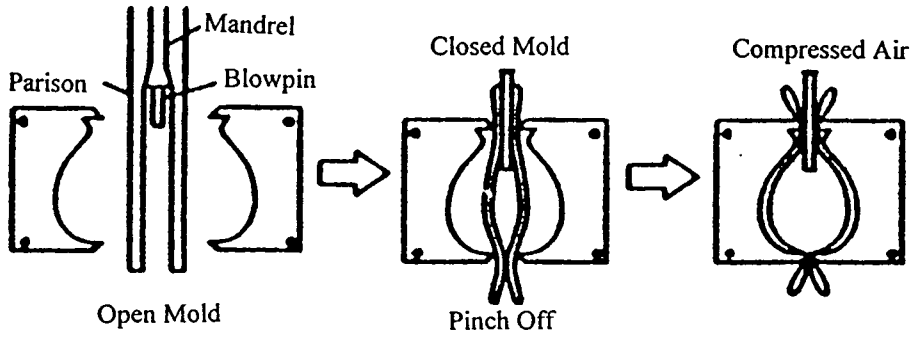

Figure 1.8 Parison inflation in the process of blow molding.

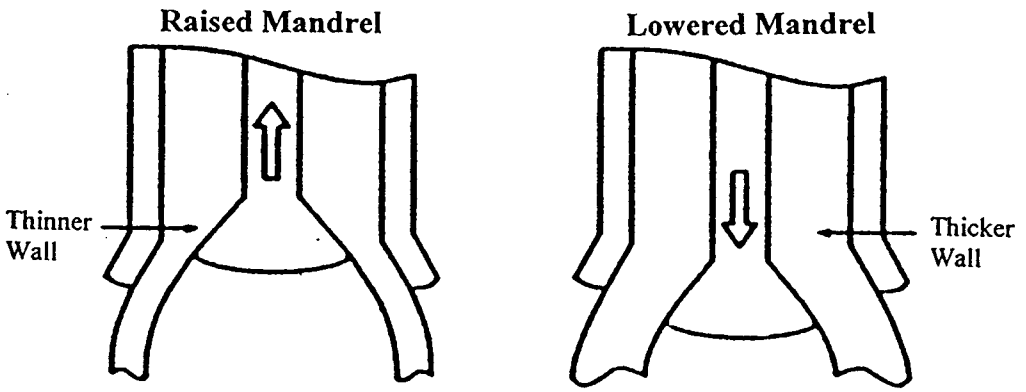

Figure 1.9 The controlling of parison wall thickness by adjustment of mandrel position.

Blow molding is an effective way to process hollow parts, and it involves relatively low tooling costs. However, the process requires long cycle times, secondary trimming, and high start-up costs.

Rheology is of central importance in the process of blow molding. During extrusion, the flow details and pressure drop in the barrel and the die are governed principally by the viscous properties of the polymer melt, and the general flow path is controlled by the geometry of the extruder and die. When the melt leaves the die, however, its behavior is no longer controlled by any contacting solid walls. Instead, the only external forces acting on the melt are gravity and the blow pressure. The parison behavior in response to these forces is governed entirely by the rheological properties of the melt. Moreover, due to the elastic nature of polymer melt, the behavior of the extruded parison reflects not only the two external forces but also the deformation it experienced in the die.

At the exit of the die, polymer melt also tends to swell. This is another manifestation of melt elasticity. Figure 1.10 illustrates the extrudate swell behavior of Newtonian and polymeric materials. The swelling of fluids (increase of effective diameter) upon the emergence from a die is not unique. For the case of polymer melts, the swell can be as much as 3 times the original diameter of the die, if not more. Generally, extrudate swell increases with increasing shear rate and decreases with increasing length to diameter ratio of the capillary die. Since this is a manifestation of the viscoelasticity of the polymer melt, there is also a time dependency involved. In general, most of the swelling takes place during the first several seconds of material emergence. However, sometimes hours are needed before the swell reaches its ultimate value. Extrudate swell may have a significant effect on the shape and weight of the final molded product.

When polymer melt exits the die, it may also exhibit 'sharkskin' or 'melt fracture', which are irregularities in the surface of the extrudate that can affect the surface finish of

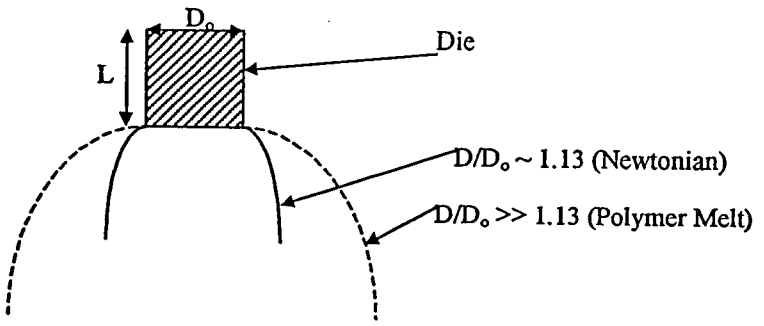

Figure 1.10 Extrudate swell behavior for (a) Newtonian fluid and (b) polymer melt.

the final blow molded product. This effect occurs above a certain critical stress in the die and is often the factor that limits the rate of an extrusion process. The distortion is most severe in narrow MWD, high viscosity resins. Sometimes, increasing the extrusion temperature or reducing the extrusion speed helps to eliminate this effect, but these actions will increase the cycle time. The detailed origins of this phenomenon are not fully understood, but it has been thought that the shape and the material of construction of the die, and the formulation of the resin may be the contributing factors [Ramamurthy (1986), Hatzikiriakos (1994)].

At the exit of the die, before the two halves of the mold close, the parison sags under its own weight. In more severe cases, sagging may cause the parison to break off. In other cases, it will cause large variations in thickness and diameter along the parison. The extent of the sag depends exclusively on the rheological properties of the polymer melt. To quantitatively analyze the sagging behavior of polymer melt, melt strength is

often defined as the ability of the melt to counteract sagging. Increasing the temperature will decrease the melt strength of the polymer melt and hence, increases sagging.

Once a molten parison is formed, the way that it inflates is again a reflection of melt viscoelasticity. The rheological properties that govern this part of the process are the extensional flow properties. The deformation is not a true uniaxial extension, but the results from uniaxial extension experiments are thought to be useful for determining inflation performance. For example, resins that exhibit 'extension thickening' are thought to be easier to inflate and unlikely to exhibit blow-out (the tendency of the parison to bulge at the centre during inflation), even if the inflation pressure is high. 'Extension thinning', on the other hand, is thought to imply unstable inflation and increased likelihood of blow-outs.

The influence of the various rheological properties on parison formation is summarized in Table 1.1.

Table 1.1 Influence of rheological properties on parison formation

Property	Effect on parison formation
High shear rate viscosity	Extrusion pressure and/or rate (length, diameter and thickness, melt fracture, curtaining)
Low shear rate viscosity	Parison sag (length, diameter and thickness, curtaining)
Extrudate swell	Parison length, diameter, thickness, curtaining
Critical stress	Melt fracture
"Relaxation" time	Sag, stretch orientation

1.3 Thesis Objectives

In order to produce acceptable blow molded products, it is necessary to understand the rheological properties and the processability of blow molding resins. Rheological properties such as shear and extensional flow properties, extrudate swell, and sensitivity of viscosity and extrudate swell to changes in deformation rate and temperature are highly influenced by the molecular characteristics of the resins. Resin processability is also affected by molecular parameters, such as M_w, PI and density. Melt strength, sagging, and weight swell are parameters which characterize the processability of blow molding resins.

The objectives of this work were, therefore, to either quantitatively or qualitatively

1. correlate the rheological properties (shear viscosity, extensional strain behavior, extrudate swell, and viscosity and swell sensitivities to changes in temperature and shear rate) of commercial HDPE blow molding resins to their molecular parameters (M_n, M_w, M_z, PI, and density),

2. correlate the processability properties (melt strength, sagging characteristics, and weight swell) of commercial HDPE blow molding resins to their molecular parameters (M_n, M_w, M_z, PI, and density),

3. determine the significance of the empirically defined parameters: stress exponent, melt index, and melt flow ratio on resin quality control, and

4. correlate processability to rheological properties.

2.0 LITERATURE REVIEW

2.1 INTRODUCTION

Numerous publications have been reported on the rheological characterization of polyethylene and the process of blow molding. However, most of these publications pertain either to pure rheological characterization, with emphasis on finding possible explanations for certain observed polymer behaviors, or to the mathematical modeling of polymer behavior during the blow molding process. Very few attempts have been made to characterize the rheological properties of resins, with the effect of rheology on resin processability as the ultimate objective.

In this chapter, some of the publications related to this work are reviewed.

2.2 RHEOLOGY

Yoshikawa *et al.* (1990) studied the influence of molecular weight distribution and long chain branching on the viscoelastic behavior of commercial HDPE melts. The two types of samples studied were produced using different kinds of catalysts. The study found that long chain branching increases the relaxation times in dynamic viscoelastic functions, relaxation modulus and elongational viscosity. It was also found that it is possible to use melt index to predict shear flow behavior. However, differences in shear viscosity corresponding to the stress for which melt index was measured were small, although reasonably large differences were obtained for the melt index values. Larger and more significant differences are observed at much lower stress levels. With regard to extensional viscosity, the authors attributed the large rises in extensional viscosity to long

chain branches and the high concentration of large molecules in the molecular weight distribution.

In another study, Yoshikawa *et al.* (1989) investigated the dependence of shear viscosity on M_w. The authors found that for HDPE with no long branches, the zero shear viscosity was proportional to $M_w^{3.5}$. For HDPE with long branches, the exponent was found to be higher than 3.5. Hence, for branched HDPE, the dependence of zero shear viscosity on M_w was stronger.

The effect of molecular weight and molecular weight distribution on the viscous and elastic behavior of other polyethylene resins have also been studied by several workers including Han and Villamizar (1978), Shroff and Mitsuzo (1977), Bersted (1976), Mendelson and Finger (1975). These studies found that increasing M_w increases the shear viscosity in the low deformation regime. Above some critical value of M_w, the zero shear rate viscosity for amorphous and linear polymers has been found to be proportional to $M_w^{3.4}$. On the other hand, the breadth of the molecular weight distribution was found to affect the shear sensitivity of the shear viscosity curves. In general, increasing the polydispersity reduces the shear rate at which shear thinning begins [Dealy and Wissbrun (1995)].

The flow of polymer depends on the availability of free volume and thermal energy. Near the glass transition temperature, the availability of free space becomes the limiting factor. However, at higher temperatures, where there is no lack of free volume, energy barriers become more significant. In this temperature regime, the activation energy is constant and it reflects the sensitivity of polymer flow to changes in temperature. It has

been found that activation energy is affected by the degree of branching. For polyethylene, increasing the percentage of long chain branching increases the activation energy significantly [Dealy and Wissbrun (1995)]. For HDPE, typical values of activation energy at high temperatures fall in the range between 20 kJ/mol to 25 kJ/mol [Van Krevelen (1990)]. Mavridis and Shroff (1992) have carried out a study on the temperature dependence of polyolefin melt rheology. They have developed a unified framework for handling the temperature dependence of rheological data.

Shenoy *et al.* (1983) proposed a simpler method to estimate the polymer flow curve and its dependence on temperature and shear rate, knowing the melt index and glass transition temperature of the polymer. The authors suggested the use of melt index as a substitute for the shift factor in time temperature superposition theory. Master curves for several types of polymers were calculated using the suggested method. It is interesting to note that the resulting master curve was a general one, applicable to any grade or class of polymer, regardless of the technology used to produce the resins, the shape of the molecular weight distribution or any other molecular parameters.

With regard to the extensional flow properties of polymers, most previous studies were conducted by subjecting polymer samples to tensile force under constant rate conditions (more detailed descriptions of extensional flow properties are provided in chapter 3). This procedure yields the extensional viscosity of the material directly. Munstedt and Laun (1981) found that increasing the polydispersity of LDPE increases the magnitude of tensile thickening in the extensional viscosity curve. However, it should be noted that the increase in polydispersity was achieved by increasing the concentration of

larger molecules. The authors did not investigate the effect of increasing the low molecular weight tail of the distribution. By increasing M_w, on the other hand, the authors found an increase in the extensional viscosity at low stress levels. The authors also concluded that extensional flow properties of polymers are affected by certain features of the molecular weight distribution, and that differences too small to be detected by chromatography can affect the extensional viscosity curve.

Rauschenberger and Laun (1997) developed a mathematical model to predict isothermal and nonisothermal elongation of an extruded filament at a given force. In the model, the pre-strain history of the material was included. The model was tested with LDPE and was found to predict the melt behavior for uniaxial elongation experiments very well.

Considering the process of blow molding, it is more useful to determine melt properties under constant stress conditions (creep). However, to date, there are not many experimental data published based on such conditions.

Extrudate swell is another important rheological property. It has been found that, for many linear polymers, increasing polydispersity increases the ultimate swell of the polymer extrudate. However, for polymers with very similar molecular weight distributions, extrudate swell profiles can differ significantly. This is thought to be due to the fact that extrudate swell is very sensitive to small amounts of high molecular weight material [Dealy and Wissbrun (1995)]. Koopmans (1988) has first recognized this. Koopmans also noted that it is misleading to use the polydispersity index as a measure of

molecular weight distribution, since it may not reflect the contribution of the high molecular weight components.

In another study, Koopmans (1992a, c) determined the effect of molecular weight distribution on the time dependency of extrudate swell. The author found that the presence of high molecular weight molecules resulted in a faster initial swell but a smaller maximum swell, which could be due to the cooling of the extrudate before the maximum swell was reached. The author also concluded that it is important to consider the full molecular weight distribution and not a few average molecular weight values, such as M_w and M_z, to understand the flow behavior of polydisperse polymers.

2.3 PROCESSABILITY

Very little information is available about the melt strength of polymers. A possible reason includes the inability to generalize such results found for a given polymer to other materials. It has also been found that melt strength is dependent on a number of parameters and cannot be used to determine the elongational viscosity of polymer melts [Mantia and Acierno (1985)].

Mantia and Acierno (1985) studied the melt strength properties of HDPE, LLDPE, and LDPE. The authors found that HDPE and LLDPE have a high breaking/stretching ratio and low melt strength values. LDPE, on the other hand, exhibits very large melt strength values but low breaking/stretching ratio values. The authors also found that it is possible to predict melt strength by measuring the melt index of the polymer. Increasing melt index was found to indicate decreasing melt strength. The breaking/stretching ratio, on the other hand, increases with melt index.

In another study, Mantia and Acierno (1983) found that it is possible to correlate melt strength to the product of M_w and polydispersity index for HDPE. The authors also investigated the effect of temperature on melt strength and found a mathematical correlation between melt strength and temperature.

Goyal (1994) performed a study on the melt strength of LLDPE having various molecular weights, densities, comonomer types and molecular weight distributions at several extrusion temperatures. The author found the same implication of melt index on melt strength in that increasing melt index indicated lower melt strength. For LLDPE with short chain branching, it was found that density did not affect melt strength significantly. On the other hand, for high pressure LDPE (with long chain branching), melt strength was found to increase with a decrease in resin density. The author also found that broadening the molecular weight distribution did not have any significant influence on melt strength. However, a change in the modality of the distribution can have a major effect on the melt strength behavior of a resin. In addition, non-reactive additives such as slip agent, anti-block and fluoroelastomer polymer processing aids did not have any effect on the melt strength of a resin, even though these additives can substantially alter the apparent shear viscosity behavior of a resin.

In the above studies, melt strength was determined by pulling polymer extrudate from a capillary barrel using a pulley at increasing speed. The force required to pull the extrudate was measured and the steady force level or the force at which the extrudate broke was taken as the melt strength value. The extrusion of the polymer in the barrel was done at some specific conditions. Considering this method of melt strength

measurement, it can be said that the reported melt strength values correspond to high shear rates and temperatures lower than the barrel temperature, since pulling was done on extrudates outside the barrel. Although this may be used to compare the melt strength properties of resins, the method is not particularly useful for blow molding processes. During parison formation, the polymer melt is subjected to very slow deformation. Hence, melt strength data obtained according to this method do not really reflect the melt strength of the polymer during parison formation. In this work, another procedure that is more useful for blow molding processes was used (see chapter 3*). No similar studies have previously been carried out using this new technique of melt strength measurement.*

Henze and Wu (1973) studied the factors affecting parison diameter swell in a blow molding process (see Figure 2.1 for the definition of parison diameter swell). The authors found that diameter swell increases with increasing shear rate (decreasing parison residence time). A correlation between the local diameter ratio and the local weight ratio has also been found. The authors found that the diameter swell ratio approximately equals the local weight swell ratio raised to the power of 0.25. In addition, it was found that the swell potential, rate of swell and melt strength strongly influence the diameter swell.

A procedure for determining parison flow behavior in regard to swell and drawdown has been described by Sheptak and Beyer (1965). The authors used a pillow mold having multiple pinch off points to determine the weight and diameter distribution of the parison. In addition, photographs were taken at different times during parison formation to

determine the relaxation behavior of the polymer melt. The qualitative analysis used by these authors is adopted in this work.

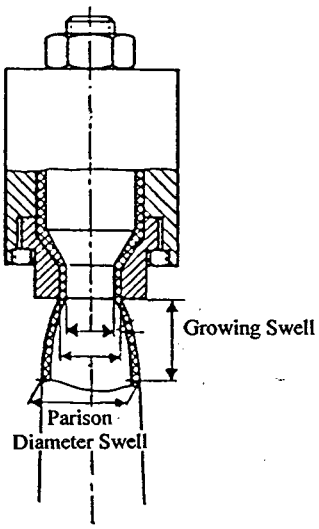

Figure 2.1 Illustration of parison diameter swell

Kaylon and Kamal (1986) also conducted a pillow mold study to investigate the relation between capillary extrudate swell and parison swell. The authors found excellent agreement between the area swell values determined on the basis of capillary and parison swell experiments. In comparing the relation between capillary and parison swell for a number of HDPE resins, Wilson *et al.* (1970) found that the relative order of magnitude of capillary extrudate swell correlates well with the relative order of parison diameter swell. In another study by Alroldi (1978), the same result was obtained.

3 EXPERIMENTAL EQUIPMENT AND PROCEDURES

3.1 INTRODUCTION

This chapter describes the experimental equipment and procedures used in the determination of the rheological properties and the processability of the HDPE resins. The theory behind each piece of equipment is discussed accordingly in each subsection. In addition, one section is devoted to the molecular properties of the resins.

3.2 EXPERIMENTAL EQUIPMENT

3.2.1 Densimeter

Density is a measure of the degree of crystallinity in a polymer and is commonly used to classify polyethylenes. A high density polyethylene has greater crystallinity than a low density polyethylene. The frequency, size and type of side branching on molecules highly influence the density value of a polymer. Increasing the frequency and the size of side branching decreases the density and affects the processing behaviour of the polymer accordingly.

In this work, the densities of HDPE resins were measured using a Toyoseiki Automatic Densimeter, Model D-H100. The densimeter is equipped with an analytical balance and a specimen clamp. A schematic diagram of the densimeter is shown in Figure 3.1.

Samples were prepared according to ASTM procedure PE-206 using a Wabash press which is equipped with electric heaters and controlled cooling rate capabilities. By measuring the sample weight in air and in distilled water by means of an analytical

balance, and knowing the density of the distilled water at the time of weighing, the absolute density of the resin can be found. The temperature of the distilled water is kept constant by circulating water of specified temperature around the beaker using a circulator. The actual temperature of the distilled water is determined manually by a thermocouple and the corresponding value of the distilled water density is obtained as tabulated in the densimeter manual.

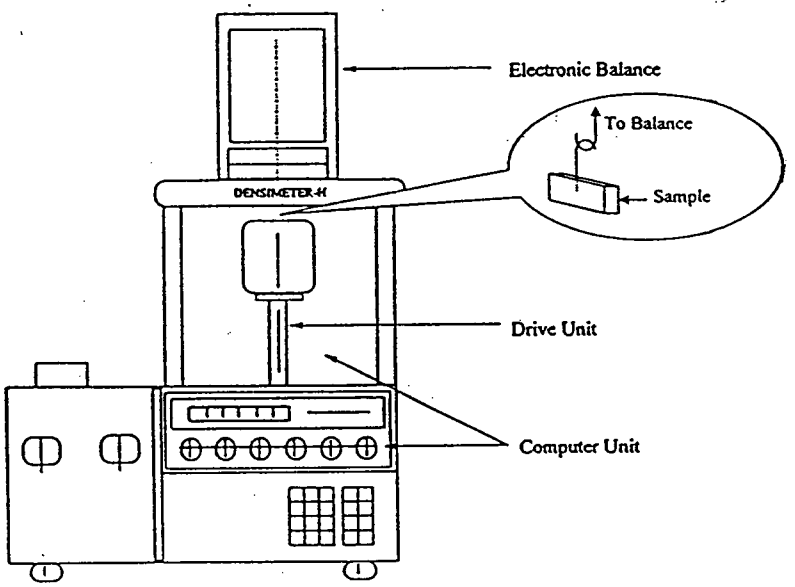

Figure 3.1 A schematic diagram of the Toyoseiki Automatic Densimeter, Model D-H100.

3.2.2 Extrusion Plastometer

Melt index is an empirically defined parameter that is critically influenced by the physical properties and molecular structure of a polymer. It serves to indicate the flow properties of a polymer at a particular low shear rate and is usually indicative of the molecular properties of the resin. It is measured as the amount of extruded polymer in a molten state through a die of specified length and diameter under prescribed conditions of

temperature and pressure. A high melt index implies ease of flow and hence, low viscosity, at the particular shear rate corresponding to the load condition. In this work, melt indexes were determined using the Tinius Olsen Manually Timed Extrusion Plastometer. A schematic diagram of the equipment is shown in Figure 3.2

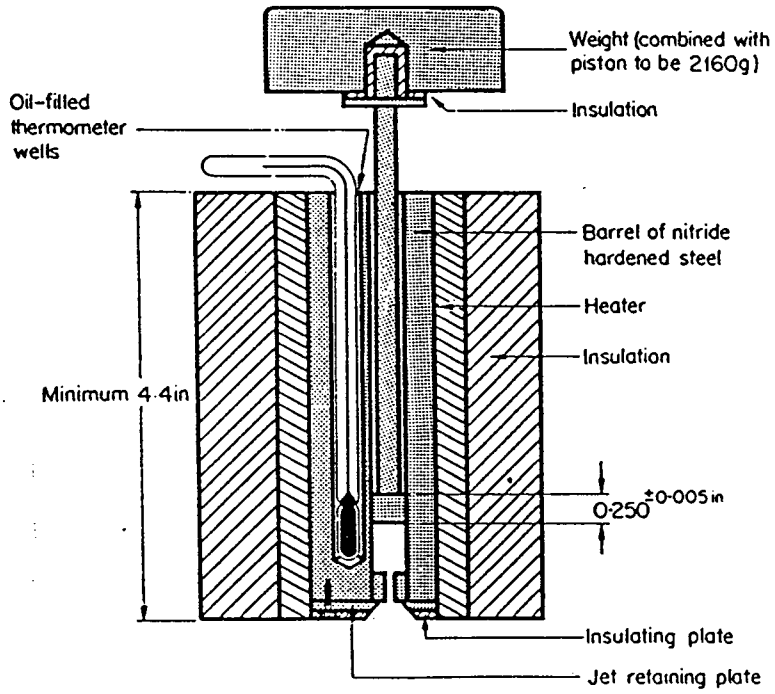

Figure 3.2 A Schematic diagram of the Tinius Olsen Manually Timed Extrusion Plastometer.

The major components of the plastometer are the electrically heated barrel, the piston, the weights, and the capillary die. The barrel is made of steel with an outside diameter of 50.8 mm and a length of 162 mm. The hole in the barrel is 9.5504 ± 0.0076 mm in diameter and is located 4.8 mm away from the cylinder axis. The electrical heater and insulator are wrapped around the barrel as shown in the figure. A thermometer is placed in the extra hole on top of the barrel to measure the actual temperature of the

barrel.

The piston used in the assembly is made of steel, 9.4742 ± 0.0076 mm in diameter and 6.35 ± 0.13 mm in length. At the top end of the piston, an insulating bushing acts as a barrier to heat transfer from the piston to the weight. The combined weight of the piston and the load is within 5% of the selected load. The load is placed on the piston as shown in Figure 3.2. When necessary, additional loads are obtained by adding more weights to the top of the first weight. The die used in this work is made of steel with the dimensions of 2.09955 ± 0.0051 mm in diameter and 8.000 ± 0.025 mm in length. For a more detailed description of the melt indexer, the reader is referred to the ASTM procedure D 1238-95.

It should be noted that small variations in the design and arrangement of the component parts may create some discrepancies in the measured melt index values. Also, it is important that the piston arrangement be kept as vertical as possible to minimize the friction between the piston and the side of the barrel. A leveling device is supplied with the melt indexer to facilitate this alignment procedure.

3.2.3 Capillary Rheometer

Capillary flow has been the most popular method for studying the rheological properties of liquids. For this particular flow, simple equations can be derived to determine the shear viscosity for both Newtonian and power law fluids. For other types of fluid, where no specific constitutive equation is known to be valid, special computational techniques are required to calculate the shear stress, shear rate and viscosity.

For a steady and fully developed flow of an incompressible fluid in a tube of radius R, a force balance can be performed to yield the absolute value of shear stress at the tube wall, σ_w:

$$\sigma_w \equiv -\sigma_{rz}\Big|_{r=R} = -\frac{r}{2}\cdot\frac{dP}{dZ}\Big|_{r=R} = -\frac{R}{2}\cdot\frac{dP}{dZ} \tag{3.1}$$

where dP is the pressure drop over the differential length dZ of the tube. For a Newtonian fluid, shear stress is related to deformation by:

$$\sigma = \eta\dot{\gamma} \tag{3.2}$$

where the viscosity η, is constant at a given temperature. Combining Equations 3.1 and 3.2, the fully developed parabolic velocity profile of Newtonian fluid can be obtained. Knowing the velocity profile, the shear rate at the tube wall can be calculated by differentiating the velocity profile with respect to the radius of the tube to yield:

$$\dot{\gamma}(Newtonian) = \frac{dV}{dr}\Big|_{r=R} = \frac{4Q}{\pi R^3} \tag{3.3}$$

where Q is the volumetric flow rate.

For non-Newtonian fluids, the same derivation procedure cannot be used. The velocity profile is no longer parabolic and a different constitutive equation is needed to determine the viscosity of the fluid, which is no longer a constant.

If a power law model is assumed, the constitutive equation is given by:

$$\sigma = K\dot{\gamma}^{n} \tag{3.4}$$

where K and n are the consistency index and the power law exponent, respectively. Note that the special case of Newtonian flow behavior is recovered for $n=1$. It can be shown that the wall shear rate for a power law fluid is given by [Dealy and Wissbrun (1995)]:

$$\dot{\gamma} = \frac{3n+1}{4n}\left(\frac{4Q}{\pi R^3}\right) \tag{3.5}.$$

It is noted that the term in bracket in the above equation is the wall shear rate for a Newtonian fluid (Equation 3.3). However, for non-Newtonian fluid, this term in itself has no significance. It is referred to as the 'apparent shear rate', $\dot{\gamma}_A$.

Using Equation 3.4 and 3.5, it can be shown that

$$\sigma_w = K\left(\frac{3n+1}{4n}\right)^{n} \cdot \left(\dot{\gamma}_A\right)^{n} \tag{3.6}.$$

The constants K and n can be determined from the intercept and the slope of the straight-line plot of the above equation in log-log co-ordinates.

If no specific constitutive equation is assumed, it is then not possible to calculate the true shear rate at the wall directly, knowing only $\dot{\gamma}_A$. A special technique which requires pressure drop data for a number of flow rates is needed. This technique makes use of a plot of $log(\sigma_w)$ versus $log(\dot{\gamma}_A)$ that yields a single curve. The true wall shear rate is then

given by

$$\dot{\gamma}_w = \left(\frac{3+b}{4}\right)\cdot\dot{\gamma}_A \tag{3.7}$$

where b is the Rabinowitsch correction given by

$$b = \frac{d\left(\log\dot{\gamma}_A\right)}{d\left(\log\sigma_w\right)} \tag{3.8}.$$

This correction term measures the fluid's deviation from Newtonian behaviour. It equals unity for a Newtonian fluid and *1/n* for a power-law fluid. A large amount of data is needed for this technique since differentiation is required to determine b.

In a capillary rheometer, the shear stress is determined by monitoring the driving pressure, P_d, in the barrel and assuming that the pressure at the outlet of the capillary is equal to the ambient pressure, P_a. P_d can be related to the force that is driving the piston (plunger), F_d, as:

$$P_d = \frac{F_d}{\pi R_b^{\,2}} \tag{3.9}$$

where R_b is the radius of the barrel. The pressure drop ($-\Delta P_w$) in Equation 3.1 is then (P_d-P_a) or, since for melts P_d is nearly always much larger than P_a, the pressure drop can simply be replaced by P_d. However, this is not the actual pressure drop that is observed for a fully developed flow in a capillary of length L. End correction is needed to take into account the large pressure drop at the entrance of the capillary and the small residual pressure at the exit. Figure 3.3 shows the pressure profile for a flow in a capillary.

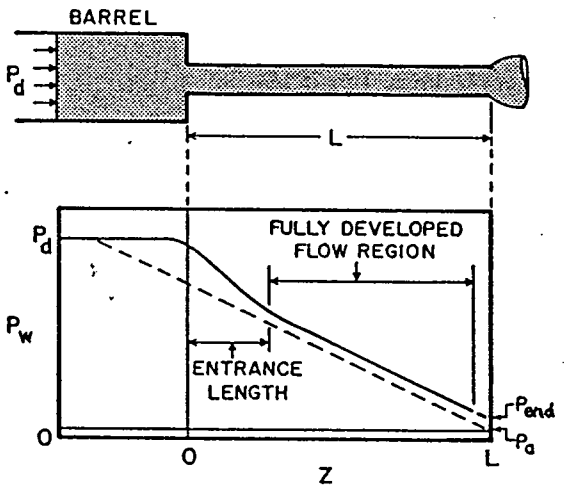

Figure 3.3 Pressure profile for a flow in a capillary.

The pressure end correction can be determined by the method outlined by Bagley (1931) in which the driving pressure, P_d, is plotted as a function of the length to diameter ratio (L/D) of capillaries of fixed diameter at fixed wall shear rate values. This plot is also referred to as the 'Bagley plot'. A typical Bagley plot is shown in Figure 3.4. The end correction is obtained by extrapolating the plot to L/D=0. Another way of determining P_{end} is by making use of an orifice die with L=0. Using the corrected pressure drop, the wall shear stress can then be calculated as

$$\sigma_w = \frac{(P_d - P_{end})}{4(L/D)} \qquad (3.10).$$

In general, the Bagley plot may include some curvature at high L/D ratio. This is due to the dependence of viscosity on pressure, the effect of pressure on polymer slip at wall, or viscous heating [Hatzikiriakos and Dealy (1992)].

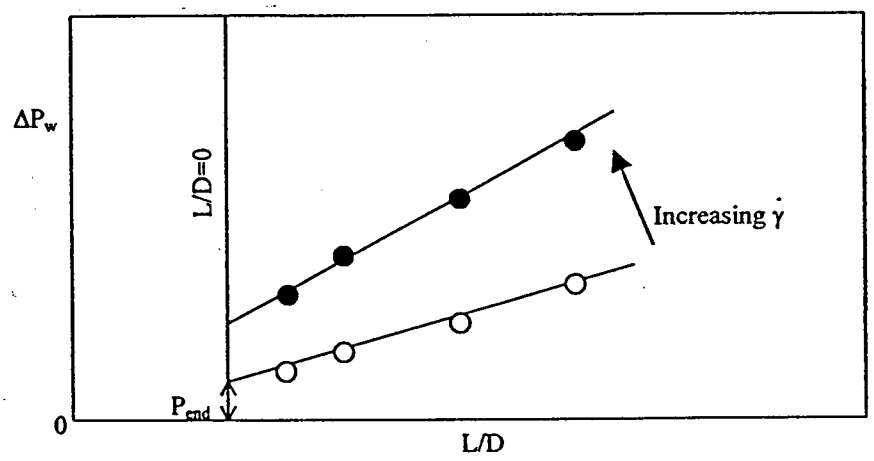

Figure 3.4 A typical Bagley plot.

In this work, a Kayeness Galaxy IV Capillary Rheometer (model 0052) was used. The barrel is equipped with a dual zone electric heater and an adaptive PID temperature controller with an accuracy of 0.1°C. The barrel is 175 mm in length and 9.55 mm ± 0.005 mm in diameter. A stepper motor is used to drive the piston from a speed of 0.5 mm per minute to a maximum speed of 250 mm per minute. Force is measured by means of a load cell installed on top of the piston driver. The rheometer also comes with data analysis software and tungsten carbide dies of different *L/D* ratios and diameters. A schematic diagram of the rheometer and a die is shown in Figure 3.5.

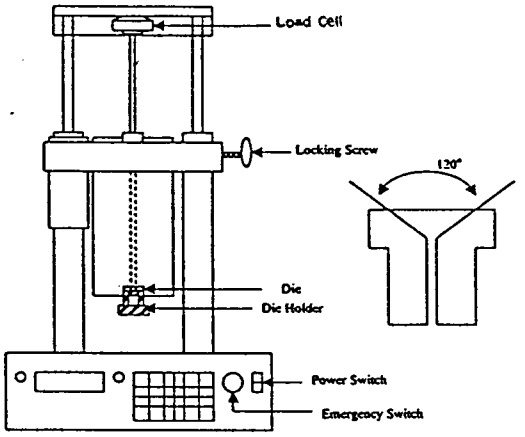

Figure 3.5 A schematic diagram of Kayness Capillary Rheometer and die.

3.2.4 Extensional Rheometer

Extensional properties of resins are very important in blow molding processes. During parison formation, the polymer melt is allowed to hang for some time before the two halves of the mold close and air is blown in. During this period, the polymer is subjected to elongational deformation by its own weight, resulting in parison sag. When air is blown to mold the parison, the polymer melt is also subjected to extensional deformation, in addition to a shearing type of deformation. For these reasons, it is therefore necessary for the extensional properties of blow molding resins to be determined before their processability can be evaluated.

'Simple extension' or 'uniaxial extension' is the type of extensional deformation illustrated in Figure 3.6. The deformation can be generated by introducing a tensile force on one end of a rod - shaped sample, which is fixed at the opposite end. The stretching

force, F and the length of the sample, L are two of the measurable parameters, which may be functions of time. Assuming that the material is incompressible, however, the following relation on the conservation of volume holds at all times

$$L \cdot A = L_o \cdot A_o \tag{3.11}$$

where L and A denote the length and the cross sectional area of the sample, respectively, and the subscript indicates the original condition of the sample before stretching.

The force applied on the sample in the longitudinal direction can easily be converted to stress by simply dividing it by the cross sectional area. This stress in itself, however, has no rheological significance. A rheologically more meaningful variable is, instead, the normal stress difference which is defined as $\sigma_{11}-\sigma_{22}$ where, referring to Figure 3.6, $_{11}$ and $_{22}$ indicate the normal directions x_1 and x_2, respectively. Note that the force is positive in the x_1 direction and, due to symmetry, $\sigma_{22}=\sigma_{33}$.

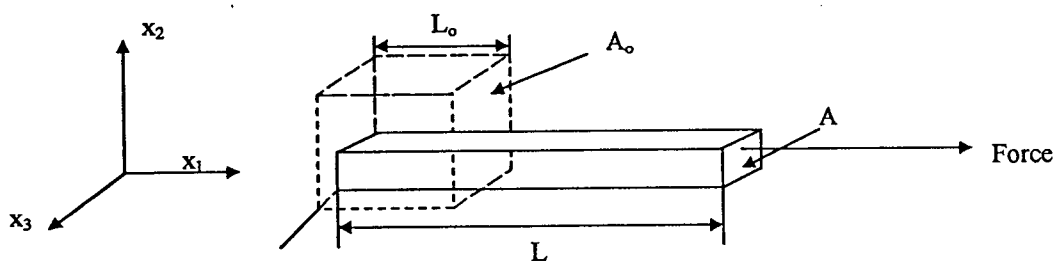

Figure 3.6 Uniaxial or simple extension

The strain experienced by the material during stretching can be defined as

$$d\varepsilon = dL / L \tag{3.12}$$

The current length of the sample, L, is used instead of the original length of the sample, L_o, as the reference length in the denominator to make the definition of strain more meaningful, since for materials with fading memory (liquid-like), the significance of L_o decreases as the stretching continues.

By simple integration, the strain for finite deformation can be obtained as

$$\varepsilon = \ln\left(\frac{L_2}{L_1}\right) \tag{3.13}$$

This is also called the Hencky strain. The strain rate can be derived from the above relation as

$$\dot{\varepsilon} = \frac{d\varepsilon}{dt} = \frac{1}{L}\cdot\frac{dL}{dt} = \frac{d\ln L}{dt} \tag{3.14}$$

Realizing that dL/dt is the velocity, V, at the end of the sample, equation 3.14 can hence be written as follows:

$$\dot{\varepsilon} = \frac{V}{L} \tag{3.15}$$

Therefore, in a constant strain rate experiment, the speed at which the sample is being pulled is controlled according to the instantaneous length of the sample, L, so that $\dot{\varepsilon}$ can be kept constant. The force required to stretch the sample is measured as a function

of time as the length, and hence the stretching velocity, change accordingly. The extensional viscosity of the material can then be calculated as the ratio of stress difference to strain rate. For a Newtonian fluid, it can be shown that the extensional viscosity is three times the shear viscosity (also observed experimentally). This is also true for polymeric materials at sufficiently small strain and shear rates, i.e.

$$\lim_{\dot{\varepsilon}\to 0} \eta_E\left(\dot{\varepsilon}\right) = 3\eta_o \tag{3.16}$$

where η_E is the extensional viscosity at diminishingly small strain rates and η_o is the zero-shear rate viscosity.

In a constant stress experiment, however, it is the stretching force that is being controlled according to the cross sectional area of the sample. The cross sectional area can be determined by measuring the length of the sample as a function of time and by using Equation 3.11, assuming material incompressibility. The measured quantity in a constant stress experiment is the strain of the material as a function of time. The strain versus time curve is useful for determining the melt strength of a polymer melt. At a particular time, a resin with lower melt strength will show a higher strain in the curve. Such a resin will hence lead to more sagging during parison formation. Constant stress experiments are, therefore, more useful for blow molding processes since the results can be related directly to processability parameters such as melt strength and sagging characteristics. Also, constant stress experiments are more representative of the parison formation stage of the blow molding process. In such experiments, the extensional viscosity of the material can be calculated as the stress to strain rate ratio by first

differentiating the strain versus time curve to get the strain rates at different times.

A Rheometrics RER-9000 Extensional Rheometer was used in this work to determine the elongational properties of the HDPE resins. The rheometer consists of a control panel, equipped with a plotter, and a dewar in which a cylindrically shaped sample is pulled in a bath of heated Dow Corning 200 fluid. To ensure temperature uniformity, the fluid is circulated through the dewar by a circulator which also functions as a heater for the fluid. The need to float the sample in the fluid is important to eliminate gravity as a driving force for deformation, which is especially critical when testing less viscous materials. Thus, the fluid is chosen so that its density minimizes the buoyancy effect on the sample during the vertical pull. The rheometer is able to perform extensional runs under constant rate or constant stress conditions and is connected to a computer for automatic data acquisition. The rheometer also comes with a set of accessories for sample making. These accessories include a 15-cavity compression mold, gluing fixture, metal clips and a rotary sample cutter. Figures 3.7 to Figure 3.9 show the schematic diagrams of the rheometer and its accessories.

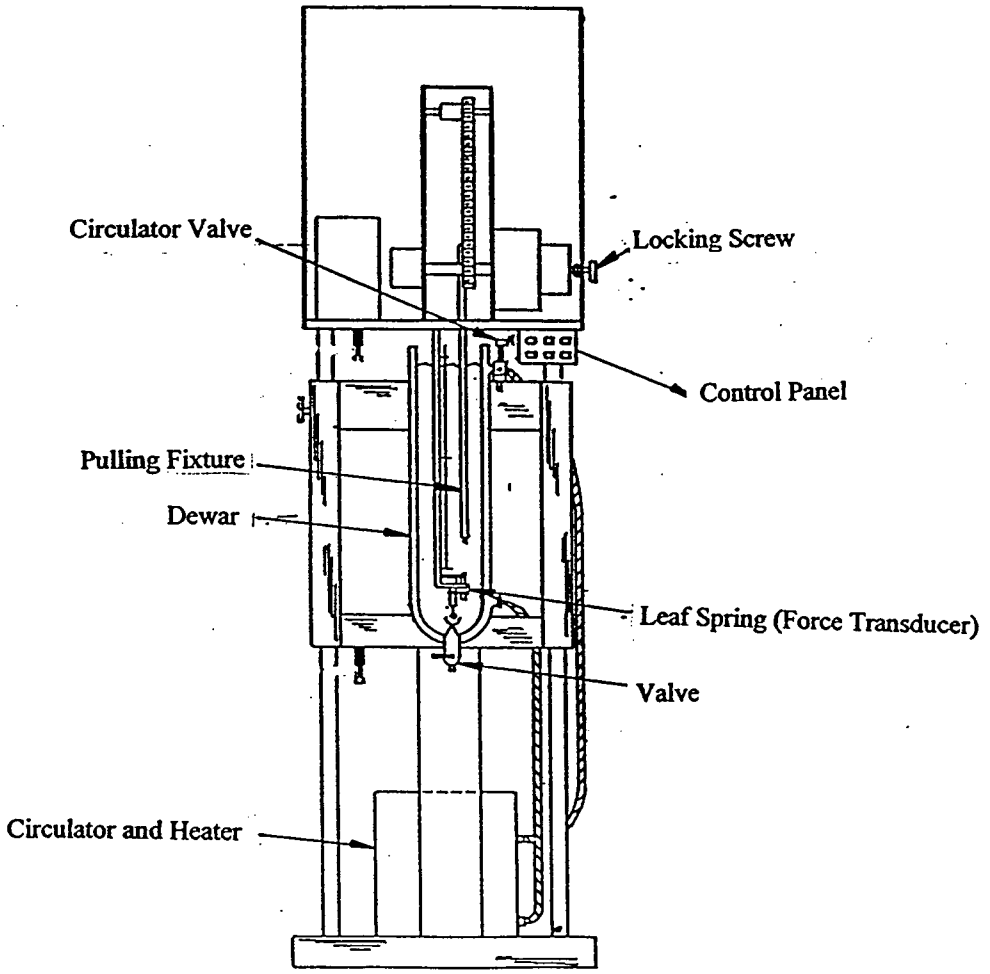

Figure 3.7 A schematic diagram of Rheometric RER-9000 Extensional Rheometer.

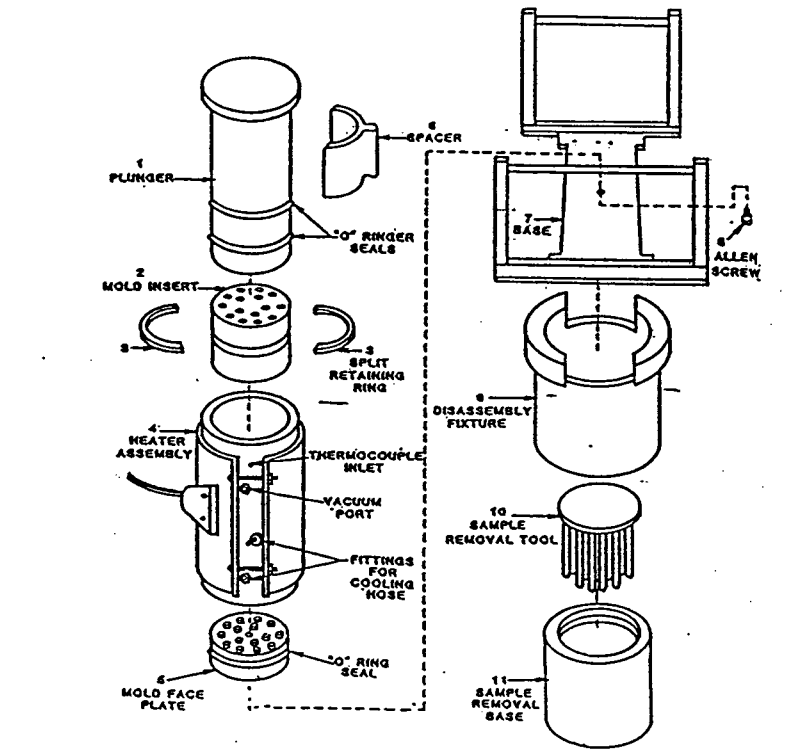

(a)

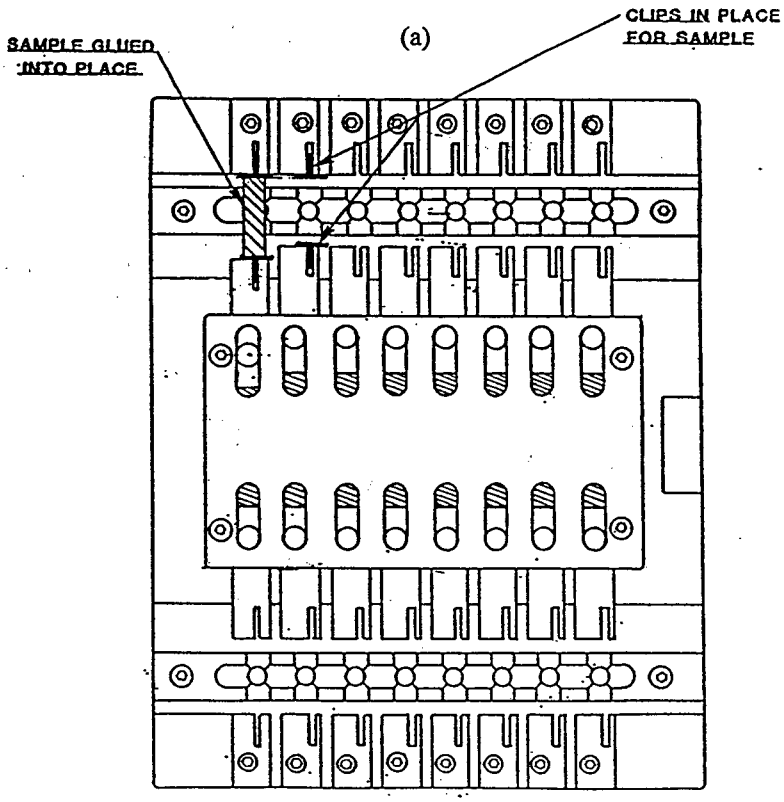

(b)

Figure 3.8 (a) Molding and (b) gluing accessories for Rheometric RER-9000 Extensional Rheometer.

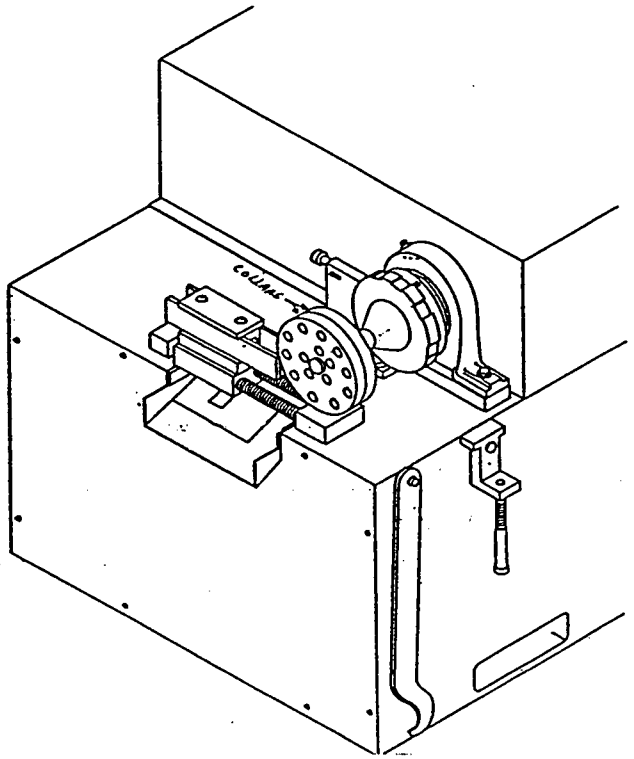

Figure 3.9 A Schematic diagram of the sample cutter supplied with RER-9000 Extensional Rheometer.

3.2.5 Blow Molding Machine

To determine the sagging and swell characteristics of the blow molding resins under actual run conditions, an Impco B-13 Blow Molder unit was used. The unit is manufactured by Ingersoll-Rand Plastics Machinery Ltd. and is equipped with an Edwards Zone-A-Matic Model CC-5 mold chiller unit. Parison programming is done through a Model A081-822 programmer supplied by Moog Incorporated. Figure 3.10 shows a schematic picture of the blow molder.

The pillow mold shown in Figure 3.11 was used with the blow molder unit. The mold facilitated the measurements of sagging and swell characteristics by providing a number of pillows, molded from different parts of the parison. This was made possible

by the multiple pinch-off points that were evenly spaced along the vertical direction of the mold. The width and weight of each pillow corresponding to the different parts of the parison could be measured to determine how wall thickness and product weight vary in the vertical direction.

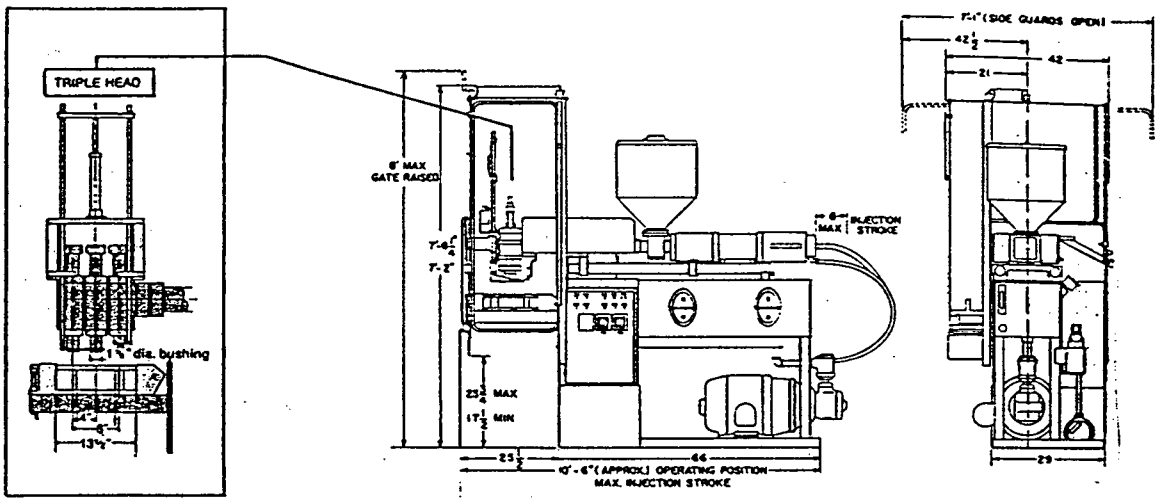

Figure 3.10 A schematic Diagram of IMPCO B-13 Blow Molder

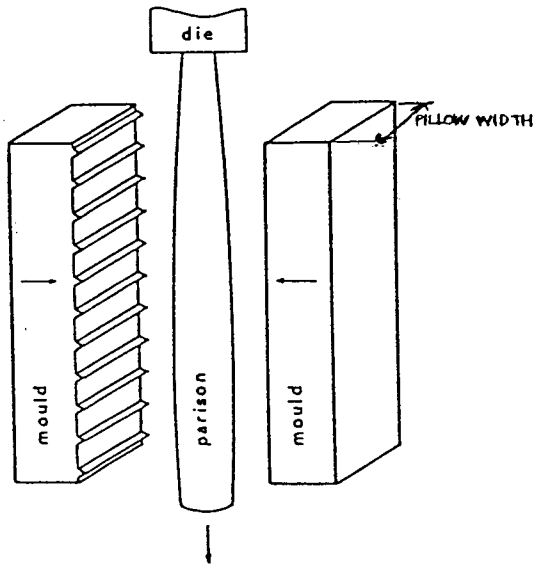

Figure 3.11 A schematic diagram of the pillow mold used in the blow molding Experiment

3.3 EXPERIMENTAL SAMPLES

Twenty four commercial HDPE blow molding resins were provided by NOVA Chemicals Ltd. to be studied in this work. The molecular characteristics of these resins are summarized in Table 3.1. The technologies used to produce the resins include gas phase, solution, and slurry technology. Due to confidentiality, it is not possible to mention the actual name of the technology used to produce the resins.

Table 3.1 A summary of the molecular characteristics of the HDPE resins that were studied in this work.

Resin	Technology	M_n	M_w	M_z	PI	Density (g/cm^3)
A	*a*	9030	152000	835400	16.83	0.9570
B	*a*	9020	157100	971500	17.42	0.9567
C	*a*	9330	133400	848400	14.3	0.9579
D	*a*	9340	153600	933500	16.44	0.9587
E	*a*	9820	131400	776600	13.38	0.9627
F	*a*	10700	143500	705000	13.41	0.9609
G	*a*	9960	147300	772000	14.79	0.9596
H	*a*	12700	104800	408900	8.25	0.9586
I	*b*	17300	104100	434600	6.02	0.9575
J	*c*	10800	108900	590600	10.1	0.9551
K	*d*	15700	137300	693200	8.75	0.9550
L	*d*	15300	133400	761200	8.72	0.9611
M	*e*	11700	130800	650900	11.18	0.9581
N	*e*	13100	174900	852200	13.35	0.9603
O	*f*	12500	101200	397000	8.1	0.9597
P	*f*	11500	116000	570800	10.09	0.9542
Q	*a*	10600	108000	503300	10.2	0.9548
R	*b*	10300	133700	676200	12.98	0.9549
S	*c*	13200	113000	640300	8.6	0.9548
T	*a*	27800	132300	462700	4.76	0.9393
U	*a*	9310	153500	776600	16.49	0.9617
V	*a*	27000	129000	377000	4.8	0.9465
W	*a*	44000	148000	423000	3.4	0.9560
X	*a*	25100	138400	535300	5.51	0.9544

The density of each resin was determined using the densimeter as described in a previous section of this chapter, and molecular weight distributions were obtained by performing GPC analysis with a polyethylene standard. Figure 3.12 shows a plot of the differential molecular weight distributions for some of the resins.

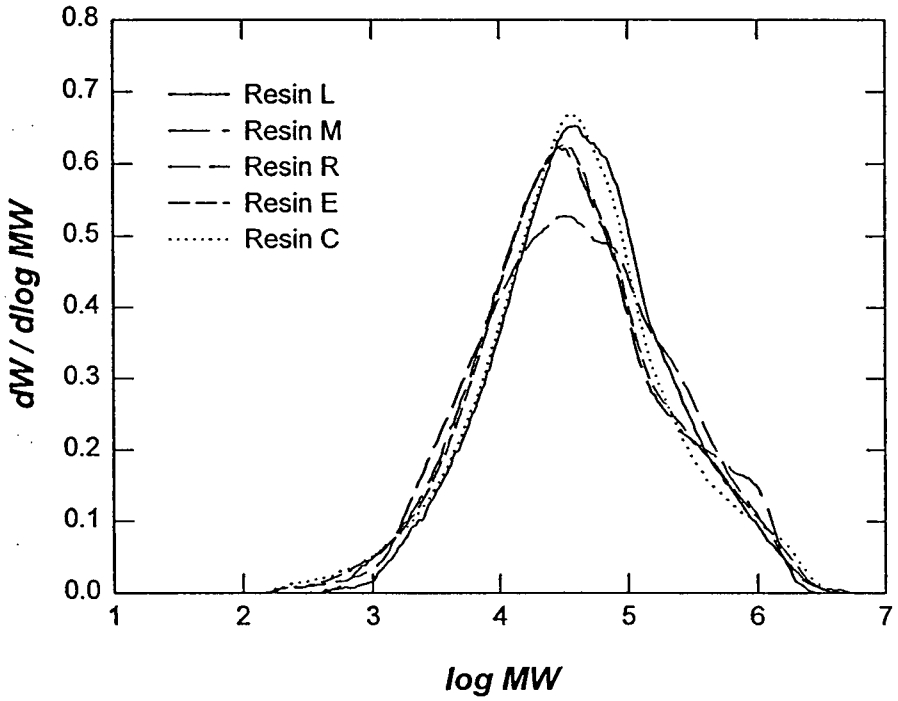

Figure 3.12 Differential molecular weight distributions for some of the resins studied in this work.

3.4 EXPERIMENTAL PROCEDURES

3.4.1 Shear Properties

The shear properties of the HDPE resins were determined using the capillary rheometry at three temperatures, namely 180°C, 200°C, and 220°C. These temperatures were chosen to closely match the processing temperature in blow molding processes,

which is around 190°C. The three temperatures facilitated the calculation of the activation energy for each resin following the time temperature superposition principle.

Each experimental run began with the loading of resin in pellet form into the heated barrel. After the barrel was filled, the piston was put in place and a pre-heat time of 360 seconds was allowed. Following the pre-heat period, the piston was allowed to travel down the barrel at a preset speed corresponding to a desired shear rate. The speed was maintained until a certain preset distance was reached, at which time the steady state force was measured and recorded through the data acquisition board. The piston was then allowed to travel at the next desired speed until the next preset distance was reached before the speed was changed again. Up to nine speeds or shear rates were allowed for each run involving a one-time sample loading. The speeds and distances were preset through the computer using the software provided with the capillary. The software also allows the interpolation of up to three shear stress and viscosity values by fitting the experimental data with the appropriate equation, such as a power law model.

After each run, the barrel, the piston and the die were cleaned thoroughly with a cloth. In addition, to avoid contamination, flushing was done prior to runs involving a different resin.

A die of $L/D = 20$ and $D = 0.7542$ mm was used throughout this work. No Bagley or Rabinowitch correction was applied to any of the data obtained for all the resins. This was decided to economize time and material and, since, the data are used for comparison purposes involving the same type of polymers, the effect of these corrections would then be non-significant. Hence, these experiments would yield the apparent, instead of the

true values of wall shear rate and viscosity.

3.4.2 Extrudate Swell Measurements

Extrudate swell was determined as a function of shear rate and temperature by manually collecting extrudates at the exit of the die during the capillary experiments. A number of extrudates were collected corresponding to each piston speed (shear rate) and their diameters were then measured in diameter using a digital caliper to determine the average swell corresponding to the shear rate and the temperature of the capillary run. Absolute care was taken during the collection of the extrudates to ensure that they were not pinched in anyway. For the same reason, measurements using the caliper were done after the extrudates had cooled off to room temperature to ensure solidity.

The extrudate swell was calculated as:

$$Die\ Swell = \frac{D}{D_o} - 1 \tag{3.17}$$

where D is the diameter of the extrudate and D_o is the diameter of the capillary die.

To ensure consistency and to minimize the error in diameter measurements due to sagging, the extrudates were cut at approximately the same distance from the die exit each time. The lengths of the extrudates were also kept to be approximately the same during each cut.

At high shear rates, melt fracture (surface distortion of extrudates) may be observed for some resins due to flow instability. In such cases, it was not possible to measure the extrudate diameter. Hence, extrudate swell data for such resins were limited to the lower

shear rate regimes. Also, since diameter measurements were done when the extrudates were at room temperature, the extrudate swell data do not represent the actual swell properties of the resins as far as the absolute magnitude is concerned. In spite of this, these data were still useful for comparison purposes between the different resins. The procedure was adopted due to its simplicity. For a more accurate determination of extrudate swell properties, much more elaborate procedure and equipment are required [Dealy (1985)].

3.4.3 Melt Index, Stress Exponent and Melt Flow Ratio Determinations

Melt Index, stress exponent and melt flow ratio are empirically defined parameters that are used mostly by industry for quality control purposes. In this work, these parameters were determined using the extrusion plastometer described in the previous section of the chapter. The difference in the procedure involved the size of the load used, depending on how these parameters are defined.

The procedure began with the loading of approximately 5 grams of resin in pellet form into the heated barrel with the die in place. The temperature was set to 190°C in accordance with ASTM procedure D1238-95. After the barrel was filled, the piston was put in place and the timer was switched on. A pre-heat time of 360 seconds was allowed before the dead weight load was placed on top of the piston (a lighter weight may be placed on the piston during the pre-heat period to improve the packing of the resin in the barrel). The polymer melt would then start to flow out of the die. After a reasonable length of extrudate was observed, a cut was made on the extrudate immediately at the exit of the die and the timer was reset to zero at the same time. When a reasonable amount of

the polymer has been forced out of the barrel, another cut was made on the extrudate and the timer was stopped. From the weight of the extrudate and the time it took to flow out of the barrel, various parameters can be calculated. To ensure that the extrusion plastometer was working properly, a test run was done with a standard resin and the results checked before the actual set of experimental runs were performed.

I_2, I_6 and I_{21} are defined as the weights of the polymer that flows out of the barrel in 10 minutes when dead weights of 2.16, 6.48, and 21.6 kg are used, respectively. The melt index takes the value of I_2 in the unit of grams/10 minutes. The stress exponent is calculated as:

$$S.Ex. = \frac{\log\left(\frac{I_6}{I_2}\right)}{\log\left(\frac{6.48}{2.16}\right)} \tag{3.18}$$

and the Melt Flow Ratio (MFR) is calculated as:

$$MFR = \frac{I_{21}}{I_2} \tag{3.19}$$

3.4.4 Melt Strength Measurements

In this work, melt strength is defined as the maximum weight of itself that a polymer melt is able to support without breaking for 3 minutes at 190°C and a preset load. All measurements were done using the extrusion plastometer described in section 3.2.2.

The procedure for melt strength measurements was similar to that described in section 3.4.3. Approximately 5 grams of resin was pre-heated in the barrel at 190°C for

360 seconds before a dead weight of 18.3 kg was placed on top of the piston. After the piston had traveled a certain distance, a cut was made immediately at the exit of the die. The piston was allowed to travel further down the barrel until it stopped, at which time the timer was immediately reset. Careful observation was then made on the extrudate at the exit of the die, which was allowed to hang under its own weight until it broke. As soon as the extrudate broke, the timer was stopped and the time recorded. The weight of the extrudate was then determined and the equipment cleaned.

The procedure was repeated four times, each time differing in the distance that the piston was allowed to travel before the first cut was made on the extrudate. This allowed a set of four different measurements of time and the corresponding weight of extrudate to be obtained. Plotting the log of time versus the log of extrudate weight yielded a straight line, and interpolating the extrudate weight at 3 minutes enabled the melt strength of the polymer to be determined. A typical plot is shown in Figure 3.13.

To ensure that the plastometer was working properly, a melt index measurement was performed on a standard resin prior to the running of the actual set of experiments.

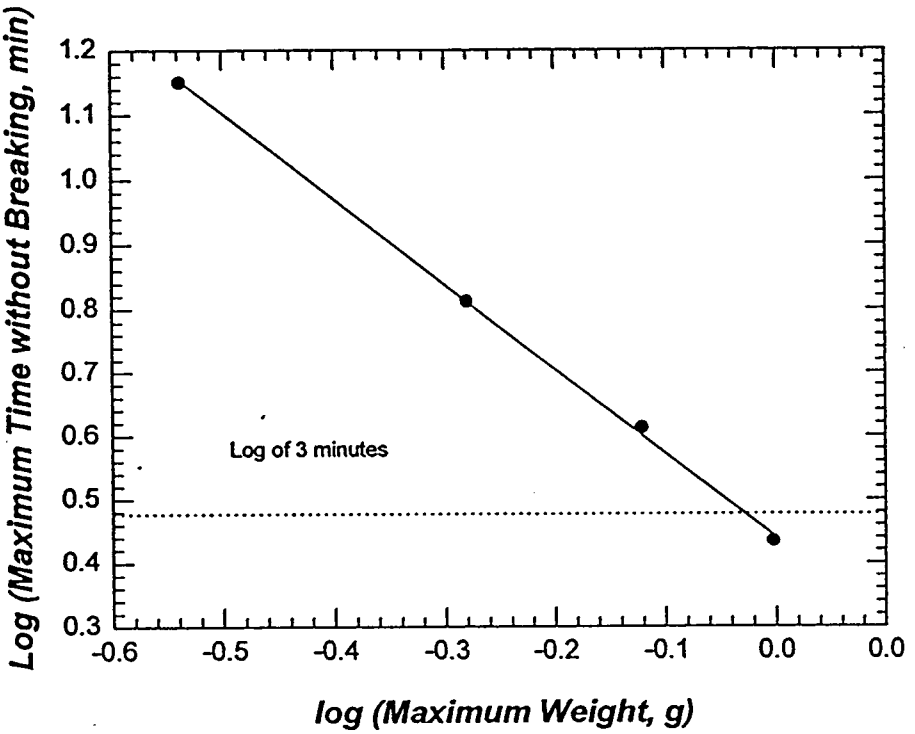

Figure 3.13 Melt strength measurement using the dead weight method. The value of melt strength is interpolated from the graph at time equal to 3 minutes.

3.4.5 Extensional Rheology

In this work, constant stress (creep), instead of constant rate experiments, were performed to determine the extensional properties of the resins, since such experiments are more applicable to the process of blow molding. As mentioned earlier, during parison formation, the polymer melt is hung from the die exit for a finite period of time before it is molded. During this period, the polymer melt is subjected to a constant downward force due to gravity, and this deformation is more appropriately described as a constant stress rather than a constant rate extensional deformation. The temperature at which the extensional properties were determined was set at 150°C and the stresses used were 7 kPa, 5 kPa, and 3 kPa. The boiling point of the oil in the dewar provided the limit as far as temperature is concerned.

Approximately 16 grams of resin were required to mold 15 rod shaped samples for the extensional rheometer. The mold assembly was first heated to 172°C before the resin was introduced. After the resin was put in the mold, a preheat period of 10 minutes was allowed with the spacer still placed in the assembly. The vacuum was then immediately switched on. After a period of 10 minutes had elapsed, the spacer was removed and the resin was heated for an additional 10 minutes. The whole assembly was then pressed in a Carver press at a load of approximately 7000 kg and let stand under pressure for 10 minutes. The pressure decreased as the polymer in the mold relaxed. After 10 minutes, the load was brought up again to 7000 kg and the polymer melt was allowed to relax for another period of 10 minutes. A final adjustment of the load to 7000 kg was then made before it was suddenly removed. Following this, an annealing period of 1.5 hours was allowed with the assembly still heated at 172°C to free the polymer in the mold from any built-in stresses. After 1.5 hours, the heater was switched off. When the whole assembly had cooled off, the sample was removed from the mold, not forgetting to switch off the vacuum beforehand. Figure 3.14 shows a diagram of the sample before and after cutting. Sample preparation is critical in this procedure since it is important to ensure that the samples contain no air voids.

To both ends of each cut sample, etching was then done with a previously stirred mixture of 2 grams $K_2Cr_2O_7$ in 100 grams of 98% H_2SO_4. A period of approximately 40 minutes was allowed for the mixture to work on each end of the sample before it was washed off the sample using distilled water. After the samples were etched, drying was done by placing the samples in the oven at 100°C for approximately 15 minutes. After the samples were completely dried, they were glued to the pulling clips using 5-minute

epoxy in the gluing fixture. The gluing assembly was then allowed to stand for a day before the samples were removed from the fixture.

After the samples were glued to the pulling clips, estimates of sample volumes at 150°C were determined. This was done by measuring the volume of each sample at room temperature and using the linear coefficient of expansivity to correct for the change in temperature. The volume at 150°C was needed to determine the cross-sectional area of the sample at each time so that the pulling force can be changed accordingly to maintain constant stress. Obviously, this is permissible assuming incompressibility and a uniform pull of the sample.

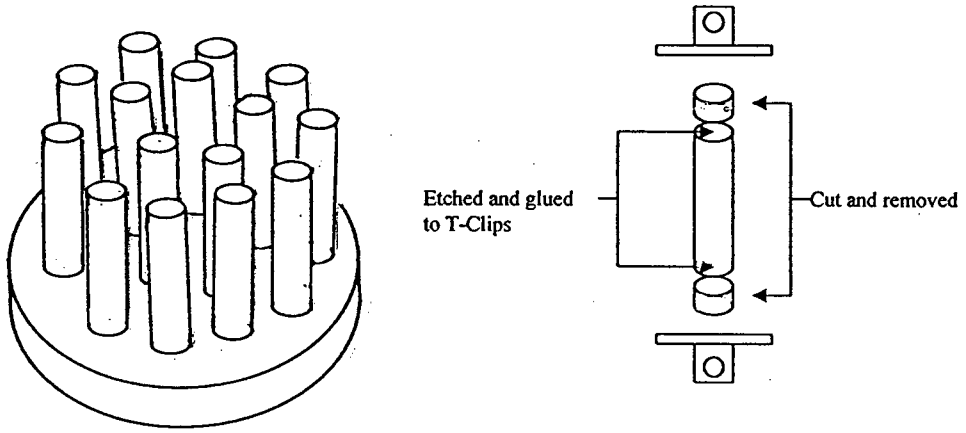

Figure 3.14 A schematic diagram of extensional sample before and after cutting.

The extensional rheometer was calibrated for length and force according to the equipment manual before each run was conducted. After the calibration and when the temperature of the oil in the dewar had reached 150°C, the sample was quickly mounted

into the pulling fixture by first adjusting the fixture to the approximate length of the sample. The high temperature in the dewar would cause the sample to expand and hence, create a compression force on the pulling fixture. To mitigate this force, the fixture was moved upward until the indicated force was close to zero. As soon as this was achieved, a timer was switched on and a pre-heat time of 3 minutes was allowed. After the pre-heat period was over, the pull was started. Data on sample length, stress, and strain as functions of time were then obtained as soon as the sample had been pulled to a maximum preset length, or a time of 300 seconds had elapsed, whichever occurred first. To ensure reproducibility, a number of runs were performed for the same sample at the same experimental conditions. A representative set of data for the particular run, possibly one from the most uniform pull, was then chosen for analysis.

3.4.6 Pillow Mold Experiments

The sagging and swell characteristics of resins E, F, and G were determined using the IMPCO B-13 Blow Molder as described in the previous section. The temperatures of the rear and front barrel of the extruder were set to 188°C and 199°C, respectively. The melt temperature was determined to be approximately 215°C and the die head was kept at 205°C. The timer was set to 12 seconds and 4 seconds for air blowing and exhausting, respectively. The screw speed of the extruder was kept constant at 125 RPM.

The wall thickness (position of the mandrel) was set arbitrarily and kept constant for all runs. The amount of resin that was extruded for each blowing cycle was also kept the same for each run by setting the shot size constant. The shot size determined how far the ram was set back during the accumulation of polymer melt before extrusion. Since the

die gap was kept constant, the ram rate determined the shear rate experienced by the polymer melt. The ram rate was determined by the shot size and the parison drop time (i.e. the time required to form the parison, or the time needed to extrude all the resin in the accumulator). Parison drop times of 1, 3 and 5 seconds were used in this work.

Prior to each run, flushing was done and the unit was tested with a standard resin.

4 RESULTS AND DISCUSSION

4.1 INTRODUCTION

This chapter is divided into four main parts. In the first part, rheological results are presented. The second part of the chapter then focuses on the effects of molecular parameters on the processability of HDPE resins. In the third section, the rheological and processing implications of melt index, stress exponent and melt flow ratio are discussed. Finally, a section is devoted to the qualitative analysis of the implications of rheology on processability.

Before proceeding to the presentation and discussion of experimental results, a brief comment has to be made with regard to the variety of samples chosen for this work. The main objective of this work was to study the effect of molecular structure on the rheology and processability of HDPE blow molding resins using resins having a broad range of molecular parameters, in terms of M_w and the molecular weight distribution. A number of studies had been done previously, some of which were partially successful in relating rheology or processability to molecular parameters. However, these studies have been performed only on resins with narrow ranges of molecular parameters. To our knowledge, no study that relates the rheological and processing behavior of resins to the broad range of molecular parameters has been reported previously.

Due to the limitations in catalyst technology and process parameters, however, it is not possible to produce resins with broad ranges of molecular parameters using only one type of technology. For example, there is no single catalyst that is capable of polymerizing a resin having a wide range of M_w and polydispersity values. For example,

solution polymerization technology produces resins with low to medium M_w. With a slurry type of polymerization technology, on the other hand, it is possible to produce resins with somewhat higher M_w and with a polydispersity range between six and ten. The gas phase catalyst technology is capable of producing resins with high M_w and polydispersity values less than five, or more than fourteen, depending on the catalyst used [Goyal (1998)]. Due to this difficulty, it was, therefore, necessary to use commercial resins produced from a number of different technologies in this study. Since commercial resins from different technologies are used, it will then be difficult to systematically determine the effect of individual parameters on resin flow properties or processability, or to perform factorial design experiments. Often, there are more than two parameters that are different for a given set of resins. Therefore, in this work, multiple regression analysis was used to study the influence of molecular parameters on the rheological and processing behaviors of the resins, wherever possible. Otherwise, qualitative analyses were conducted to investigate the influence of these variables. However, it should be noted that the objective of performing multiple regression analysis was to obtain general trends on various rheological and processing properties of the resins, with the molecular parameters being the independent variables. The analysis was not intended to produce predictive mathematical models. Hence, in the regression analysis, the dependencies of various rheological and processing parameters on molecular structure was kept as simple as possible. Also, in some cases, outliers in the data set were not included in the analysis.

4.2 RHEOLOGY

4.2.1 Shear Properties

The shear properties of the resins were determined using a capillary rheometer at 180°C, 200°C, and 220°C. The range of shear rate used was from approximately 5 s^{-1} to 900 s^{-1}. Duplicate runs on some resins indicate excellent reproducibility of results. For example, variations in the viscosity data were found to be much less than 5%. Figure 4.1 shows the apparent shear viscosity plot for one of the resins.

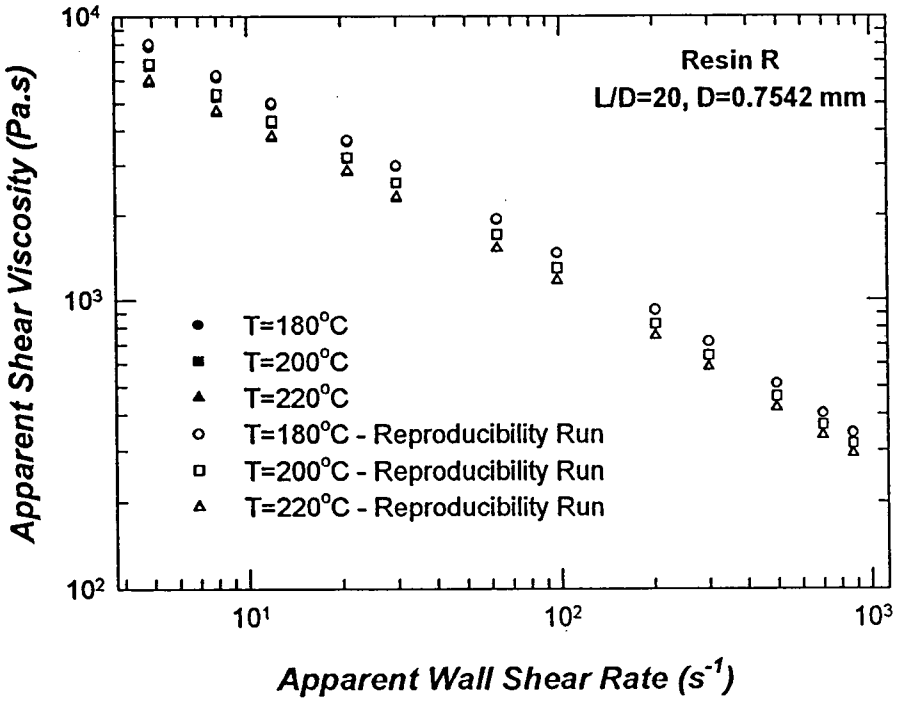

Figure 4.1 Reproducibility of apparent flow curves for resin R, determined at 180°C, 200°C, and 220°C. Data variation at each shear rate is estimated to be less than 5%.

To determine the effect of molecular weight on shear viscosity, the resins were grouped according to their polydispersities. Viscosity plots such as those shown in Figure 4.2 were then analyzed. Previous studies have shown that increasing M_w while keeping the polydispersity constant increases the zero shear rate viscosity, or the viscosity at lower shear rates. However, this is not very apparent in the data obtained using the capillary rheometer. One reason is that the shear rate range does not cover sufficiently low values. To see this effect, experiments may have to be carried out using other equipment such as parallel plate rheometer, which is capable of generating very low deformation rates. Another possible reason is the one mentioned previously. Variations in other molecular parameters, such as M_z, may be affecting the viscosity profiles in different way. Moreover, the number of resins in each polydispersity group is too small for a definite conclusion to be drawn.

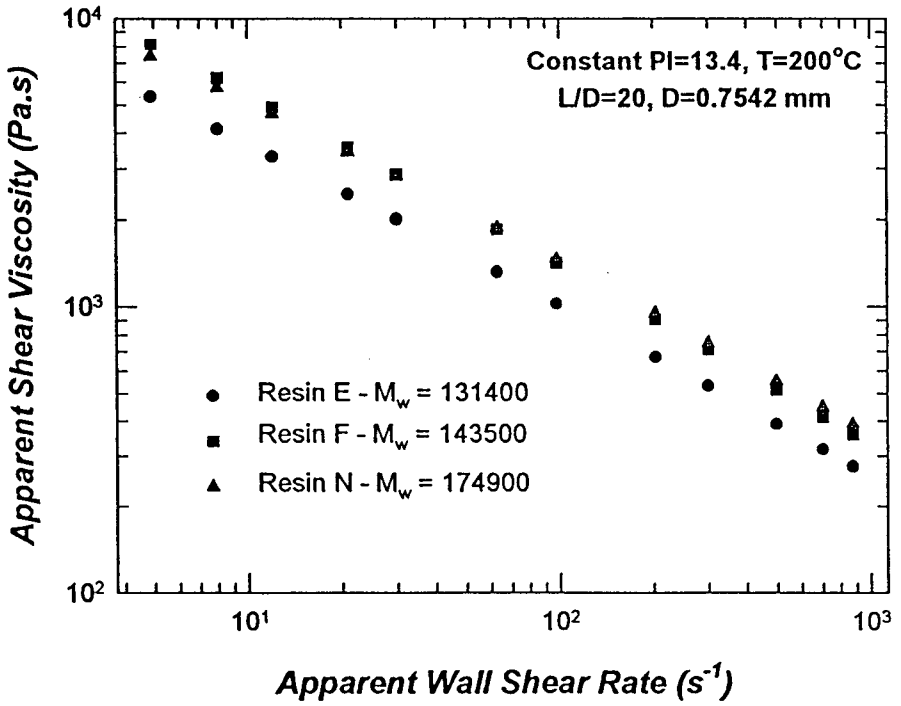

Figure 4.2 Apparent flow curves for resins with similar polydispersities determined at 200°C.

Plotting the shear viscosity data for resins with similar molecular weight yields results such as those shown in Figure 4.3. Similarly, it is difficult to extract a reasonable trend from this figure. As the polydispersity of a resin is increased, the viscosity curve is expected to be steeper, as has been shown in previous studies. In this work, however, due to the limited number of resins having similar M_w, such a conclusion cannot be drawn as easily.

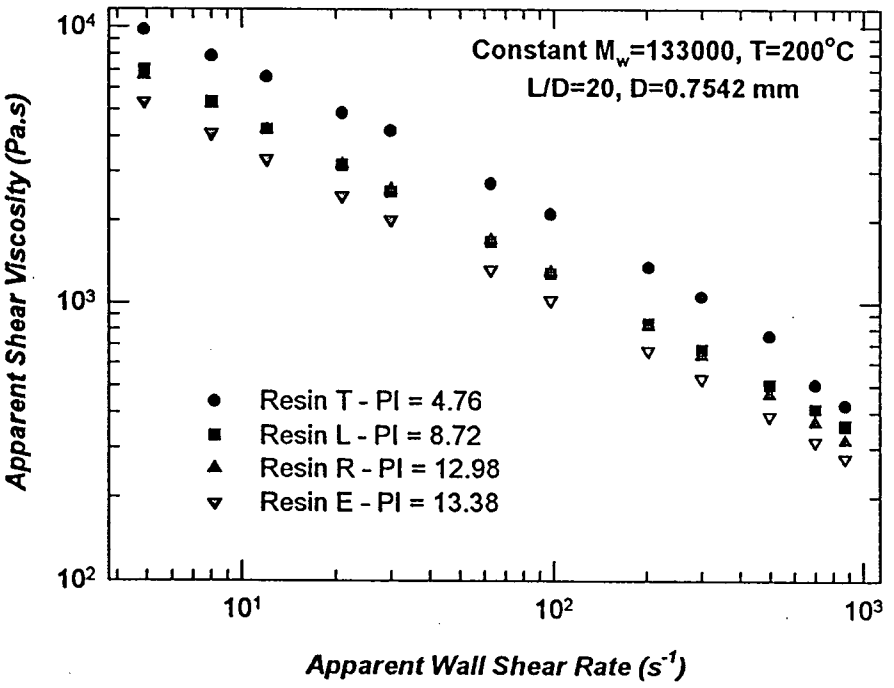

Figure 4.3 Apparent flow curves for resins with similar M_w determined at 200°C.

To overcome the problem of having too few resins in each group having similar polydispersity or M_w, another approach to data analysis was used. Based on the knowledge from previous studies that the viscosity profile is affected mainly by polydispersity and M_w, it was then decided that multivariable regression should be performed on the viscosity data. By performing such analyses, it will then be no longer necessary that the resins be grouped according to polydispersity or M_w. A statistical software, STATGRAPHICS PLUS v2.0, was used in this work for this purpose. In each analysis, the magnitude of the apparent shear viscosity at a particular shear rate was regressed with polydispersity and M_w as the independent variables. The result from each regression was statistically analyzed by the software to ensure that the independent variables were in fact significant, and that the correct form of dependency was used for each independent variable.

A good correlation could not be found between shear viscosity and the two independent variables, polydispersity and M_w. However, when the data analyzed were only those for resins manufactured using the same technology (e.g. technology '*a*' in Table 3.1), clear trends were observed. A plot of the predicted values versus the observed values for one analysis is shown in Figure 4.4. Figure 4.5 shows the predicted and observed viscosity values from the same analysis as a function of polydispersity. The need to include only the resins produced from the same technology in the analysis implies that different technologies produce resins with non-comparable shear viscosity profiles. Hence, if molecular parameters are to be used to predict the relative profile of shear viscosity, it is important to make sure that the resins are produced from the same technology. Surprisingly, this finding has not been reported in any previous studies.

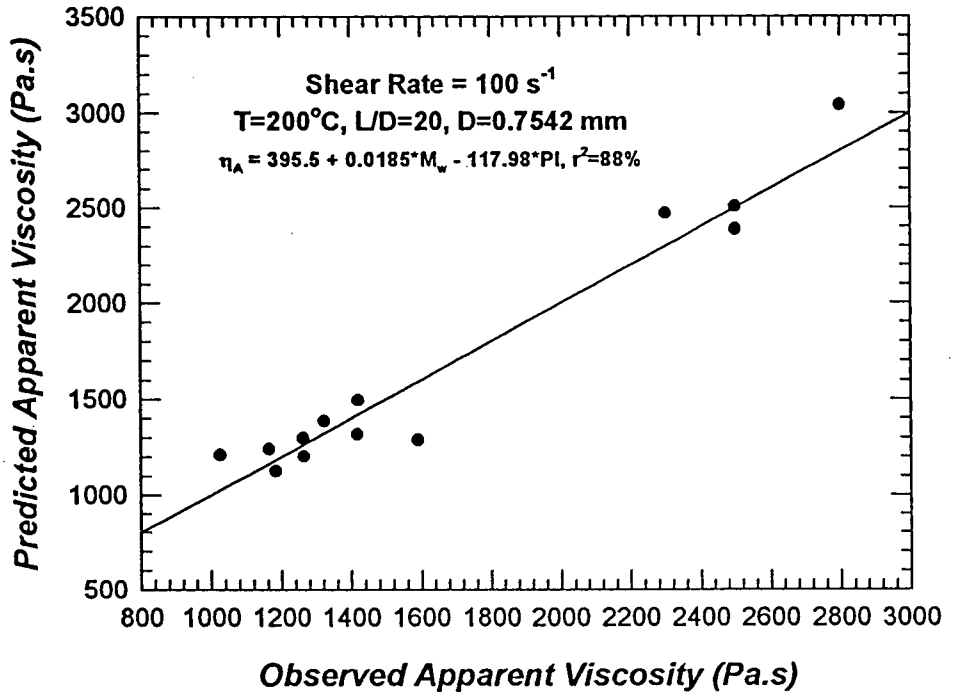

Figure 4.4 Predicted apparent viscosity values at 100 s^{-1} and 200°C as determined using STATGRAPHICSv2.0. Only resins manufactured using technology '*a*' are included in the analysis.

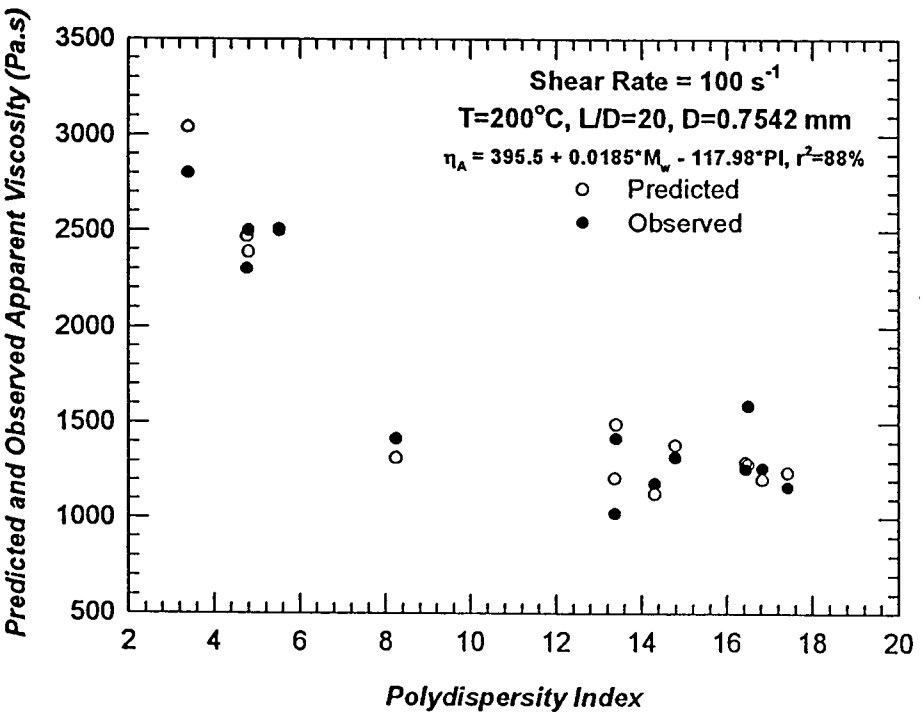

Figure 4.5 Predicted and observed apparent shear viscosity at 100 s^{-1} and 200°C.

For the range of shear rates studied in this work, it was found that increasing M_w at a constant polydispersity tends to increase shear viscosity, while increasing polydispersity at a constant M_w decreases the viscosity. This is the expected trend, considering the molecular properties of a polymer. Increasing M_w implies that, on average, molecules are longer in size. This means that there are more entanglements between molecules, which results in greater resistance to flow, or higher viscosity. As far as the effect of polydispersity is concerned, the trend is consistent with previously published results that polymer melts exhibit steeper viscosity curves with increasing polydispersity (increasing shear thinning behavior) [Dealy and Wissbrun (1995)]. However, at much lower shear rates, viscosity is expected to increase with increasing polydispersity. To see this effect more clearly, Figures 4.6 and 4.7 were prepared using the equations obtained from the regression analysis performed at each shear rate. Arbitrary values of polydispersity and M_w were used to simulate the plots. In Figure 4.6, it can be seen that increasing M_w at a constant polydispersity increases the shear viscosity, and in Figure 4.7, increasing polydispersity at a constant M_w decreases the shear viscosity. The shear thinning effect of polydispersity on the viscosity can also be seen in Figure 4.7.

It is interesting to note that, in Figure 4.7, although the polydispersity index covers a broad range of values, the differences in the shear thinning behavior depicted by the simulated viscosity curves are comparatively less obvious. This is due to the way polydispersity index is defined, which can be misleading. By defining the polydispersity index as the ratio of M_w to M_n, only changes in the molecular weight distribution which involve smaller molecules are reflected in the value of the index. Altering the molecular weight distribution by changing the concentration of larger molecules will not be

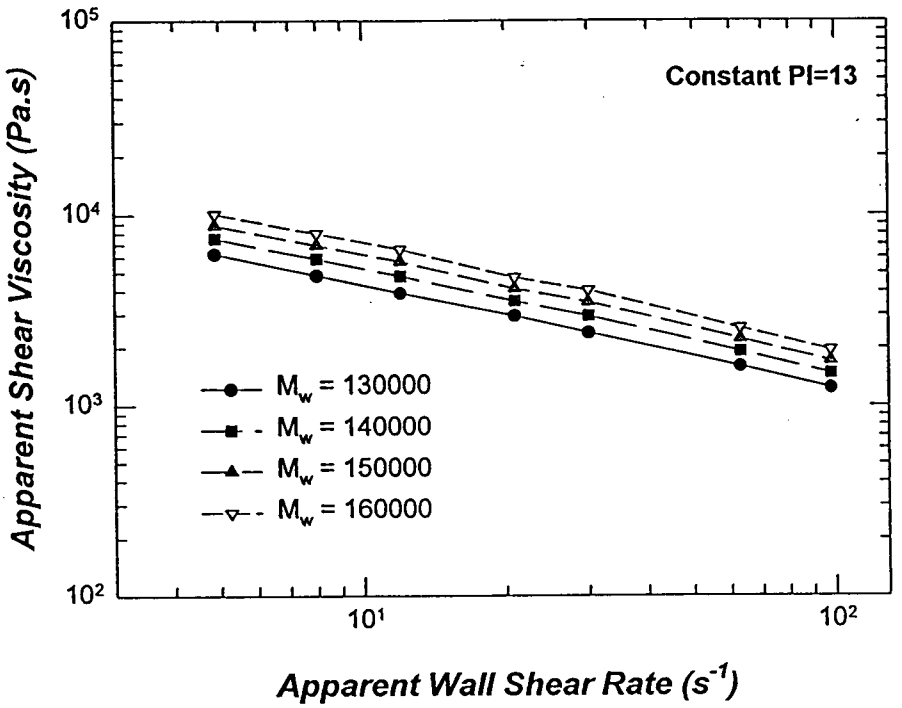

Figure 4.6 Apparent shear viscosity curves simulated at constant *PI* using the regression relationship at each shear rate.

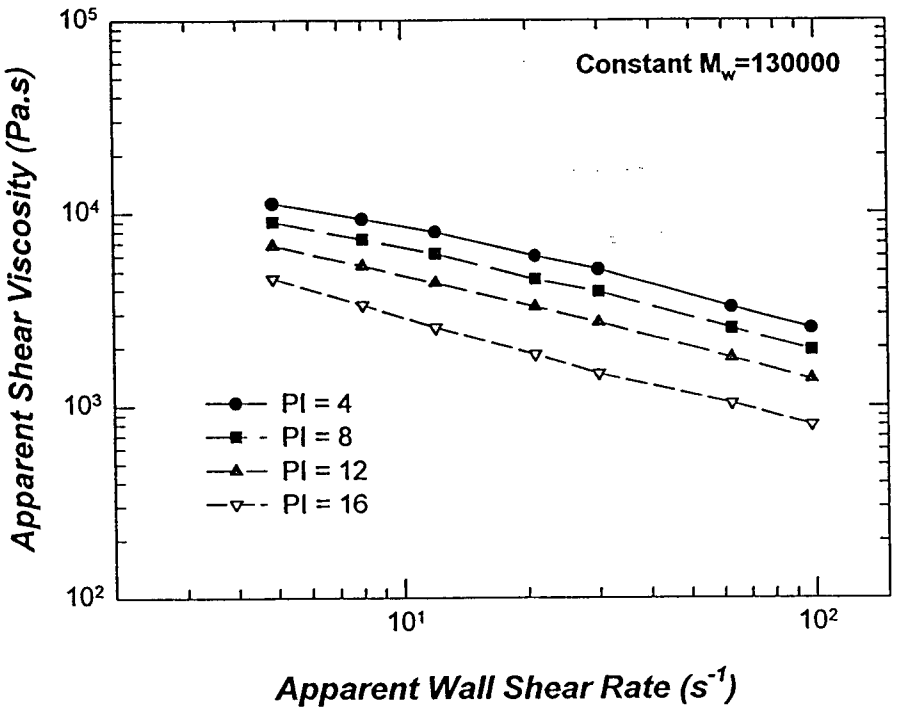

Figure 4.7 Apparent shear viscosity curves simulated at constant M_w using the regression relationship at each shear rate.

reflected in the value of the polydispersity index. Hence, it is often more useful to consider the whole molecular weight distribution curve than to only consider polydispersity index as a measure of the breadth of the molecular weight distribution, especially when the distribution curve is skewed. There may be portions of the distribution which are not reflected by the polydispersity index. These may significantly affect the rheology and processability of a resin.

To further determine the effect of molecular weight distribution (MWD) on the shear properties of the resins, a FORTRAN program that calculates the normalized areas of slices under the differential MWD curves was written. The objective of this approach was to determine the portions of the distribution that affect the shear properties the most. The differential MWD curves obtained from GPC for all resins were first arbitrarily divided into several slices as shown in Figure 4.8. The normalized area corresponding to each slice was then calculated using the 4-panel Adaptive Newton-Cotes numerical integration method (normalization was done by dividing the area of each slice by the total area under the MWD). Splines with fitted ends were used to facilitate this integration (see Appendix A). The critical molecular weight range would then be implied by the slice, which, for all resins, has a normalized area that correlates the best with, in this case, the shear viscosity. All possible combinations of molecular weight ranges (slice areas) were considered for correlation in the program.

Correlating the normalized areas with the shear viscosity of all resins determined at 5 s^{-1} and 200°C indicated that there are two portions of the MWD that are relatively critical in affecting the shear viscosity. Figure 4.9 shows 3-D plots of the correlation

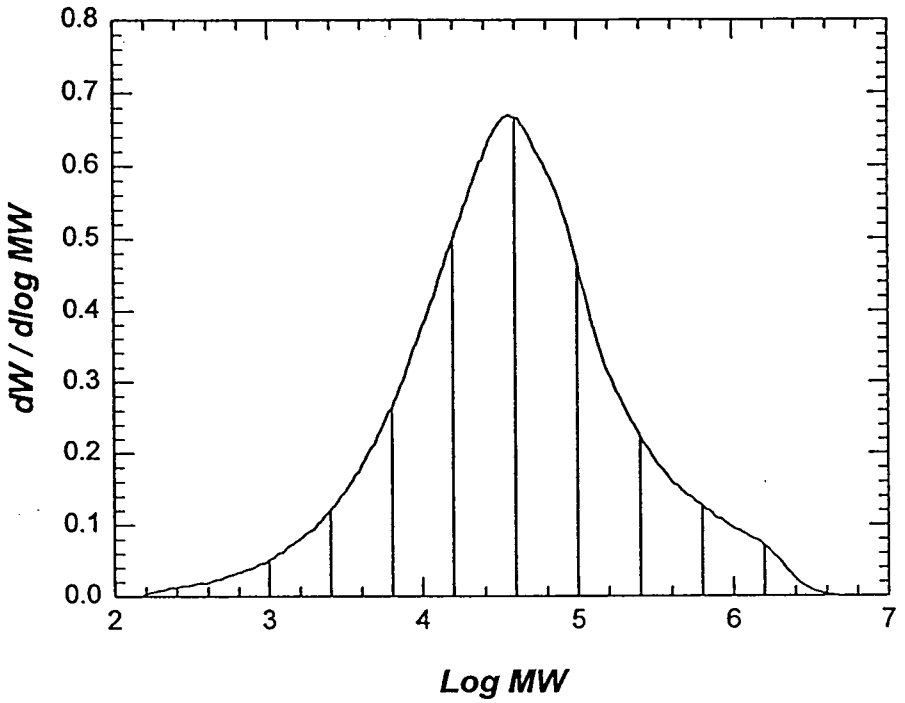

Figure 4.8 Determination of molecular weight ranges that are critically affecting a certain property of a resin. Slices were made arbitrarily.

coefficient, obtained from correlating the shear viscosity to the normalized areas bounded by the two molecular weight limits, as a function of the upper and lower molecular weight limits. It can be seen from Figure 4.9(a) that one critical portion is in the molecular weight range of approximately 9,000 to 22,000. In this range of molecular weight, the correlation was found to be negative, i.e. increasing this portion of the distribution results in a decrease of viscosity. This is the lower molecular weight range that is reflected by M_n. This finding is consistent with the previously described analysis, which shows that lower viscosity is obtained when polydispersity is increased or M_w is decreased. By increasing the portion of the MWD that lies on the left side of the peak, M_n, M_w, and M_z are reduced, while polydispersity is increased (M_n is more significantly decreased than M_w – MWD is broader), and hence, lower viscosity is observed.

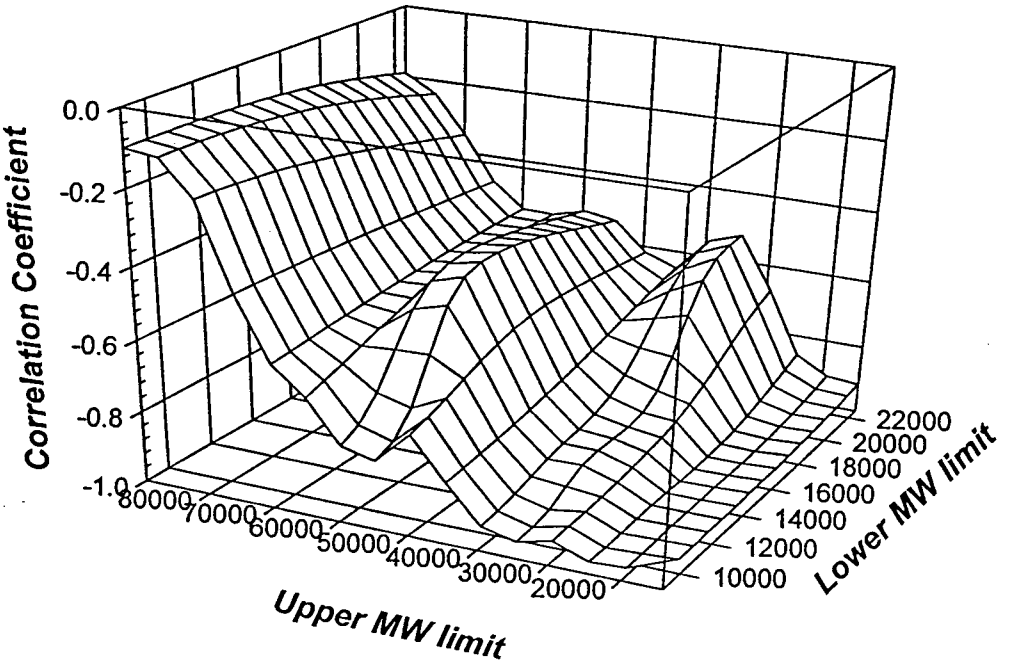

(a)

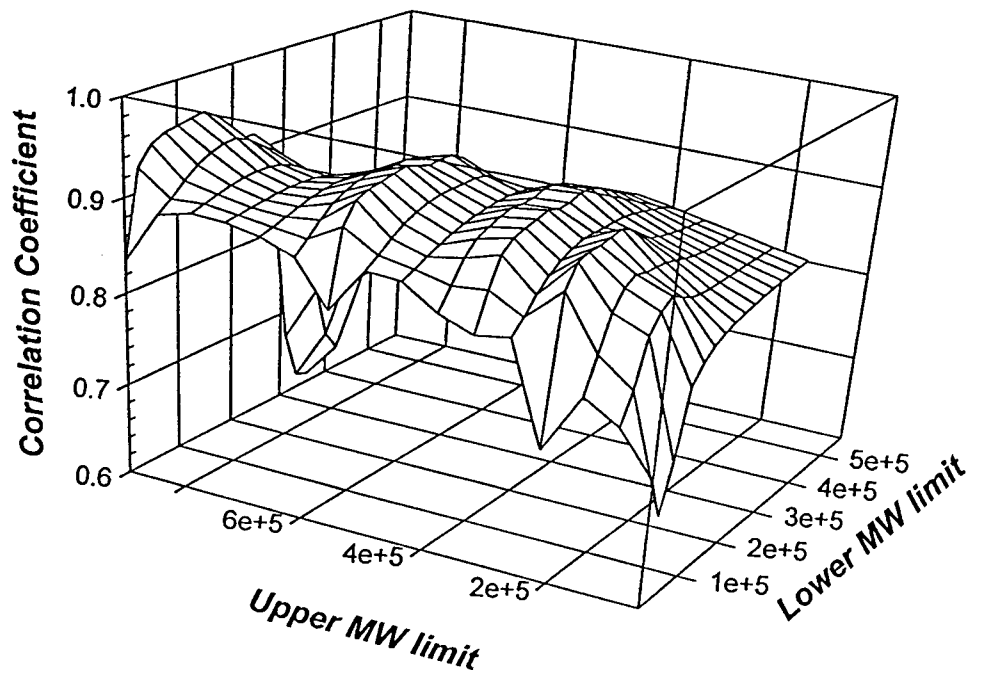

(b)

Figure 4.9 Correlation coefficients relating various molecular weight ranges to shear viscosity at 5 s^{-1} and 200°C (a) negative correlation (b) positive correlation. Correlation coefficient (x,y) = *COV* $(x,y)/\sigma_x.\sigma_y$

From Figure 4.9(b), the other critical molecular weight can be determined to range from approximately 140000 to 900000. In this case, the correlation is positive. This molecular weight range lies on the right of the MWD peak. It implies the concentration of larger molecules and is reflected by M_w and M_z. Increasing this portion of MWD, increases the weight average molecular weight, M_w, and hence, higher viscosity is observed. By doing this, however, the MWD is also broadened and, hence, polydispersity is increased. The previously discussed effect of polydispersity on the shear thinning behavior of the resins is not observed using this analysis. Therefore, it seems that the observed effect of polydispersity on shear thinning is only true if changes in polydispersity are made by changing the concentration of smaller molecules. Broadening the MWD by increasing the concentration of larger molecules does not seem to affect shear sensitivity significantly, although it increases the magnitude of the shear viscosity.

Comparing Figure 4.9(a) to Figure 4.9(b), one can see that the variation in the correlation coefficient is stronger in the case of the lower molecular weight ranges [Figure 4.9(a)]. This implies that shear viscosity is more sensitive to changes in the concentration of smaller molecules.

To determine the effect of temperature on shear viscosity, the activation energy term, E_a, in Equation 1.14 was calculated using the time-temperature superposition principle. Resins with greater values of E_a have flow characteristics which are more sensitive to temperature changes. A FORTRAN program was written to facilitate the shifting of data and is included in Appendix B. Instead of calculating the shift factor by performing a

two way shift on the shear viscosity data, the program considers the shear stress data and performs only a horizontal shift. After the master curve data on shear stress and shifted shear rate is determined, the master shear viscosity curve is calculated. The golden search optimization method was used in the program to determine the shift factor that minimizes residuals involved in each shift. In this analysis, a reference temperature of 180°C was used throughout and the values of E_a were found to range from 20 kJ/mol to 28 kJ/mol which are comparable to other reported literature values for HDPE [Van Krevelen (1990)]. Figure 4.10 shows a master curve for one of the resins and the fit of shift factors to the Arrhenius type of equation.

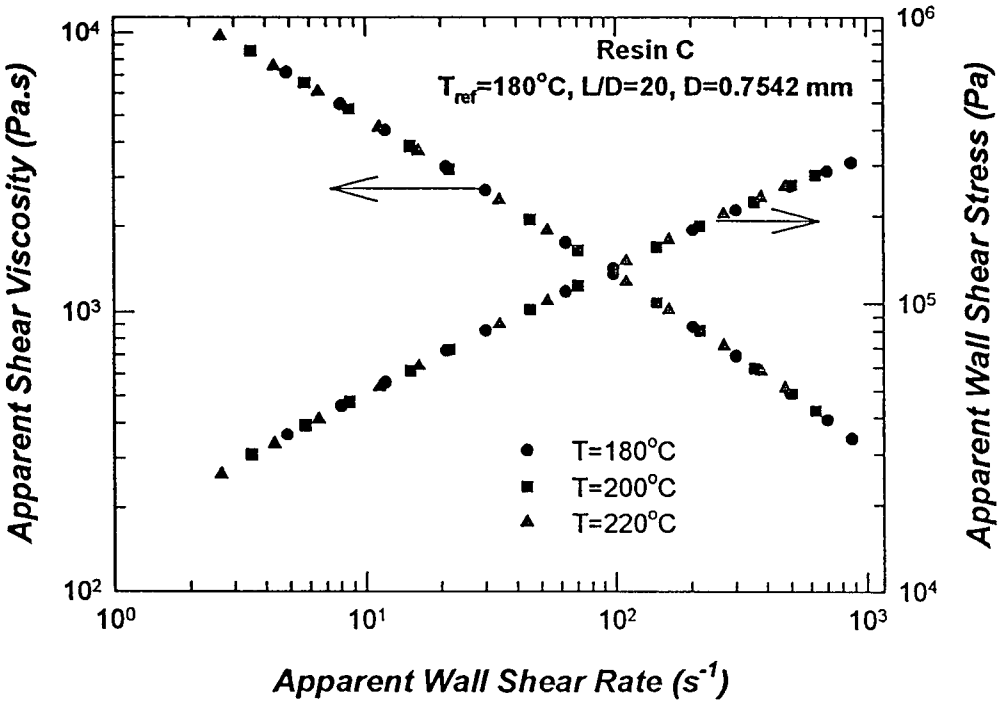

(a)

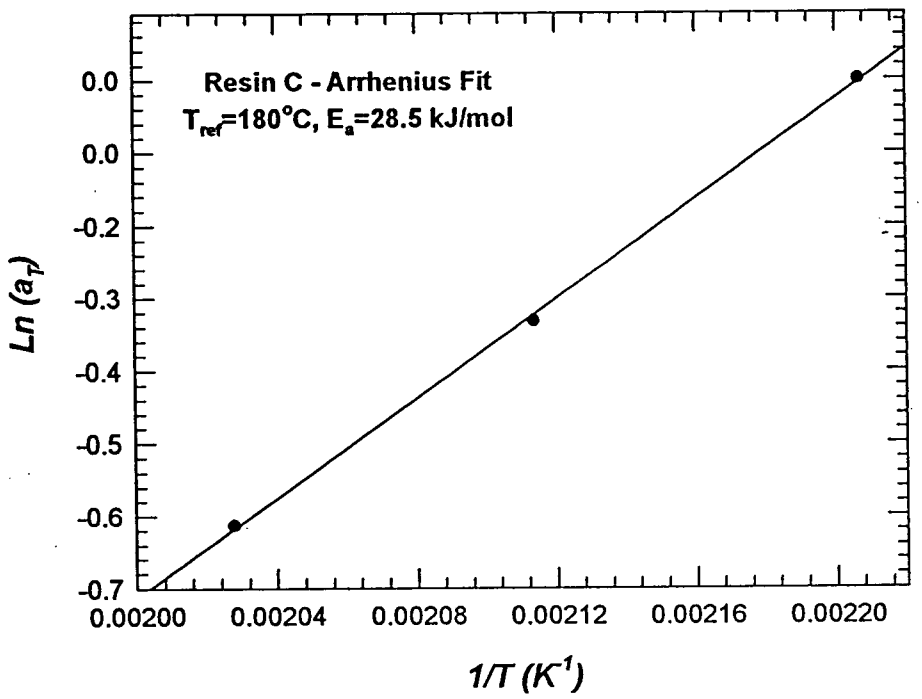

(b)

Figure 4.10 (a) Master curve and (b) Arrhenius fit generated by the FORTRAN program.

To determine the effect of MWD on the flow sensitivity of the resins, multivariable regression was again performed. The activation energy was set as the dependent variable and M_n, M_w, and/or M_z as the independent variables. Using the results for all resins, it was found that no general trend could be extracted. However, if the activation energy data were grouped according to the polydispersity ranges of $PI>10$, $8<PI<10$, and $PI<8$, good correlations were obtained. The need to separate the resins into three groups has also been reported by Kazatchkov *et al.* (1997) in his melt fracture study of LLDPE's. It seems that the resins undergo a change in behavior around the polydispersity bracket of

eight to ten. A change in the general trend in some properties, or a discontinuity in the general trend seems to happen at approximately this range of polydispersity.

For polydispersity greater than ten, it was found that E_a could be related to the molecular parameters with an excellent correlation coefficient. Figure 4.11 shows a plot of the observed and predicted values. In mathematical form, the correlation can be written as

$$E_a = 1.69 + 7.8\text{E}-4 \cdot M_n + 1.02\text{E}-5 \cdot M_z + 1.31\text{E}6 / M_w \qquad (4.1).$$

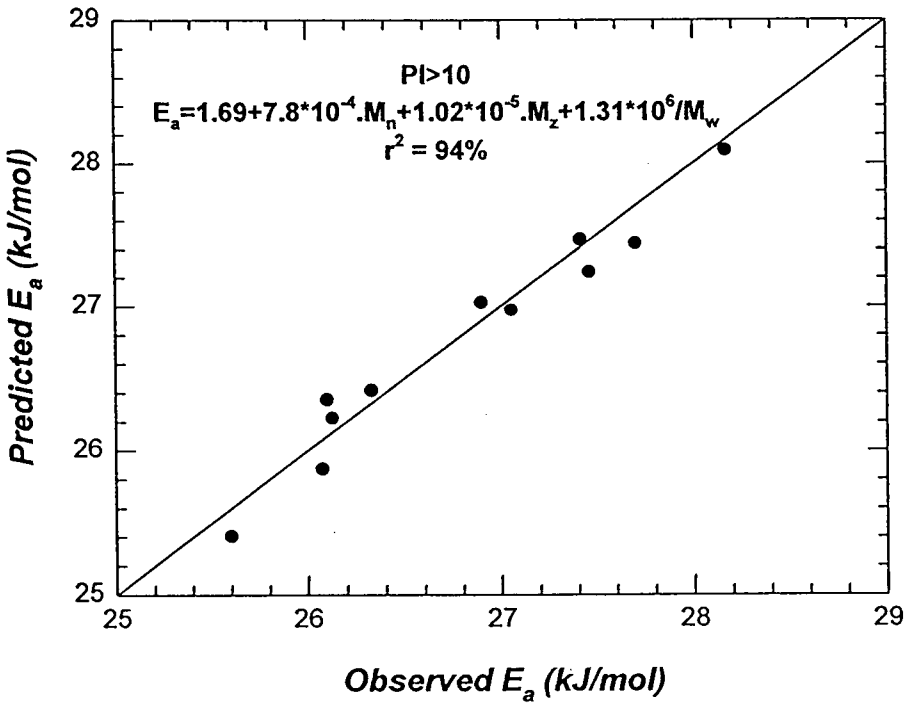

Figure 4.11 Observed and predicted E_a values as obtained from STATGRAPHICS v2.0 (PI>10).

From the equation, it can be deduced that by increasing M_n and M_z, shear properties become more sensitive to temperature change. The opposite can also be deduced when

M_w is increased. The trend, however, will be more useful if it is expressed in terms of polydispersity index, M_w, and M_z, which are more commonly used to describe a molecular weight distribution. The effect of these variables is summarized in Figure 4.12. In Figure 4.12(a), the polydispersity index is fixed arbitrarily at thirteen, while in Figure 4.12(b), 130,000 is arbitrarily used as the value of M_w. One can see that, at constant polydispersity index, increasing M_w affects the magnitude of E_a non-linearly, but in a relatively non-significant manner. The effect of M_z is more significant: increasing M_z increases the magnitude of E_a. This same trend is also observed at constant M_w, as shown in Figure 4.12(b). The effect of polydispersity index is also shown in the figure. One can see that the effect of polydispersity index on E_a is relatively significant, and that increasing the polydispersity index decreases the temperature sensitivity of shear flow. Of course, this is achievable only if changes are made in the concentration of smaller molecules, considering the definition of polydispersity index.

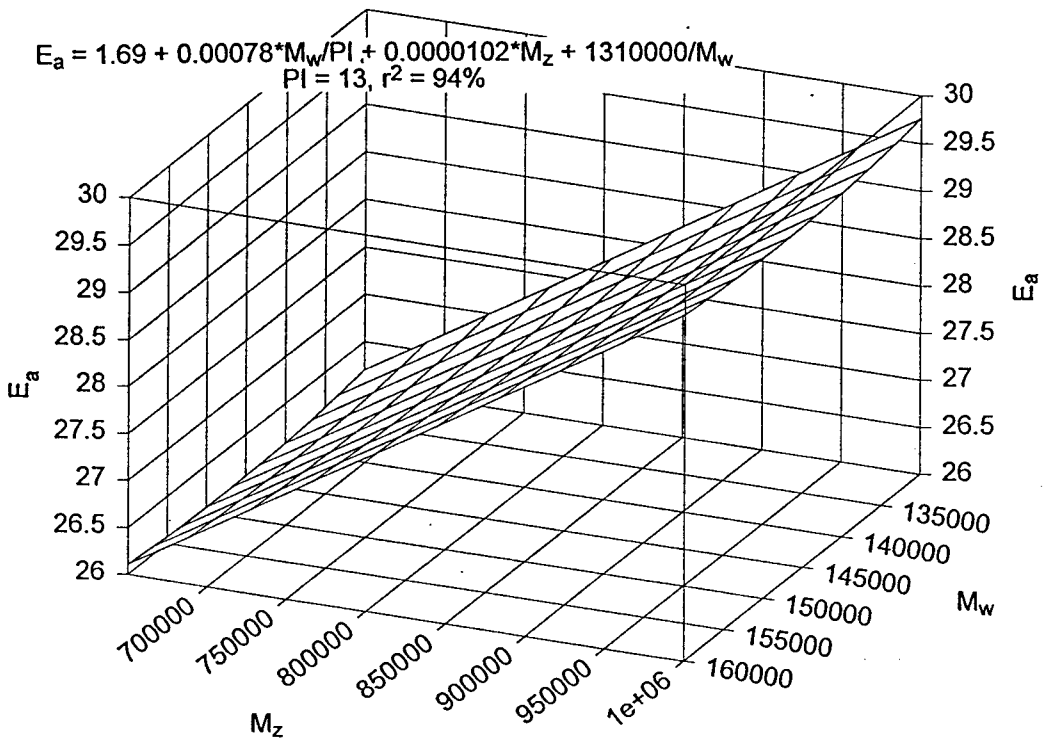

(a)

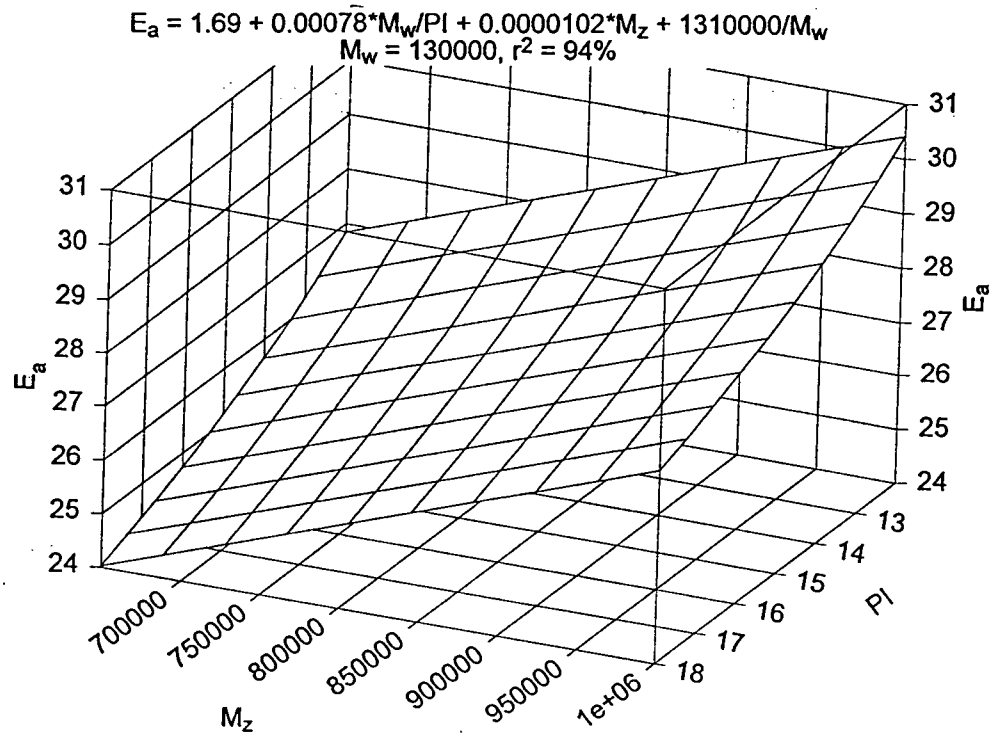

(b)

Figure 4.12 The effect of *PI*, M_w and M_z on temperature sensitivity of shear flow properties. *PI* and M_w were arbitrarily set to be constant in (a), and (b), respectively.

This analysis is only particularly useful for resins which have skewed molecular weight distributions, as is the case with most of the resins studied in this work. For resins with molecular weight distributions which are describable by Gaussian curves, the individual effect of molecular parameters is not as obvious. This is true since, for a Gaussian distribution, these variables are very dependent on one another. For example, it is not possible to increase M_w while keeping polydispersity index constant without increasing M_z and decreasing M_n proportionally, as shown in Figure 4.13. Hence, for resins with Gaussian - type molecular weight distributions, the effects of molecular parameters have to be considered collectively.

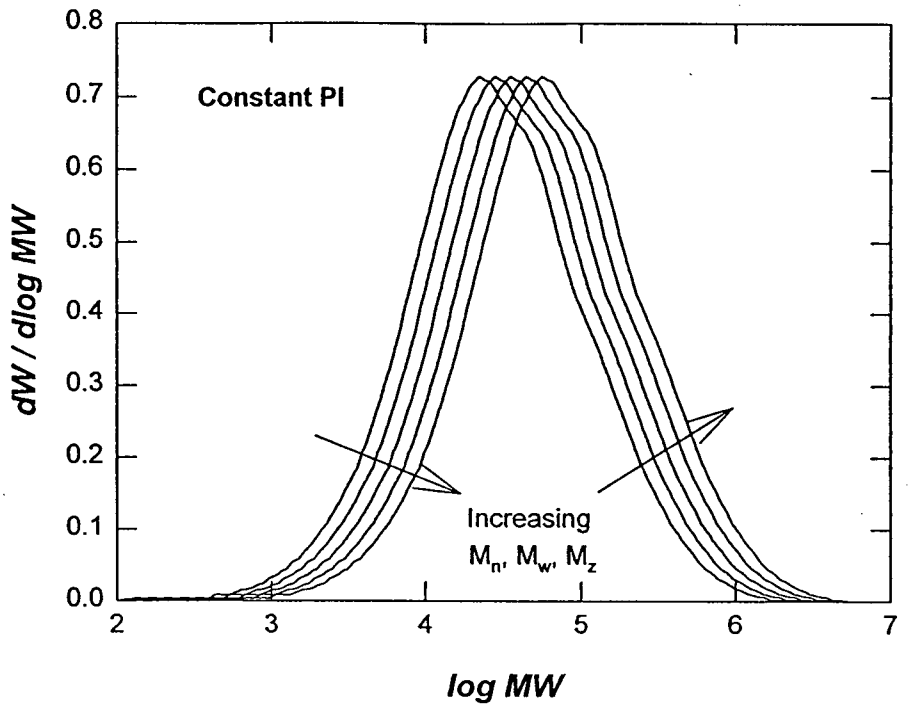

Figure 4.13 Hypothetical MWD showing the shift in M_n, M_w, and M_z at constant *PI*.

For the polydispersity range between eight to ten, the correlation obtained was

$$E_a = 35.3 - 1.31\text{E}-3 \cdot M_n + 5.53\text{E}-5 \cdot M_w \qquad (4.2).$$

Similarly, a good r-squared statistic (degree of freedom corrected) was obtained in this case. Figure 4.14 shows the observed versus predicted E_a values obtained by using the equation. The analysis indicated that the effect of M_z is statistically non-significant. From the equation, it can be deduced that increasing polydispersity while keeping M_w constant, increases E_a. This, of course, is true only if the broadening of the molecular weight distribution is done by decreasing M_n (or by increasing the concentration of smaller molecules). If polydispersity is increased by increasing M_z, no significant effect should be observed. From the equation, it can also be deduced that when M_w is increased

at a constant polydispersity, temperature sensitivity is reduced. This is the case since, for polydispersity between eight and ten, the second term, which can be written in terms of M_w/PI, dominates the equation.

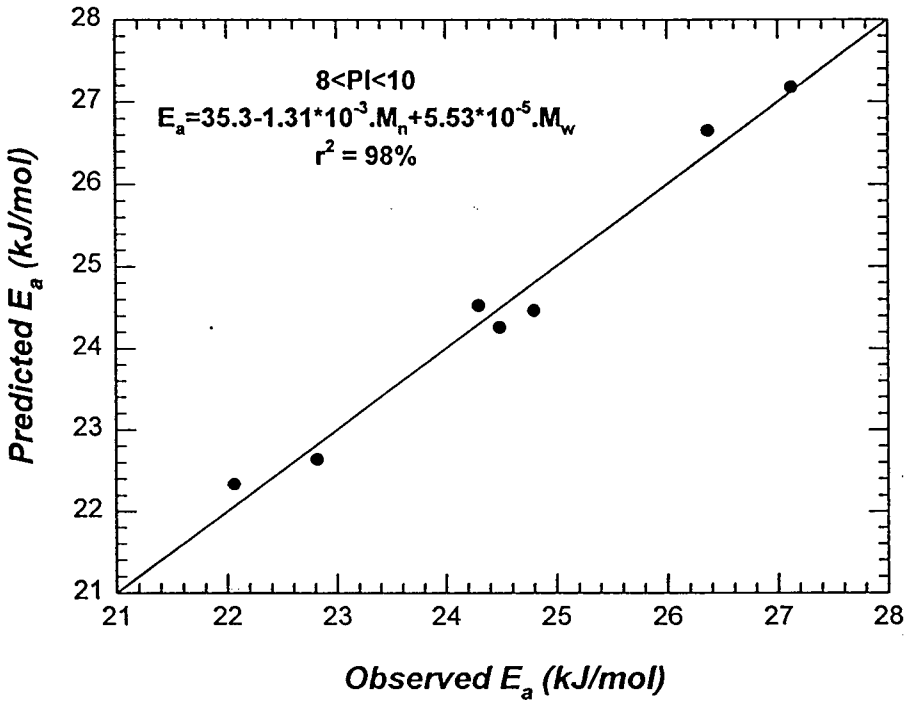

Figure 4.14 Observed and predicted E_a values as obtained from STATGRAPHICS v2.0 (8<PI<10).

For the lowest polydispersity range (PI<8), no good correlation between E_a and the molecular parameters could be obtained. Moreover, for most resins in this polydispersity range, melt fracture was observed, making it hard for the shear stress curves to be superposed. Hence, no definite trend can be stated.

In summary, increasing M_w at a constant polydispersity increases shear viscosity, while increasing polydispersity at a constant M_w increases the shear sensitivity of the

viscosity curve. This is true only if polydispersity is increased by increasing the concentration of smaller molecules. More generally, it was found that shear viscosity is most strongly affected by molecules in the molecular weight ranges of approximately 9,000 to 22,000 and 140,000 to 900,000. Decreasing the concentration of molecules in the lower molecular weight range or increasing the concentration in the higher range has the same effect of increasing the shear viscosity for the shear rate range studied in this work. However, the shear flow properties of the resins are more significantly affected by the concentration of the smaller molecules. It was also found that the temperature sensitivity of the viscosity ranged from 20 kJ/mol to 28 kJ/mol. For resins with polydispersity less than eight, no definite conclusion can be drawn with regard to the effect of molecular parameters on E_a. For resins with polydispersity greater than eight, it was found that, at constant M_w, increasing polydispersity increases E_a with the effect entirely contributed by the increase in the concentration of smaller molecules. Above a polydispersity of ten, however, the concentration of larger molecules becomes more important. Increasing the concentration of smaller molecules now tends to decrease E_a, while increasing the concentration of larger molecules tends to increase E_a. Comparing the values of E_a for resins with $PI<10$ and $PI>10$, one can see that, generally, the range of activation energy values for resins with $PI<10$ is smaller than that for resins with $PI>10$. This is consistent with what is observed in the actual industrial blow molding process, in which resins with broader molecular weight distributions are found to be more sensitive to changes in temperature relative to the resins with smaller polydispersity index values [Goyal (1998)]. It is interesting to note that although different technologies

produce resins with non-comparable viscosity profiles, the activation energy of these resins can still be correlated regardless of the technology used.

4.2.2 Extensional Flow Properties

The extensional properties of the resin were determined through 'constant stress' (creep) experiments at 150°C. Three stress levels were used in each run: 7 kPa, 5 kPa, and 3 kPa. The experiments yielded Hencky strain versus time data, some of which are plotted in Figure 4.15.

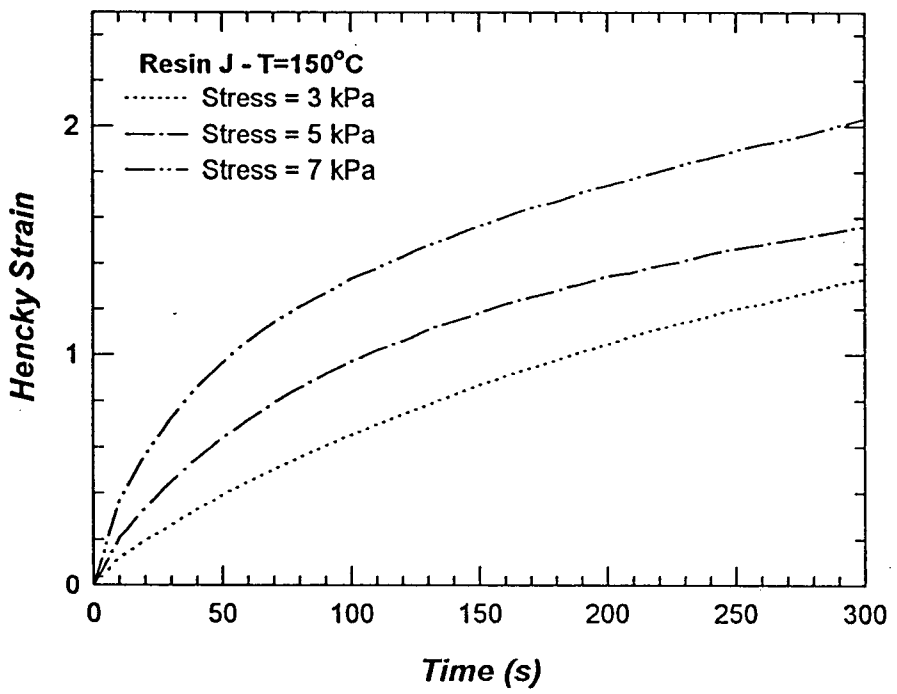

Figure 4.15 Hencky strain as a function of time determined at different stress levels.

The Hencky strain at a particular time signifies the degree of deformation that the polymer is experiencing when subjected to a particular stress for that period of time.

Hence, it reflects the melt strength properties of the polymer. For the same stress level, a larger Hencky strain at a particular time implies that the polymer has a lower melt strength. From Figure 4.16, it can be seen that increasing M_w decreases the Hencky strain. This is not surprising since increasing M_w means an increase in molecular entanglements and hence, greater melt strength.

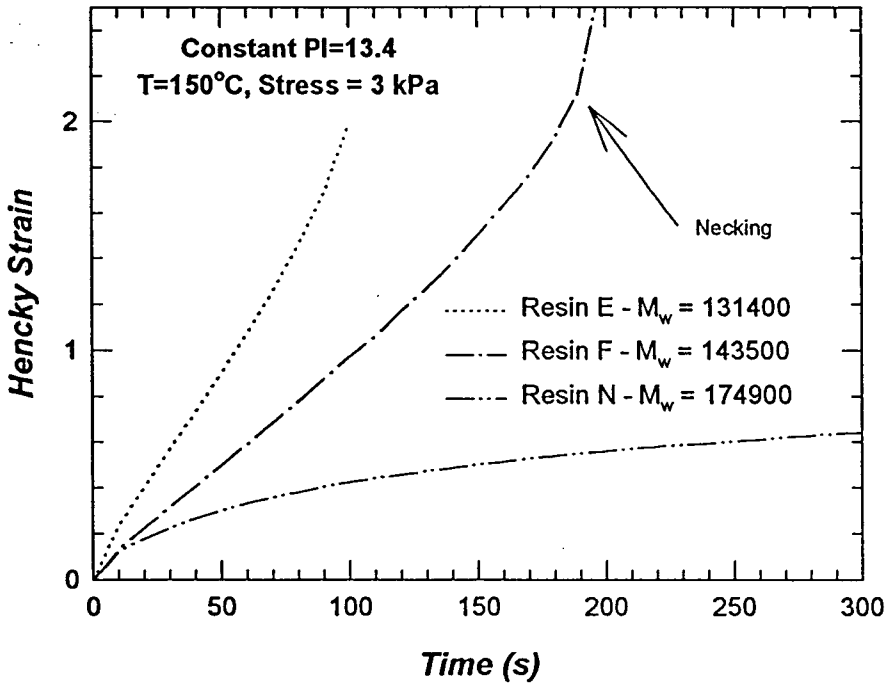

Figure 4.16 The effect of M_w on Hencky strain.

To obtain extensional viscosity data, the strain versus time curves were fitted with suitable polynomial equations, which were then differentiated to obtain the extensional rate data. Knowing the stresses and the extensional rates, viscosities could then be calculated. For one group of resins with similar polydispersities, the extensional

viscosities are plotted versus strain in Figure 4.17. It can be seen that increasing the molecular weight has a clear effect on the magnitude of the extensional viscosity. Higher molecular weight materials exhibit greater tensile viscosity as expected. As the molecular weight of the polymer is increased, more entanglements will occur, resulting in an increase in viscosity as the strain increases. Figure 4.18 shows the molecular weight distributions of these resins. It can be seen from the figure that it is the concentration of larger molecules which is contributing most to the observed effect (although this is not really reflected by M_z values). The same was also found for other sets of resins. Figures 4.19 and 4.20 illustrates this finding based on another set of resins.

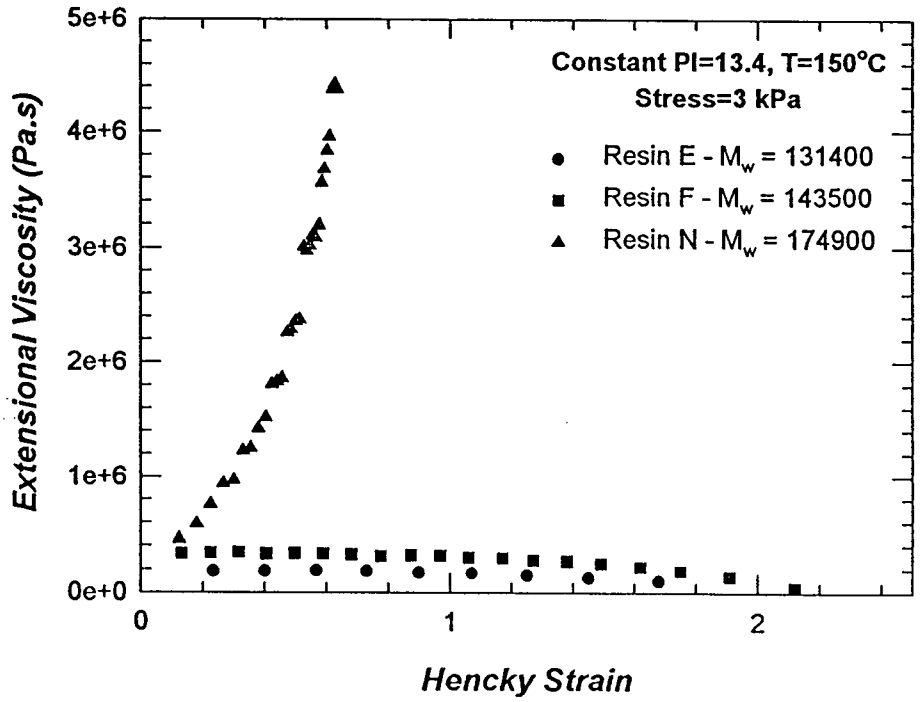

Figure 4.17 The effect of M_w on tensile viscosity.

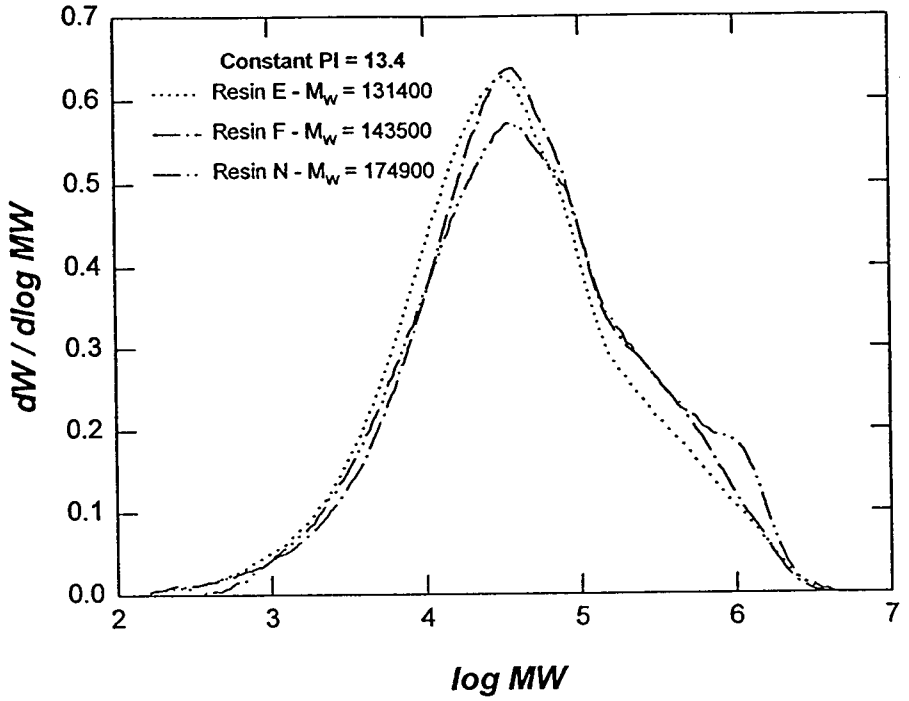

Figure 4.18 Differential molecular weight distribution for resin E, F, and N.

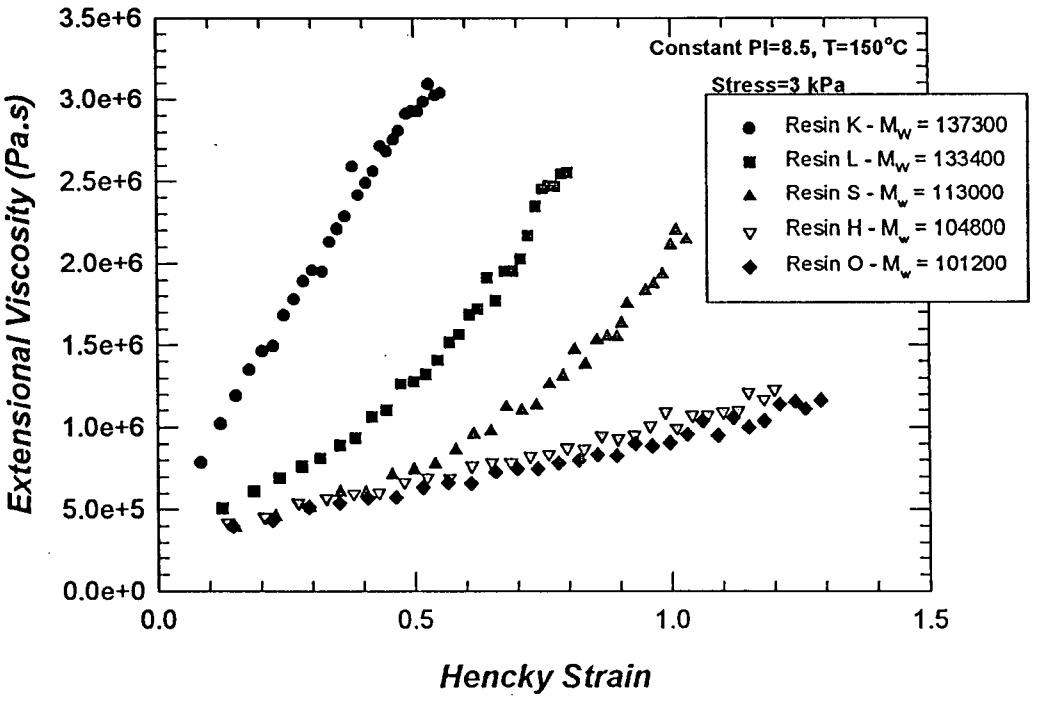

Figure 4.19 Effect of M_w on tensile viscosity.

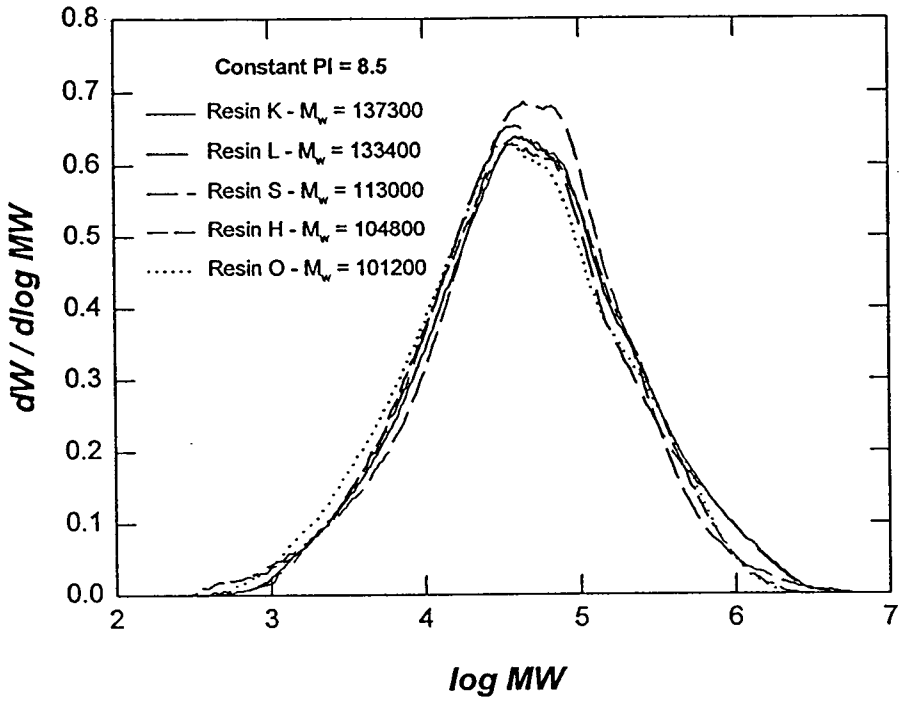

Figure 4.20 Differential molecular weight distribution for resin K, L, S, H, and O.

The relationship between extensional viscosity and zero shear rate viscosity cannot be established using the current set of results, since deformations were not low enough to be in the linear viscoelastic regime. In addition, it was found that the effect of polydispersity on extensional viscosity is not very clear from this data. Figures 4.21 and 4.22 show the extensional viscosity data for a group of resins with similar M_w, and their molecular weight distribution curves, respectively. It can be seen that the effect of polydispersity depends on the part of the distribution that is broadened. It appears that the extensional viscosity is significantly influenced by the concentration of larger molecules, which is consistent with the study reported by Munstedt and Laun (1981).

Also, as will be shown later, melt strength or extensional flow property is also affected by resin density.

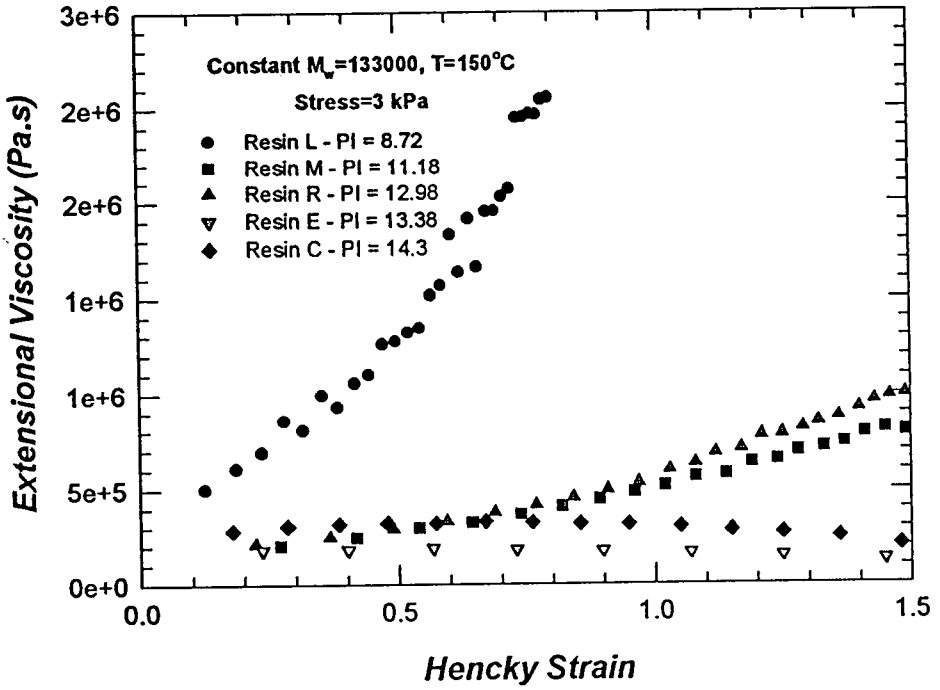

Figure 4.21 The effect of *PI* on tensile viscosity.

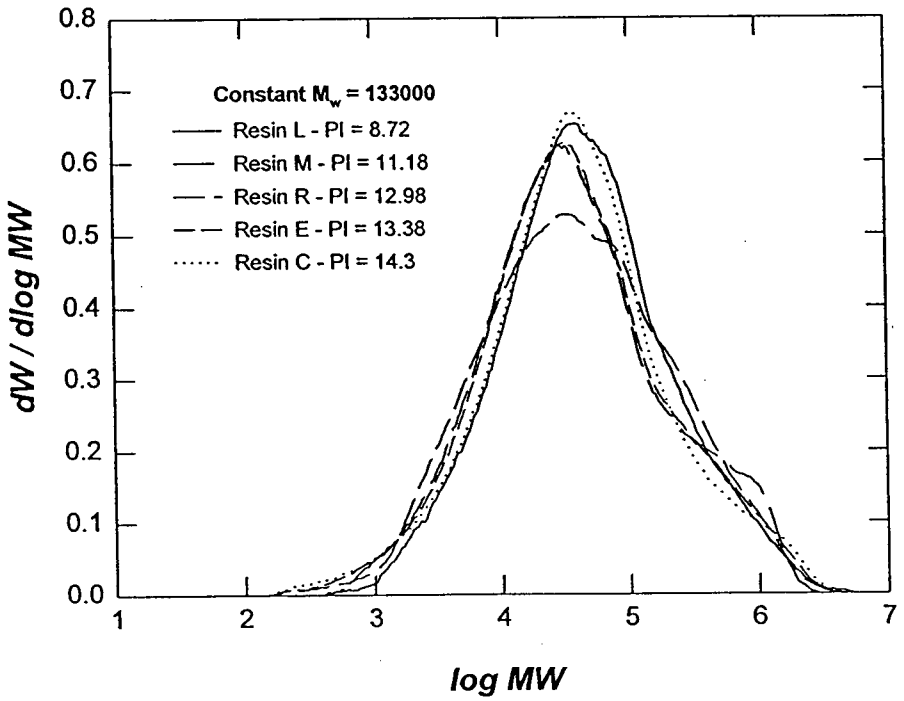

Figure 4.22 Differential molecular weight distribution for resin L, M, R, E, and C.

It is emphasized that the extensional viscosities in this work were determined using constant stress experiments. Hence, the typical viscosity versus strain rate graph is not useful, since, for the same stress level, the resulting viscosity curves corresponding to different resins will coincide. The viscosity will be proportional to the inverse of strain rate with the proportionality constant being the stress level. This is obvious from Equation 4.3. Since σ_E is constant, extensional viscosity will be related to strain rate by the equation

$$\eta_E = \sigma_E / \dot{\varepsilon} \tag{4.3}$$

regardless of the rheology of the resins.

By using the data on Hencky strain, the effect of polydispersity on melt strength was determined. For a group of resins with essentially constant M_w, the Hencky strains at different times are plotted versus polydispersity. The result for one set of resins is shown in Figure 4.23. Although, there is a fair amount of scatter in the plot, it can generally be seen that Hencky strain decreases as polydispersity is increased to about nine (the scatter can be attributed to experimental error and the effects of other parameters such as density, as will be discussed later). As polydispersity is increased further beyond nine, the Hencky strain starts to increase. At higher polydispersity, however, the effect dies off as shown in Figure 4.24 for another set of resins. Therefore, in terms of melt strength, it implies that increasing polydispersity up to about nine increases the melt strength of the resin. Increasing polydispersity beyond nine, however, decreases the melt strength, and at higher polydispersity, the melt strength is essentially not further affected by MWD.

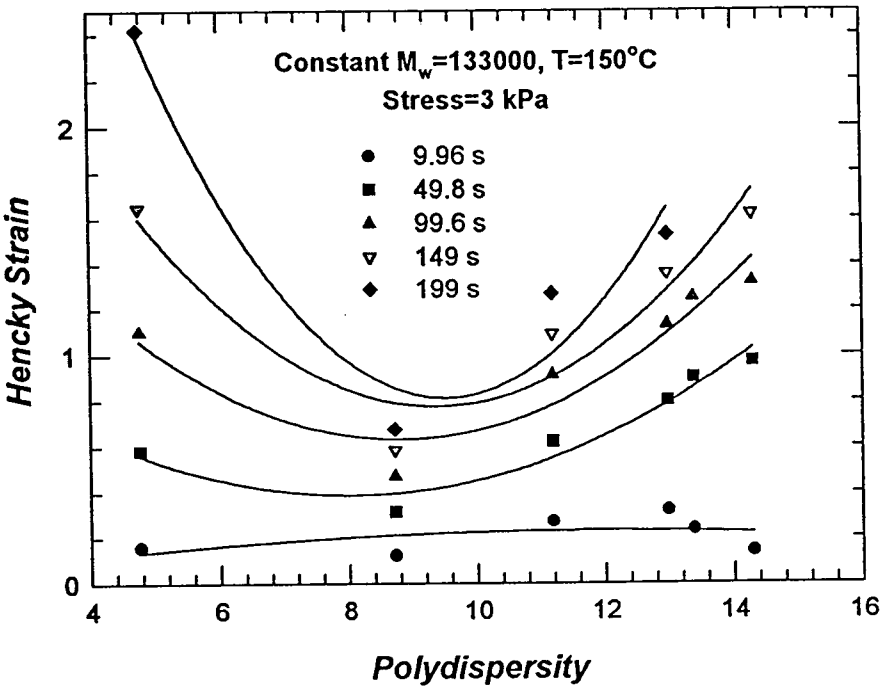

Figure 4.23 The effect of *PI* on Hencky strain at different times (strain rates). At shorter times, the effect of polydispersity is non-significant.

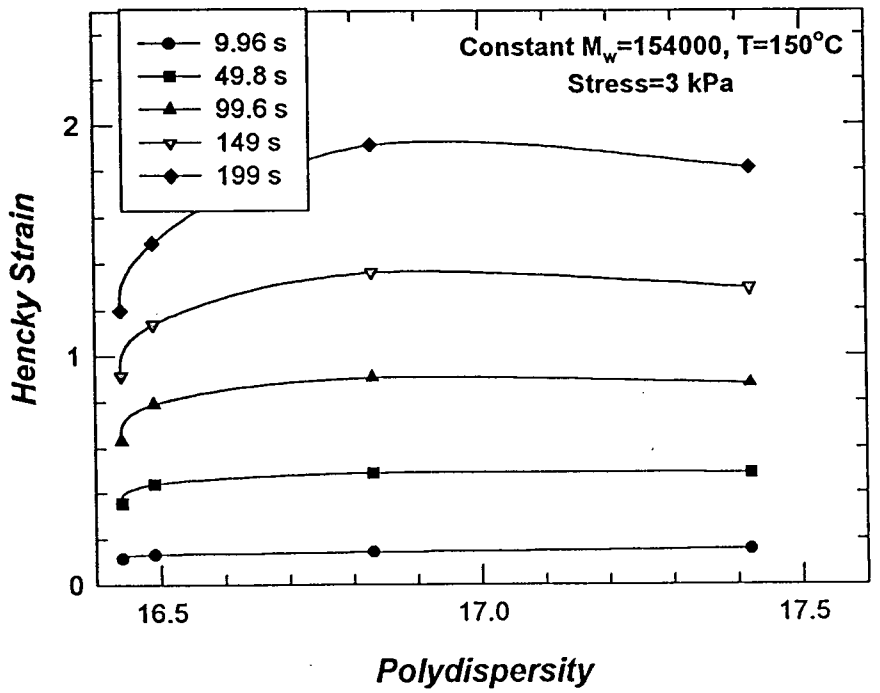

Figure 4.24 The effect of large *PI* on Hencky strain.

This observation again indicates the change in behavior experienced by the resins in the polydispersity range of about eight to ten, as discussed previously and observed by Kazatchkov *et al.* (1997). It seems that at this range of polydispersity, polymer molecules have reached a certain limit in molecular arrangements or entanglements that increasing polydispersity further would only reverse or drastically change its effect on polymer properties. This observation on melt strength is confirmed in section 4.3.1. No theoretical reason has been found for this observation.

In summary, increasing M_w was found to increase the tendency of tensile viscosity. Also, it was found that extensional flow properties of a polymer can be related to its melt strength by considering the Hencky strain curve as a function of time in a constant stress experiment. At a constant M_w, the effect of polydispersity on Hencky strain is such that increasing polydispersity up to about nine decreases the strain, while increasing polydispersity further reverses the trend. However, for broadly distributed resins ($PI>16$), it was found that increasing the polydispersity no longer affects the strain significantly.

4.2.3 Extrudate Swell Characteristics

The method of extrudate swell measurements used in this work was a simple one. However, there were a number of possible error sources associated with the procedure. Most importantly, since measurements were done after the extrudates had cooled to room temperature, the absolute magnitudes of the swell data obtained were obviously not the actual swell at the processing temperature. Secondly, there was a problem associated with sagging, which was especially pronounced at low shear rates. Sagging produces

higher swell in the lower portion of the extrudates and makes them thinner near the die. Collection of extrudates was another source of experimental error. Although extreme care was taken during the collection of extrudates, some pinching may have happened. This also caused a problem in measuring the actual extrudate diameters using a caliper. However, the results are still useful qualitatively and comparatively. Figure 4.25 shows the reproducibility of extrudate swell data for one of the resins as a function of shear rate and temperature. Data at each shear rate was estimated to vary by approximately 5%.

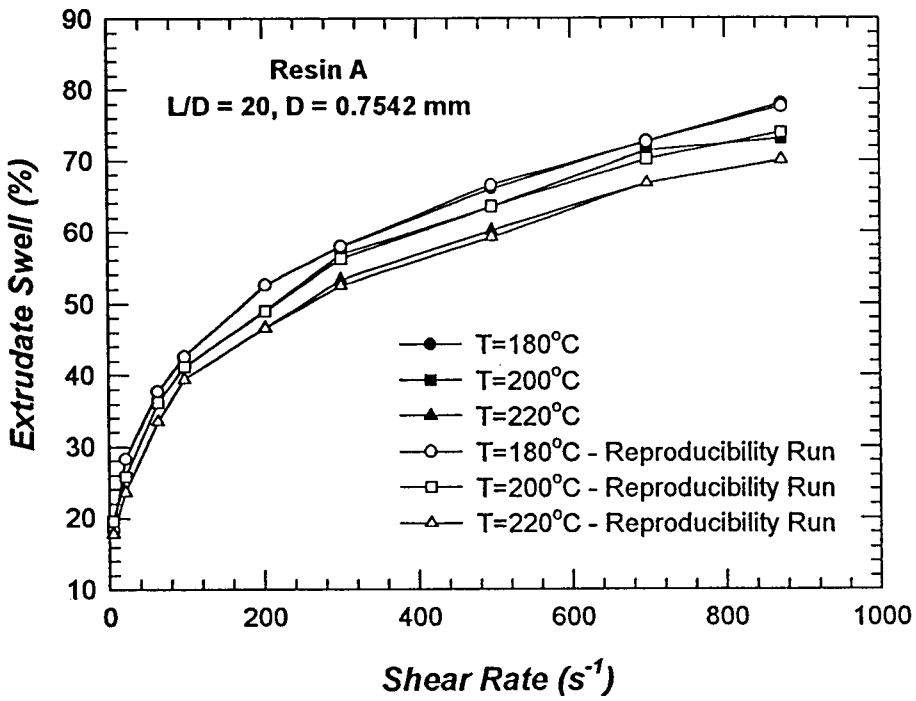

Figure 4.25 Reproducibility of extrudate swell data.

To determine the effect of molecular weight on the relative magnitude of swell, the resins were grouped according to their polydispersities. Figures 4.26 and 4.27 show the extrudate swell data for two groups of resins. The molecular weight distributions for

these resins are plotted in Figures 4.28 and 4.29, respectively. One can see that although the molecular weight distributions of the resins are very similar, extrudate swell data varies relatively significantly. This shows that extrudate swell is very sensitive to the various parts of the MWD. Attempts were also made to correlate the swell to various areas under the MWD curve, but it was not possible to determine the molecular weight range that is most critical in its affect on extrudate swell. This observation has also been reported by Koopmans (1988), who finally concluded that polydispersity is not a useful parameter to be used in the analysis of extrudate swell. However, extrudate swell is expected to increase with the increase of concentration of larger molecules. This may not show in the plot because of the possibility of the extrudates cooling before the ultimate swell is reached.

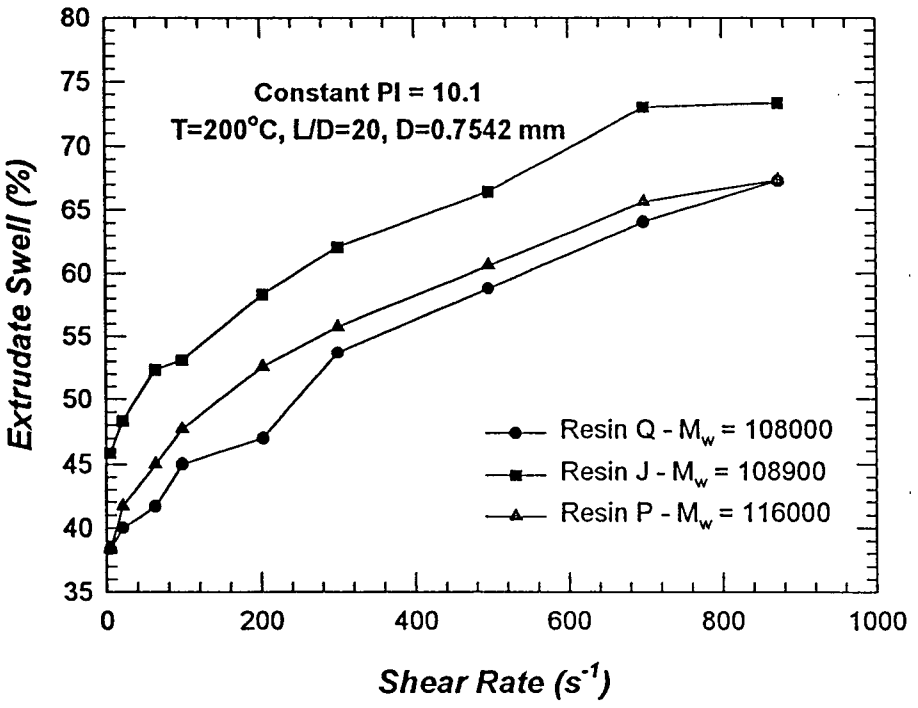

Figure 4.26 Extrudate swell data for resins Q, J, and P having similar *PI*.

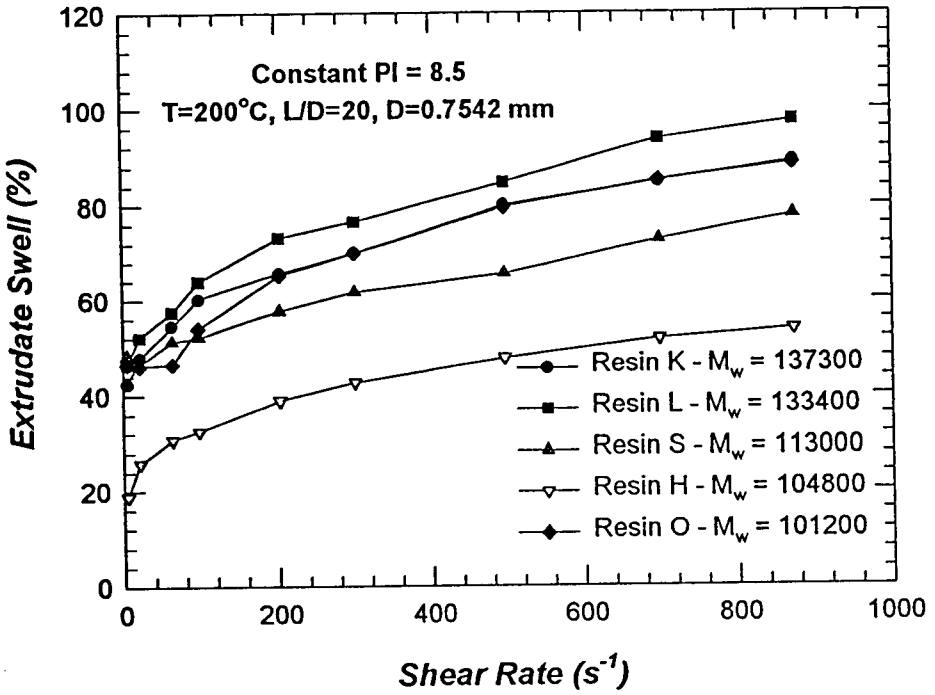

Figure 4.27 Extrudate swell data for resin K, L, S, H, and O having similar *PI*.

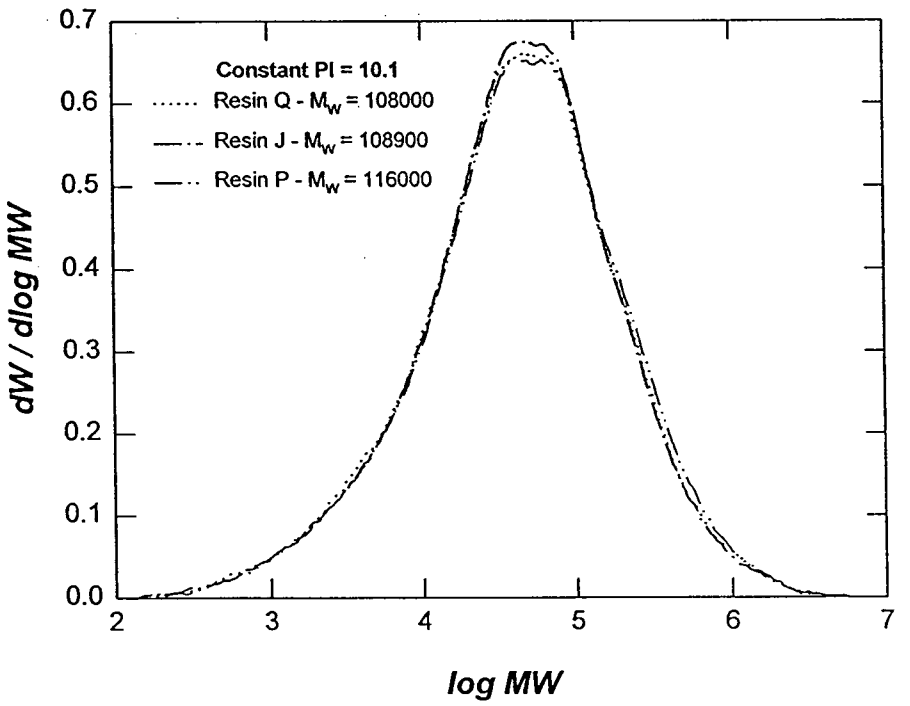

Figure 4.28 Differential molecular weight distribution for resin Q, J, and P.

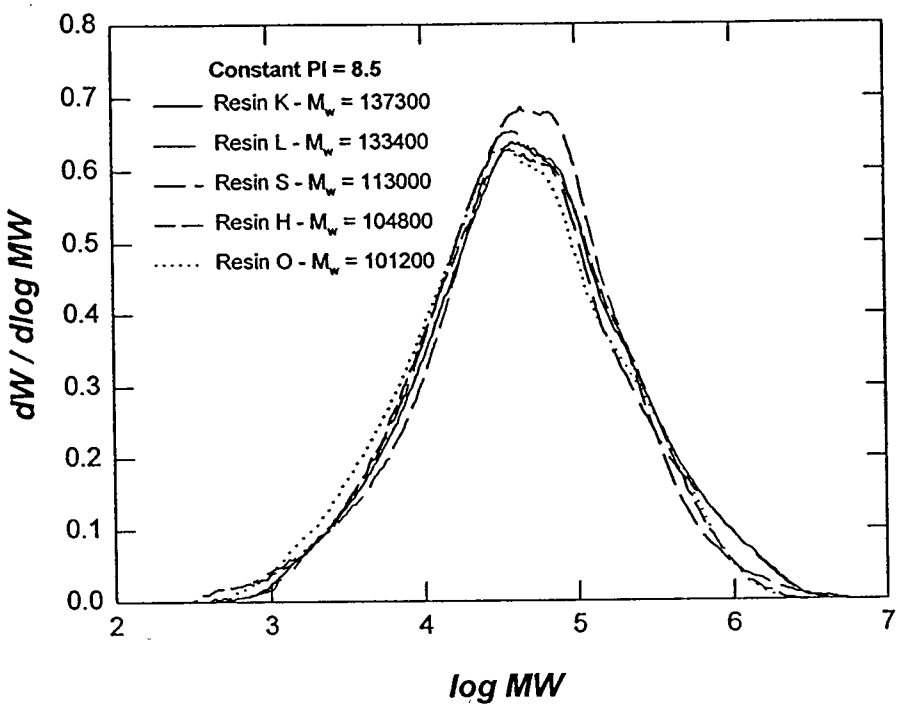

Figure 4.29 Differential molecular weight distribution for resins K, L, S, H, and O.

Plotting extrudate swell data for resins with similar M_w resulted in the same conclusion. It is not possible to qualitatively correlate extrudate swell with polydispersity, because extrudate swell is very sensitive to the different parts of the MWD. This is shown in Figures 4.30 and 4.31.

Extrudate swell is a manifestation of the elastic property of a polymer. Since the elastic property of a polymer is very much affected by the pre-shear history experienced during the various parts of resin production, a possible reason for the inability to correlate extrudate swell to molecular parameters could be due to the different pre-shear history experienced by the different resins. This seems to be a valid reason. Previous studies

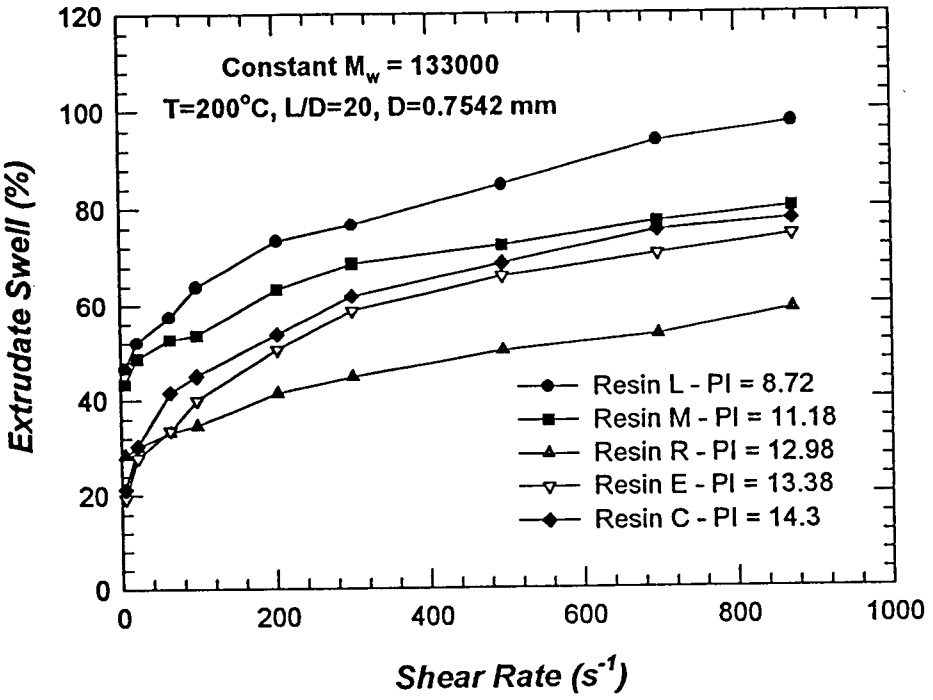

Figure 4.30 Extrudate swell data for resins L, M, R, E, and C having similar M_w.

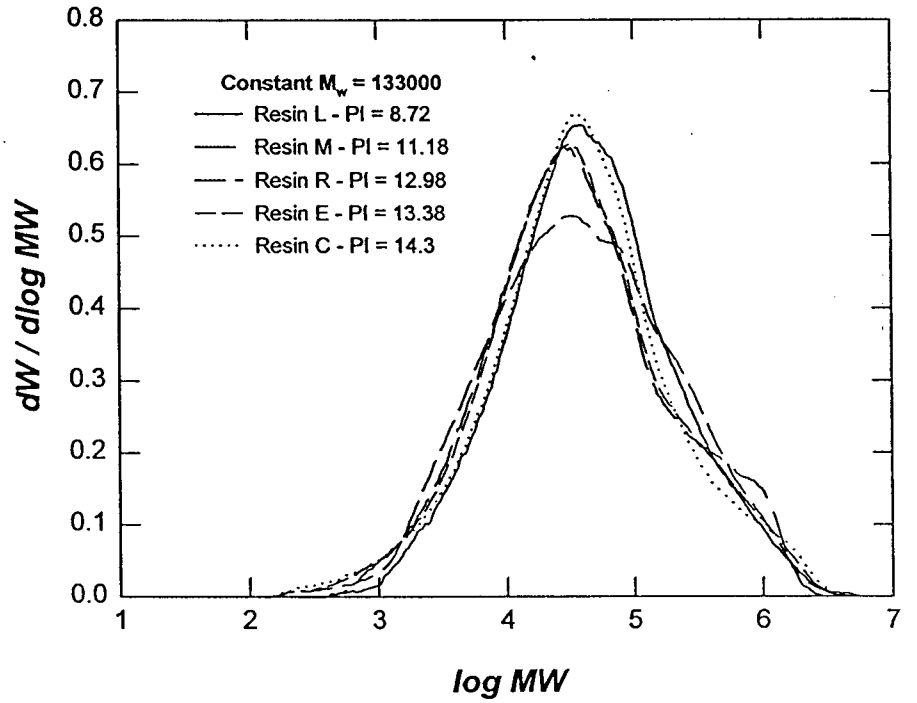

Figure 4.31 Differential molecular weight distribution for resins L, M, R, E, and C.

have also failed to determine such a correlation, and possibly, the effect of pre-shear history is more significant than previously thought. Also, differences in polymerization technology may render the resins non-comparable as far as die swell is concerned. The rate and mechanism of termination of a polymerization process, and the amount of additives used may differ greatly among the different technologies, and may result in a varying degree of unsaturation in the resulting polymer. This affects the amount of crosslinking and chain scission in the polymer. Although this variation may not be reflected as being significant in the molecular weight distribution curves, the elastic properties of the resins may very well be affected significantly.

In regard to the sensitivity of swell to changes in shear, it was found that M_z and polydispersity are useful parameters. Figures 4.32 and 4.33 show the effect of M_z and polydispersity on the slope of extrudate swell data. In the plots, all curves are normalized linearly by shifting the data so that the swell value at the lowest shear rate coincide. One can see from the figures that at a constant M_w, broadening the molecular weight distribution by increasing the concentration of larger molecules increases the swell sensitivity in the lower shear rate regime and decreases it in the shear rate range of 350 s^{-1} to 700 s^{-1}. Hence, swell is very sensitive at lower shear rates due to the presence of larger molecules. In the processing range of shear rates (350 s^{-1} – 700 s^{-1}), however, the sensitivity tends to decrease with polydispersity. Figures 4.34 and 4.35 show the molecular weight distributions of the two sets of resins. However, this analysis seems to be true only for resins manufactured using the same technology, *'a'*. If resins manufactured using other technologies are included in the analysis, as shown in Figure 4.36, one can see a breakdown in the pattern. Hence, not only does the manufacturing

technology affect the viscosity profile of a polymer, but it seems to affect its extrudate swell profile as well.

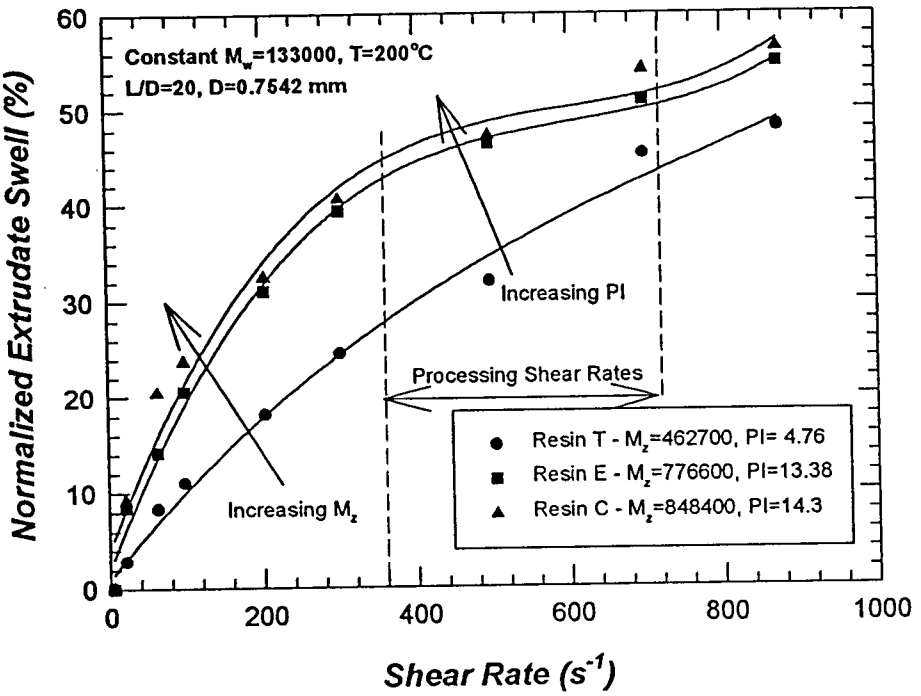

Figure 4.32 Sensitivity of extrudate swell to changes in shear rate. All resins are manufactured by technology *'a'* (set 1).

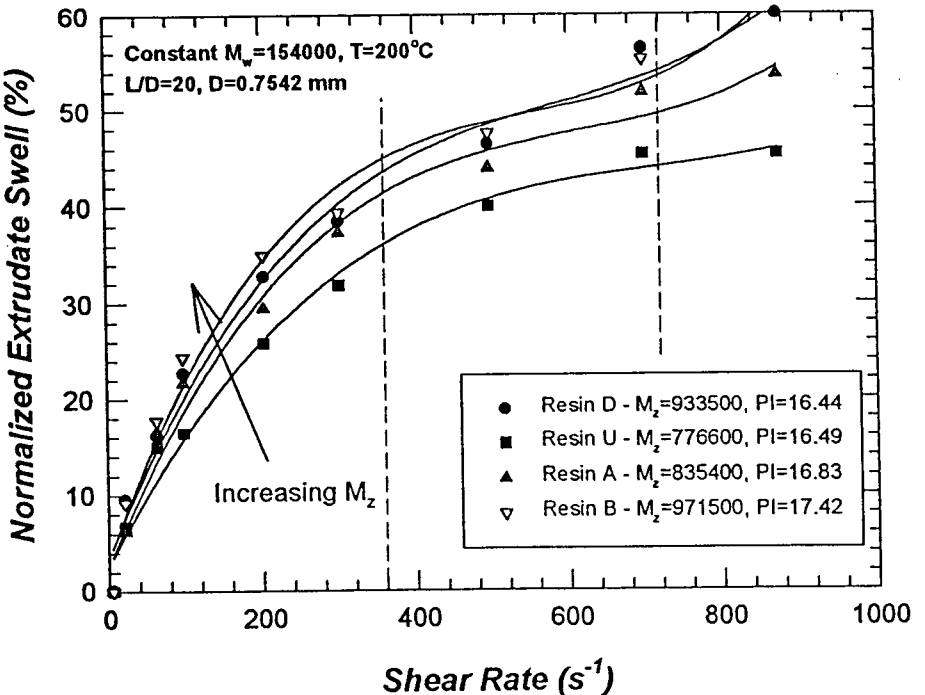

Figure 4.33 Sensitivity of extrudate swell to changes in shear rate. All resins are manufactured using technology *'a'* (set 2).

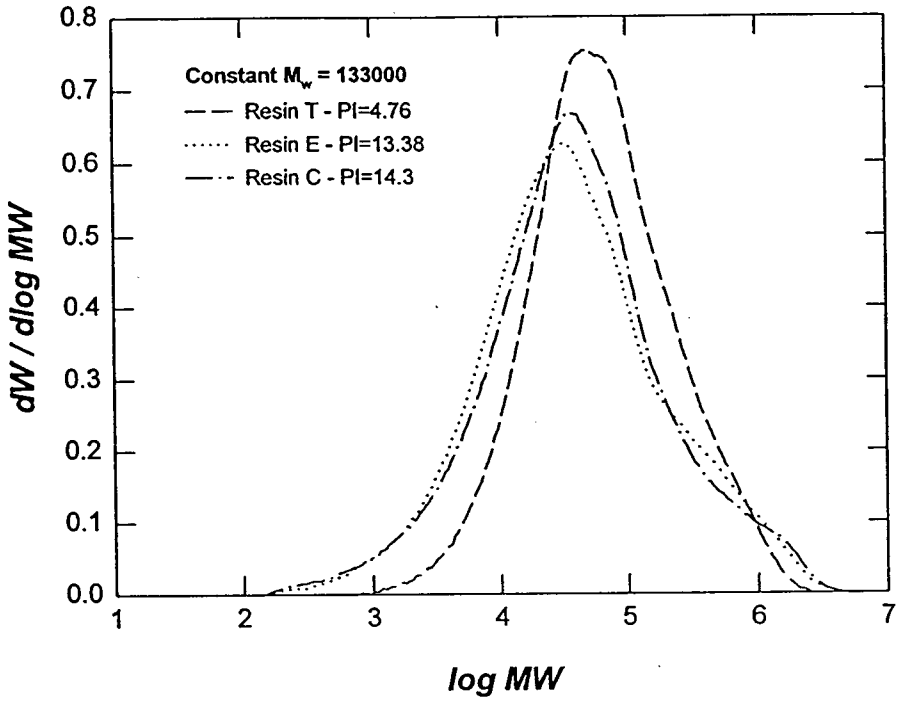

Figure 4.34 Differential molecular weight distribution for resins T, E, and C.

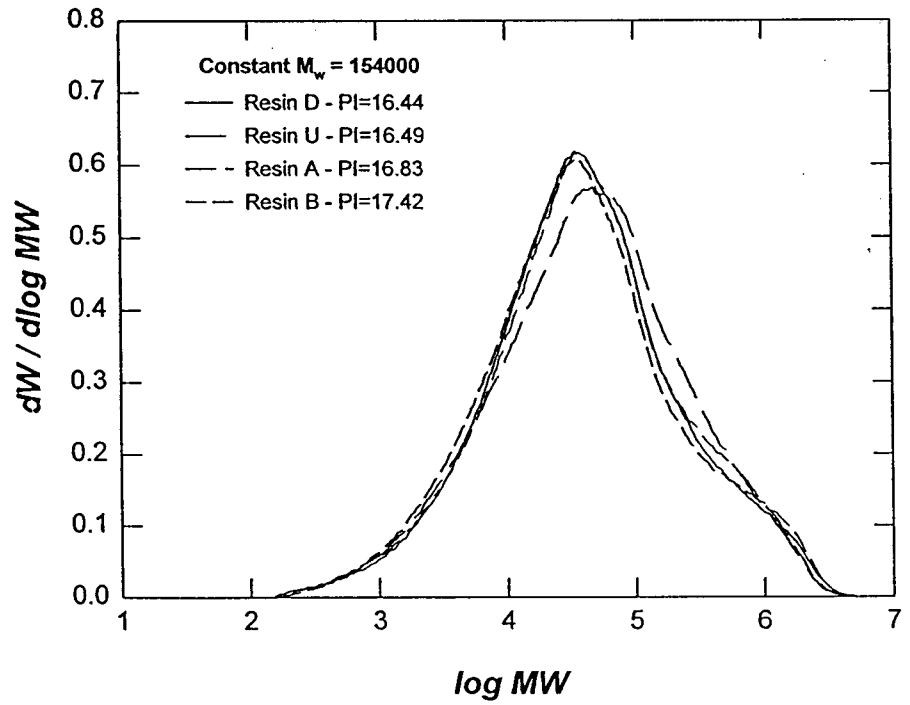

Figure 4.35 Differential molecular weight distribution for resins D, U, A, and B.

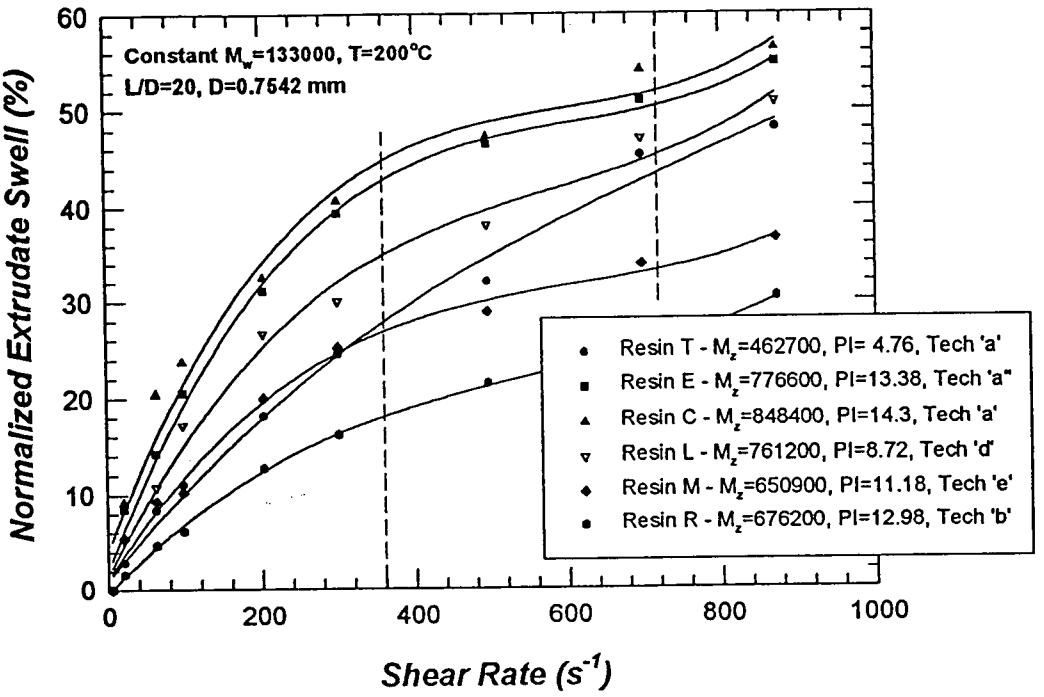

Figure 4.36 Sensitivity of extrudate swell to changes in shear rate. Included in the plot are resins produced from different technologies. One can see a breakdown in the pattern.

In summary, it was found that no useful correlation could be made between the relative magnitude of extrudate swell and various molecular weight parameters. This could be due to the fact that the resins studied have different pre-shear history, and that the effect of pre-shear history is more significant than that of molecular weight distribution. Also, polymerization technology may influence the degree of unsaturation and hence, the degree of crosslinking and chain scission in a polymer melt, which will affect its elastic behavior significantly. This renders the resins produced from different technologies to be non-comparable. However, it was found that the sensitivity of swell to changes in shear rate correlates well with M_z and polydispersity. Increasing M_z was

found to increase the shear sensitivity of extrudate swell at low shear rates. In the processing shear rate range of 350 s^{-1} to 700 s^{-1}, however, shear sensitivity is affected more significantly by polydispersity. In this range, increasing polydispersity tends to decrease the shear sensitivity of extrudate swell. It should be reiterated that only resins manufactured using the same technology show this trend.

4.3 PROCESSABILITY

4.3.1 Melt Strength

In this work, melt strength is defined as the maximum weight that a polymer is able to support for a period of three minutes without breaking, and was determined using the extrusion plastometer at 190°C. The detailed procedure for the experiment was described in Section 3.4.3. In performing the experiments, it was made sure that the range of data obtained included the three-minute period so that interpolation would be required instead of extrapolation. A plot of maximum weight versus maximum time before breaking is shown in Figure 4.37 for some resins.

The analysis of the melt strength properties of the resins studied in this work was based on the extensional properties of the resins. In this section, the analysis of the data obtained using the melt indexer is emphasized.

To determine the effect of molecular properties on melt strength, it was necessary to group the resins into three groups having $PI>10$, $8<PI<10$ and $PI<8$. Without doing so, it was found that no useful correlation could be obtained. This is consistent with the results obtained from the extensional experiments. From the analysis of Hencky strain as

a function of polydispersity and time, it was found that the melt strength properties of the resins change in behavior at a polydispersity range of around eight to ten.

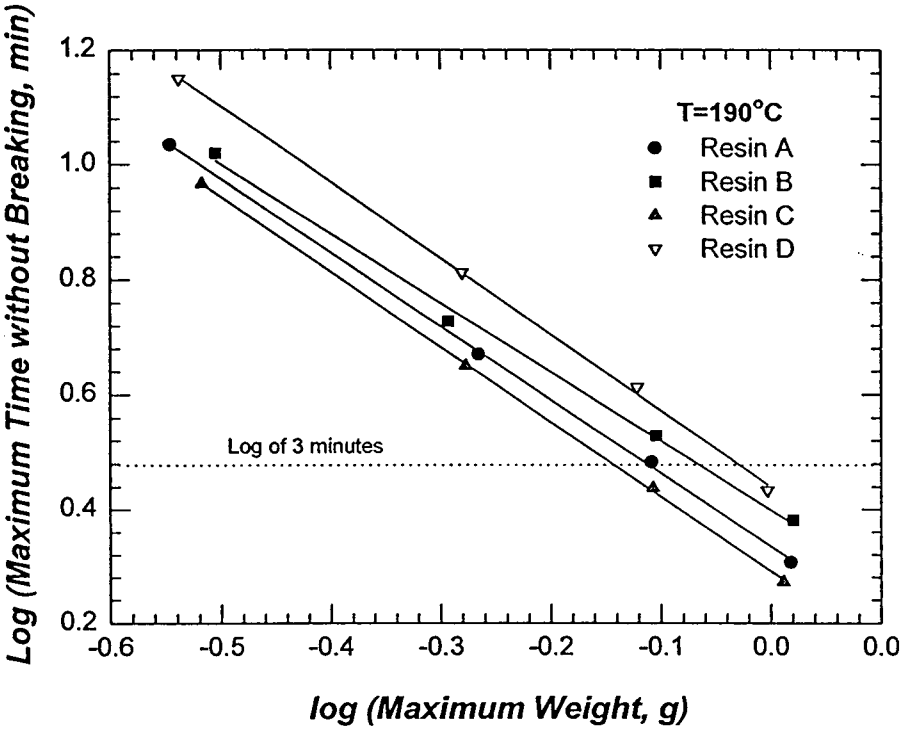

Figure 4.37 Determination of melt strength using the melt indexer.

In trying to correlate melt strength directly to M_n, M_w, M_z, or polydispersity, a difficulty was encountered associated with the fact that melt strength may not be affected by only a single molecular parameter, but two or more. Hence, STATGRAPHICS was used for the analysis. For resins with $PI>10$, it was found that melt strength is dependent on M_w, M_n (hence, polydispersity), and density. The model obtained with the best r-squared statistic was

$$Melt\ Strength = 75.5 + 1.47\text{E}-5 \cdot M_w + 4.68\text{E}-4 \cdot M_n - 84.78 \cdot Density \qquad (4.4).$$

The plot of observed versus predicted melt strength values using this model is shown in Figure 4.38. In Figure 4.39, predicted and observed melt strength values as a function of M_w are shown. It can be seen that the model closely predicts the melt strength values. It should be noted, however, that this trend is valid only for the range of M_w, M_n, polydispersity and density studied in this work.

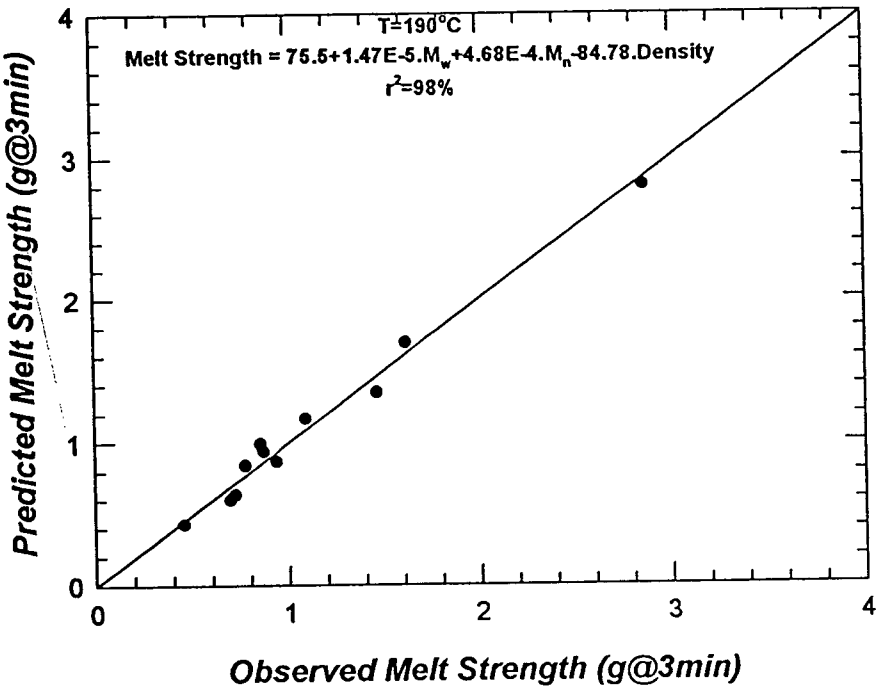

Figure 4.38 Observed and predicted melt strength values obtained from STATGRAPHICS (*PI*>10).

Equation 4.4 implies that melt strength decreases with increasing polydispersity (for *PI>10*), which is attainable by decreasing M_n. Moreover, by rewriting M_n as M_w/PI, one may see that for large polydispersity, melt strength becomes essentially independent of the breadth of the molecular weight distribution. This is consistent with the analysis performed earlier, which was based on the extensional flow properties of the resins. The equation also shows the effect of M_w. By increasing M_w, melt strength tends to increase,

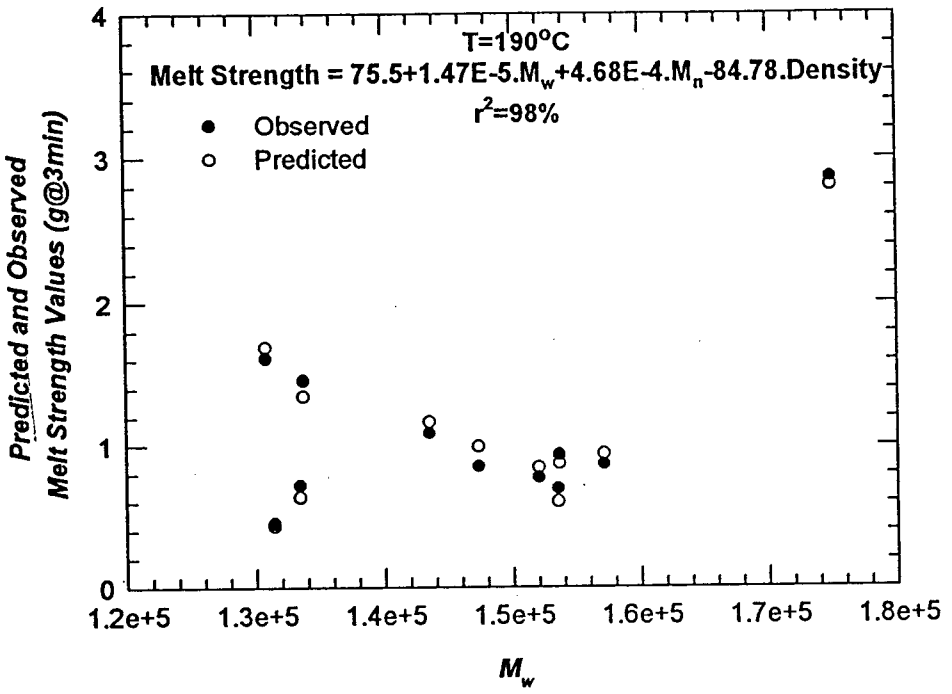

Figure 4.39 Observed and predicted values of melt strength as a function of M_w (PI>10).

which is as expected due to the increase in entanglements in molecular levels. In addition, it can be seen from the equation that melt strength is also significantly affected by density. Resins with lower density are found to have higher melt strengths, due to the greater branching associated with them. Figure 4.40 shows graphically the effect of M_w and polydispersity on melt strength. For resins with $PI>10$, higher melt strength can, therefore, be achieved by narrowing the molecular weight distribution, by increasing the weight average molecular weight, M_w, or by increasing the degree of branching.

For resins with $8<PI<10$, the following correlation was obtained:

$$Melt\ Strength = 50.31 + 4.19 * 10^{-5} \cdot M_w - 55.08 \cdot Density \qquad (4.5).$$

A plot of the observed and predicted values is shown in Figure 4.41. It can be seen

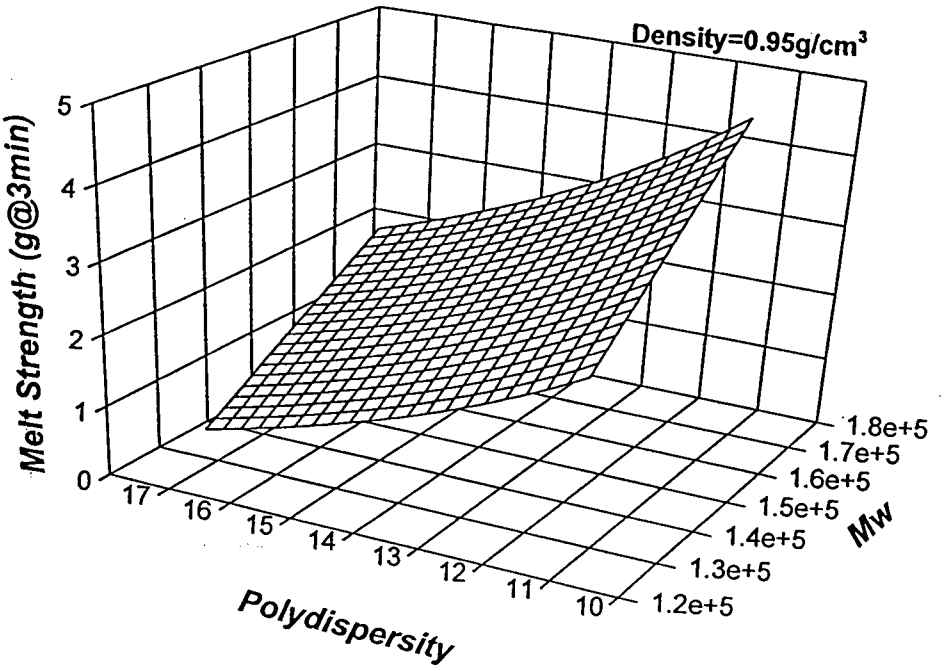

Figure 4.40 3-D plot showing the effect of *PI* and M_w on melt strength. The density value is fixed arbitrarily. Changing the density value would shift the curve upward or downward accordingly. Note that M_w is related to *PI* and M_n, and hence, when considering the plot, it has to be ensured that M_n is reasonable, so that *PI>10*.

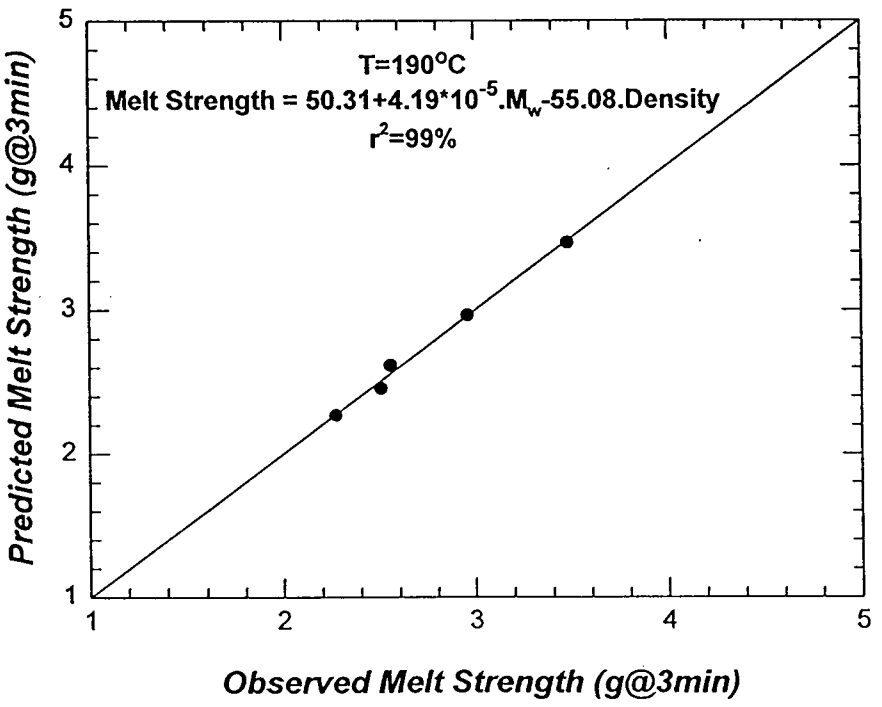

Figure 4.41 Observed and predicted melt strength values obtained from STATGRAPHICS v2.0 *(8<PI<10)*.

that the equation predicts melt strength values very well. The trend implied by the equation is the same as that implied by Equation 4.4, i.e increasing M_w and decreasing density have an increasing effect on the melt strength. M_n (or polydispersity) was found not to have a significant effect for resins with this range of polydispersity. A possible reason is the narrow range of polydispersity associated with this group of resins.

For resins with $PI<8$, it was not possible to obtain good correlation using STATGRAPHICS. Therefore, there may be portions of the molecular weight distribution that are affecting the melt strength, which are not reflected in M_n, M_w, or M_z. The FORTRAN program described earlier was then used to analyze the different portions of the MWD. The resulting correlation coefficients are plotted as a function of molecular weight limits in Figure 4.42. It can be seen that melt strength is significantly affected by the molecules in the molecular weight range of 9,000 to 220,000 in a positive manner and by molecules in the molecular weight range of 35,000 to 55,000 in the negative manner. However, the molecular weight range of 35,000 to 55,000 is relatively small and is inclusive in the larger range of 9,000 to 220,000. Hence, it can be said that melt strength is affected by the molecules in the molecular weight range of 55,000 to 220,000, and that increasing the concentration of molecules in this range increases the melt strength. Therefore, by increasing the polydispersity of a polymer (with $PI<8$) in the direction of increasing the concentration of moderate to larger molecules, one may increase its melt strength. It is interesting to note that there is not much difference in the correlation coefficient for various molecular weight ranges, implying that all portions of the distribution are relatively significant in their effect on melt strength.

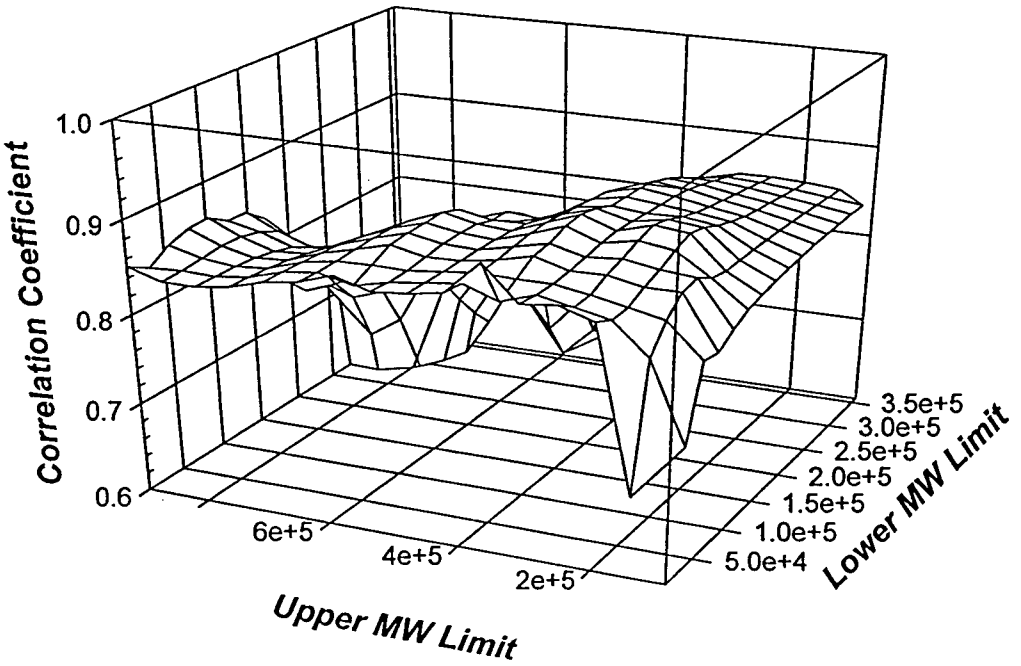

(a)

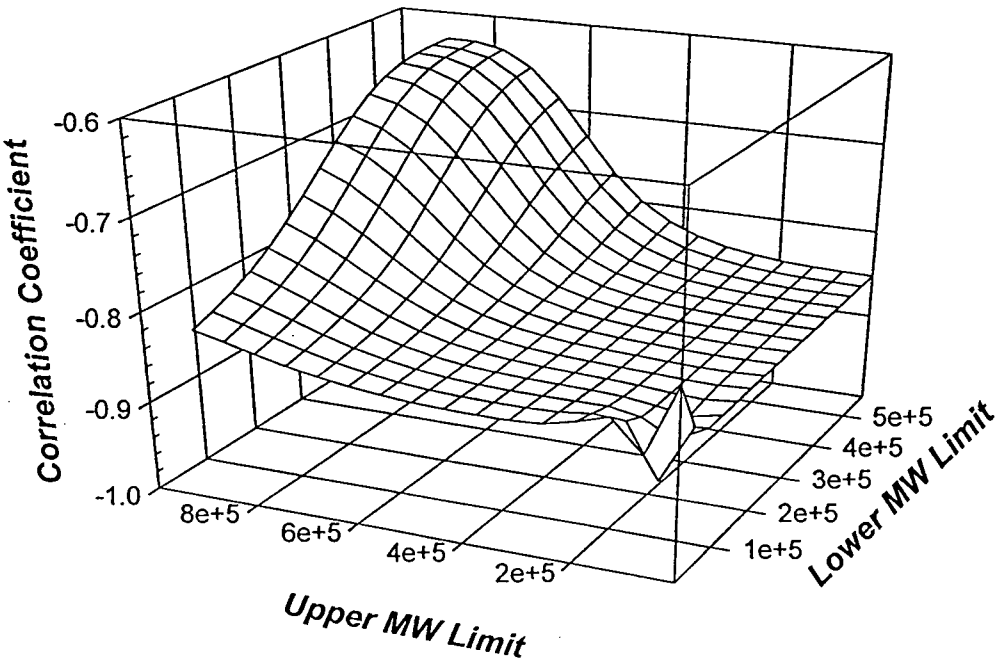

(b)

Figure 4.42 Correlation coefficients relating various molecular weight ranges to melt strength *(PI<8)* (a) positive correlation (b) negative correlation. Correlation coefficient (x,y) = *COV* $(x,y)/\sigma_x.\sigma_y$

In summary, melt strength was found to increase with increasing M_w and decreasing density. Analysis had to be done separately according to the three polydispersity groups of *PI<8*, *8<PI<10*, and *PI>10*. This is consistent with the results obtained when analyzing the Hencky strain data. For narrowly distributed resins, up to a polydispersity in the approximate range of eight to ten, broadening the molecular weight distribution increases the melt strength. Beyond the critical range of eight to ten, however, increasing polydispersity decreases the melt strength. For resins with high polydispersity, further broadening the molecular weight distribution has been found to result in insignificant change in melt strength.

4.3.2 Sagging and Weight Swell Characteristics

Sagging and weight swell characteristics for three of the resins, E, F, and G, were determined by performing pillow mold experiments. The results show the exact behavior of the resins under industrial operating conditions.

In performing the experiments, five replicate runs were carried out each time, and the average results were determined. Figure 4.43 shows a plot of pillow weight versus parison number for one of the resins to demonstrate the reproducibility of the experiments. The numbering of the pillows is such that pillow number one is that which is nearest to the exit of the die and, hence, extruded last. From the figure, one can see that the reproducibility in these experiments was excellent.

During parison formation, uneven wall thickness is attributable to both the swell and sagging characteristics of the resin. However, it is difficult to perform experiments that would differentiate the effect of either factor individually. Although useful results may

be obtained by doing pillow mold experiments, it is nonetheless not possible to determine if a certain parison flow behavior is solely due to swell or sagging. The effect of each factor is equally important and opposite.

In the analysis of the results, it was found that it is easier to relate weight swell and sagging to extrudate swell and melt strength, respectively. It was not possible to relate the results to the molecular parameters due to the limited number of resins used in the pillow mold experiments. However, knowing how the molecular distribution affects melt strength and extrudate swell, one can always relate molecular distribution to sagging and weight swell.

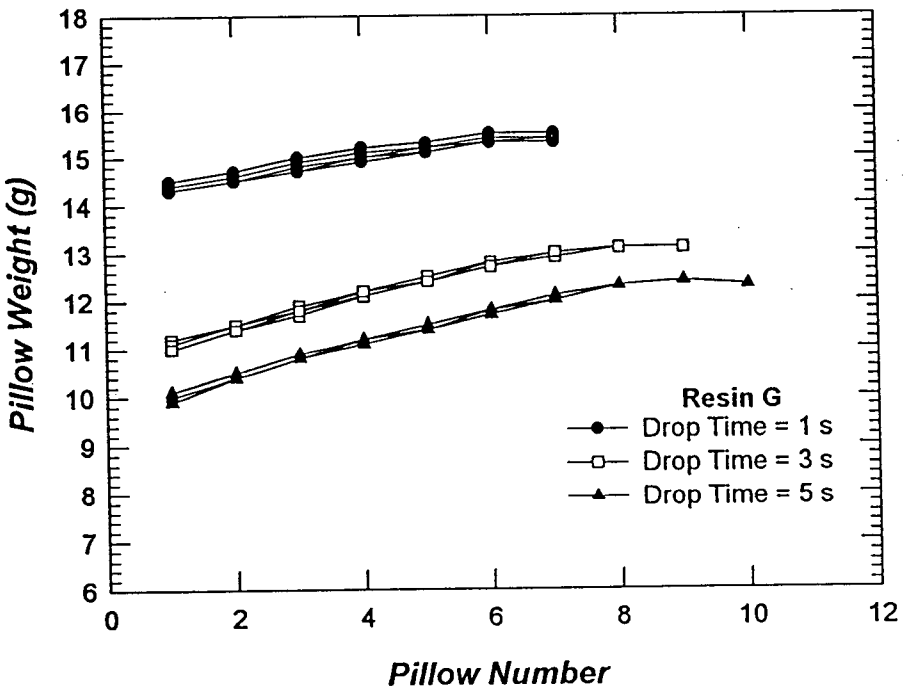

Figure 4.43 Variation of pillow weight with pillow number. Multiple curves indicate replicate runs.

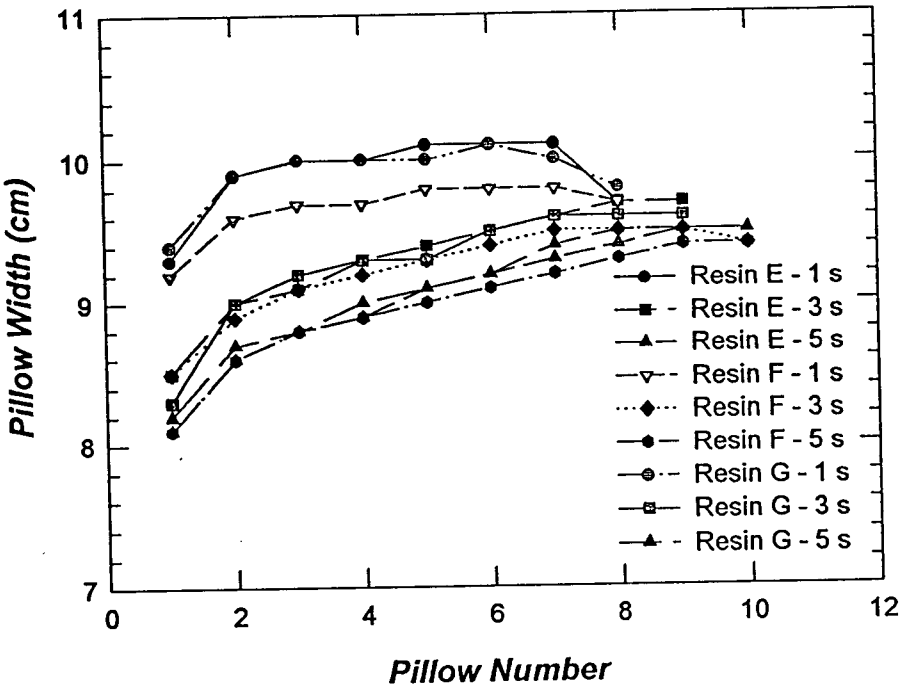

Figure 4.44 Variation in pillow width for different resins extruded at different drop times.

The results from the pillow mold experiments seemed to indicate that weight swell is proportional to extrudate swell, while sagging is inversely proportional to melt strength, which is obvious. Figure 4.44 shows a plot of pillow width versus parison number for the three resins and for parison drop times of 1 s, 3 s, and 5 s (see Figure 3.11 for definition of pillow width). As mentioned earlier, decreasing parison drop time means faster parison formation and hence, higher shear rate. One can see that as the parison drop time is increased, the width for each pillow is decreased. This shows the effect of extrudate swell and hence, weight swell which decreases with decreasing shear rate (or increasing drop time). On the other hand, as the pillow number increases, the width of each pillow also increases, due to parison sag, which causes the lower part of the parison

to become thicker than the upper part. It is also interesting to observe that each line has curvature, which provides an indication of the elastic properties of the resins. The pillow which was extruded first would have spent the most time in the die and hence, it showed lower swell (fading memory effect). On the other hand, pillows which were extruded later would show greater swell. However, this does not show on the plot due to parison sag. Instead, it is shown as a curvature. One can see that as parison drop time increases, the curvature becomes less obvious, implying the significance of swell at shorter parison drop times. To relate melt strength and extrudate swell of each resin to parison sag and weight swell, respectively, it is useful to consider Figures 4.45 and 4.46. In Figure 4.45, extrudate swell data as a function of shear rate are plotted for the three resins. In Figure 4.46, the melt strength data for the three resins are presented. It can be seen that, on average, resin E has the highest extrudate swell, while resin F has the lowest. As far as melt strength is concerned, resin G has the highest, while resin E has the lowest.

Referring back to Figure 4.44, for a parison drop time of 1 s, it can be seen that resin E has the largest width on average, followed by resin G. This can be understood by considering the extrudate swell properties of the three resins. The short parison drop time causes extrudate swell to be a significant factor and since resin E has the highest swell in general, followed by resin G, this is the trend observed in Figure 4.44. However, the effect of melt strength starts to show for longer parison drop times. For drop time of 3 s, for example, the curves corresponding to resin E and G are brought closer together. This is because of the competing effect of melt strength and extrudate swell. Although resin E has the highest swell, it has the lowest melt strength. Resin G, on the other hand, has the highest melt strength. As far as resin F is concerned, it has the lowest swell and moderate

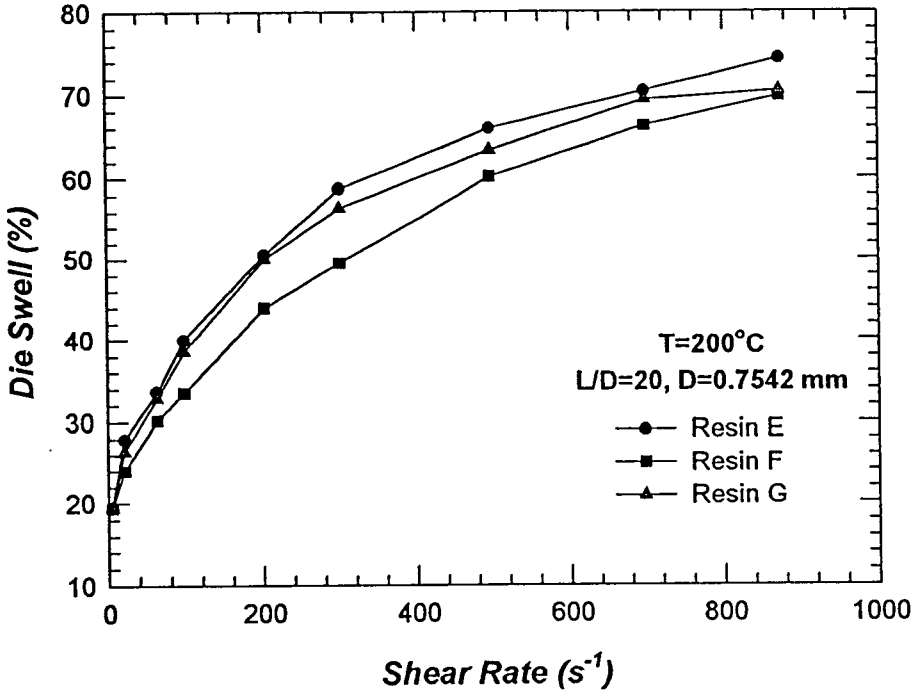

Figure 4.45 Extrudate swell profile for resin E, F, and G.

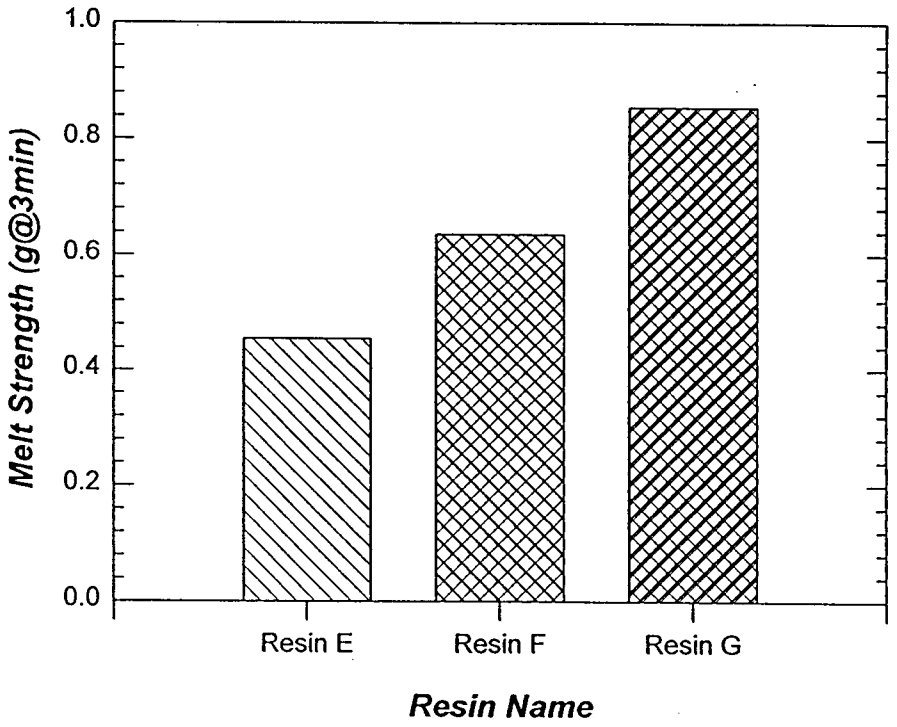

Figure 4.46 Melt strength values for resin E, F, and G.

melt strength and hence, its position in the plot is still unchanged. This is also true for the parison drop time of 5 s. Resin F still maintains its position in the plot, while the positions of resin E and G have been reversed. Parison sag has become the deciding factor for this drop time, such that resin G, which has the highest melt strength, shows larger pillow width in general.

Figure 4.47 shows a plot of pillow weight versus pillow number. Similar observations can be made. Weight swell and parison sag cause the opposite effects, resulting in the observed behavior. For fast parison drop times, swell dominates and hence, resin E which has the highest extrudate swell property, shows the largest weight for each pillow. As parison drop time increases, sagging becomes increasingly important and this brings the curve corresponding to resin E, which has the highest swell and lowest melt strength, closer to that corresponding to resin G, which has a lower swell and highest melt strength. Resin F is not affected as far as relative position in the plot is concerned since it has the lowest extrudate swell behavior, but moderate melt strength. It is noted that for a parison drop time of 5 s, the weight for each pillow corresponding to resin E is still larger than that corresponding to resin G due to the difference in density. Figure 4.48 compares the densities of the three resins. It can be seen that resin G has the lowest density, making it possible for it to have larger width and smaller weight for a parison drop time of 5 s.

Figure 4.49 shows a plot of pillow weight, normalized to the weight of the first pillow, versus pillow number for one of the resins. This plot is useful for slope analysis, which should give an indication of sagging and swell characteristics. It can be seen that

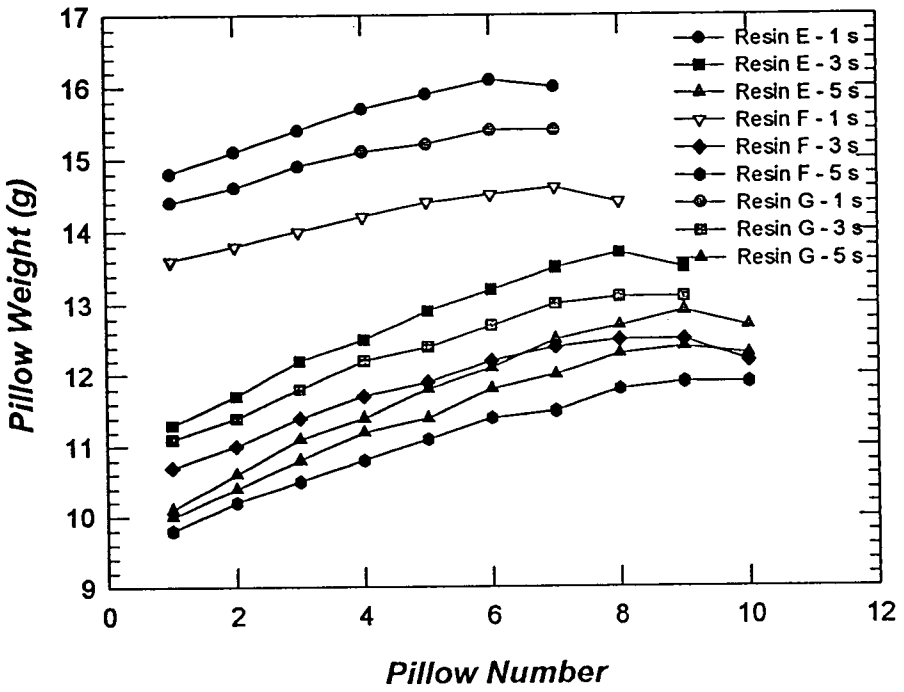

Figure 4.47 Variation in pillow weight of the three resins extruded at different drop times.

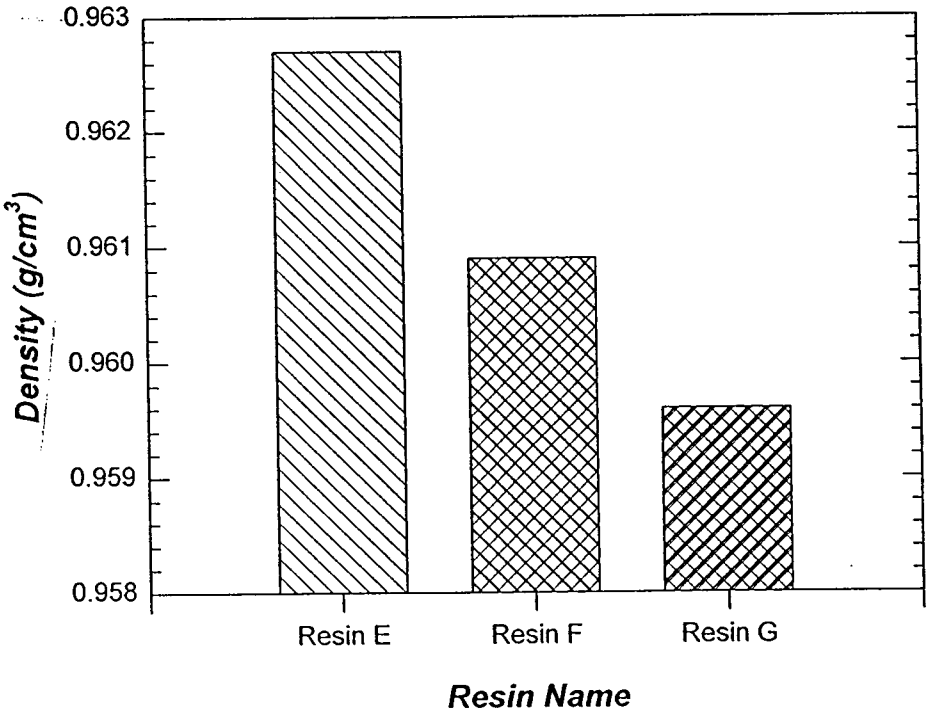

Figure 4.48 Density values for resin E, F, and G.

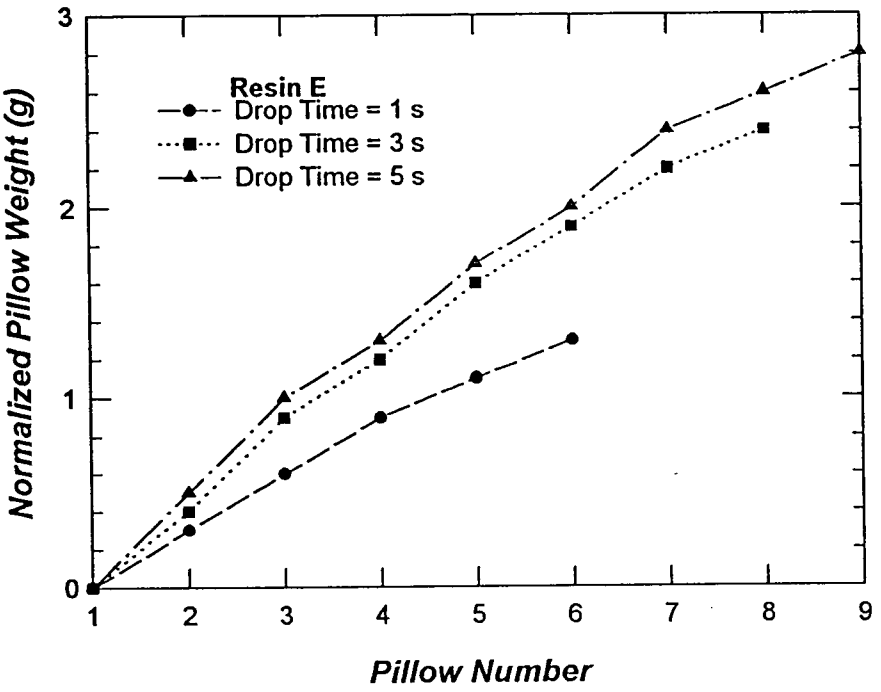

Figure 4.49 Pillow weight normalized to the weight of pillow number one to show the magnitude of sagging.

increasing parison drop time increases the slope of the curve. A steeper curve implies greater difference in the weight of the first and the last pillow, and hence, is an indication of greater sagging, provided no swell occurs. Therefore, for the same resin, having the same extrudate swell property, it can be seen that increasing parison drop time increases sagging.

When three resins having different swell properties and melt strengths are compared as in Figure 4.50, the slope of the curves is an indication of both the swell and sagging effects. One can see that for resin E, which has the lowest melt strength and highest swell, the slope is the steepest. Resin G, which has the highest melt strength, however,

has a curve which is steeper than that for resin F, which has a comparatively lower melt strength. This is due to the greater swell exhibited by resin G. The swell results in a downward force that is greater in the case of resin G. Hence, the difference in weight between the first and the last pillow for resin G is larger than that for resin F.

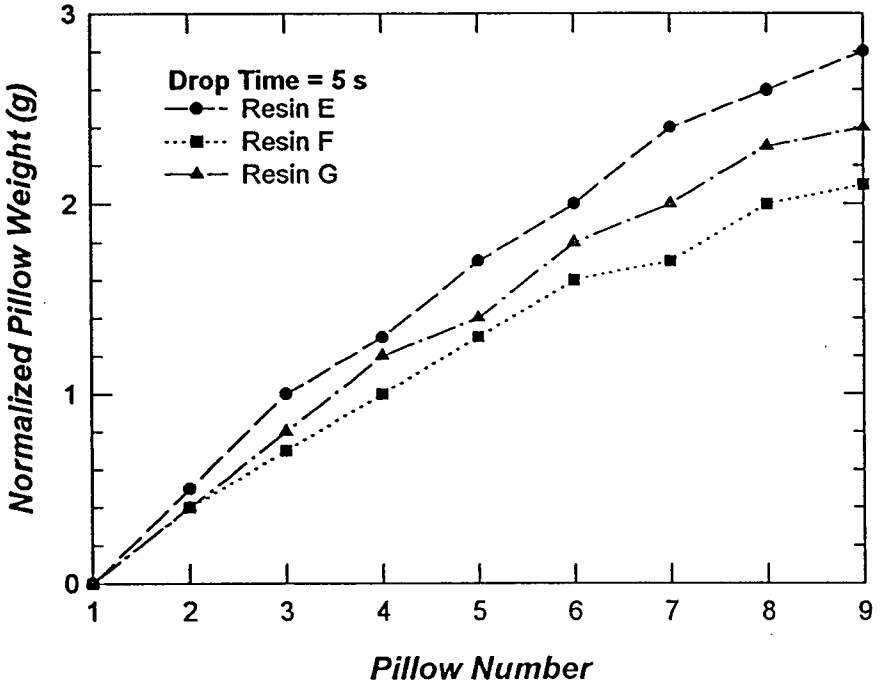

Figure 4.50 Comparison of parison sag between resin E, F, and G.

Figure 4.51 shows a plot of total parison length and weight for the three resins versus drop time. Considering the total length of the parison, the general trend is that parison length increases as drop time increases. Of course this is as expected, since longer parison time means more sagging. Also, for shorter drop times, swell dominates and tends to shorten the total parison length. The effect of swell can be seen more clearly by comparing the curves for the three resins. It can be seen that resin E, which has the highest swell, has the shortest parison length, while resin F, which has the lowest swell,

has the longest parison length. Note that the curves are closer for higher parison drop times, implying the competing effect of melt strength. When parison drop time is increased, sagging becomes more important, and the curves are expected to intersect and be ranked according to melt strength.

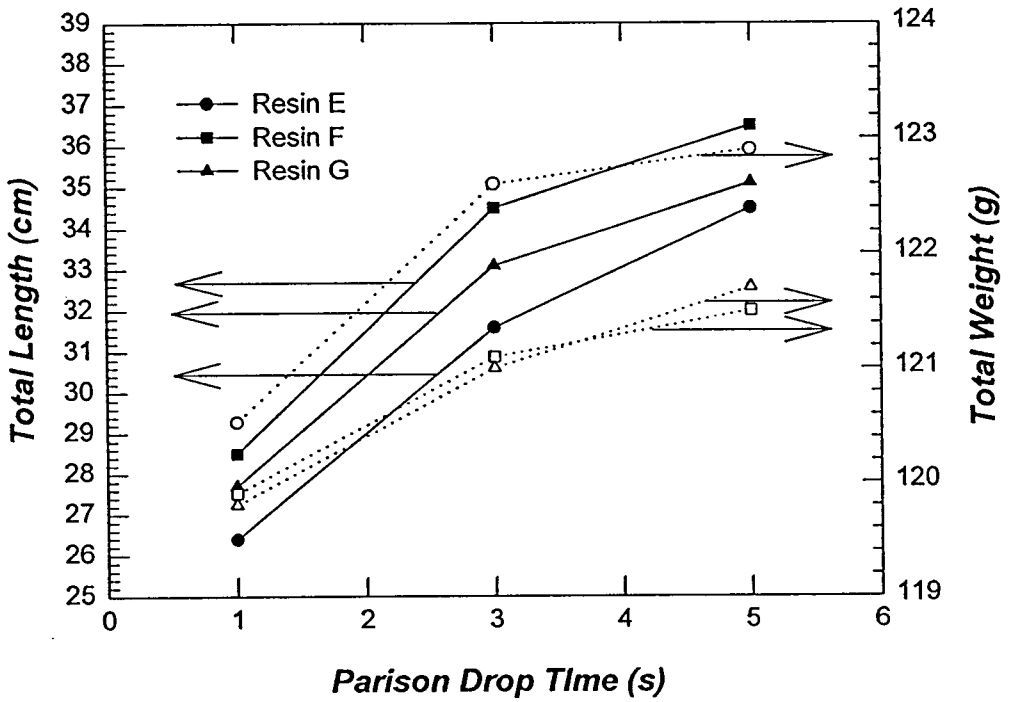

Figure 4.51 Total length and weight as a function of parison drop time. Although the total melt volume before extrusion was kept the same, the total length and weight of the parison were not constant, due to the fact that the mold was located at some distance below the die.

The competing effect of weight swell and parison sag can also be seen by considering the total parison weight versus drop time, though not as clearly. The same trend is observed when parison drop time is increased. However, resin E having the lowest melt strength and highest swell is shown to have the highest parison weight for all drop times. This is as expected since both lower melt strength and higher swell tend to increase total parison weight. For resin F and G, however, the trend is not as clear. Resin

G is expected to have higher total parison weight, since it has a higher swell. However, resin G has a higher melt strength compared to resin F. Since the two factors have opposite effects, the two curves become similar. Moreover, resin G has a lower density which should be taken into consideration.

From the above discussion, it can be concluded that melt behavior during parison formation is critically affected by melt strength and the swell properties of the resin. From the pillow mold experiments, however, it is difficult to determine the individual effects of these factors. Higher melt strength tends to reduce sagging, while higher swell reduces total parison length. Hence, the two effects are competing in opposite directions. It was also found that parison drop time has a significant effect on parison formation considering the dependence of shear rate on the drop time. A shorter drop time implies higher shear rate and higher swell, but shorter time for parison sag to occur.

4.4 MELT INDEX, STRESS EXPONENT AND MELT FLOW RATIO

Although melt index (*MI*) is not a material function, it is a convenient parameter that is often used by industry for resin comparisons. The main advantage of using *MI* is the ease at which it can be determined. It does not require elaborate equipment and can be done frequently and quickly. However, the reproducibility of *MI* data is very much dependent on the design of the equipment and the procedure used. It was mentioned earlier that a small change in the design of the equipment or the procedure may result in a very significant variation of the *MI* data.

Generally, *MI* is used for the analysis of reaction quality control. It serves to indicate the uniformity of the flow behavior of a polymer made by a particular process, and may

also be indicative of the uniformity of other properties. The value of *MI* is affected by the molecular weight of the polymer, as is the case with all other rheological and processing parameters. By performing experiments at different conditions, the stress exponent (*S.Ex.*) and melt flow ratio (*MFR*) can also be determined. In this work, an attempt was made to relate molecular, rheological and processing parameters to *MI*, *S.Ex.*, and *MFR*, to determine the possibility of using *MI*, *S.Ex.*, and *MFR* as an additional set of parameters to predict polymer behavior.

Figure 4.52 shows the relationship of *MI* to M_w. No useful mathematical correlation can be found as can be seen by the large scatter in the plot. However, approximate trends can be observed if the results are sorted according to polydispersity. Generally, the data

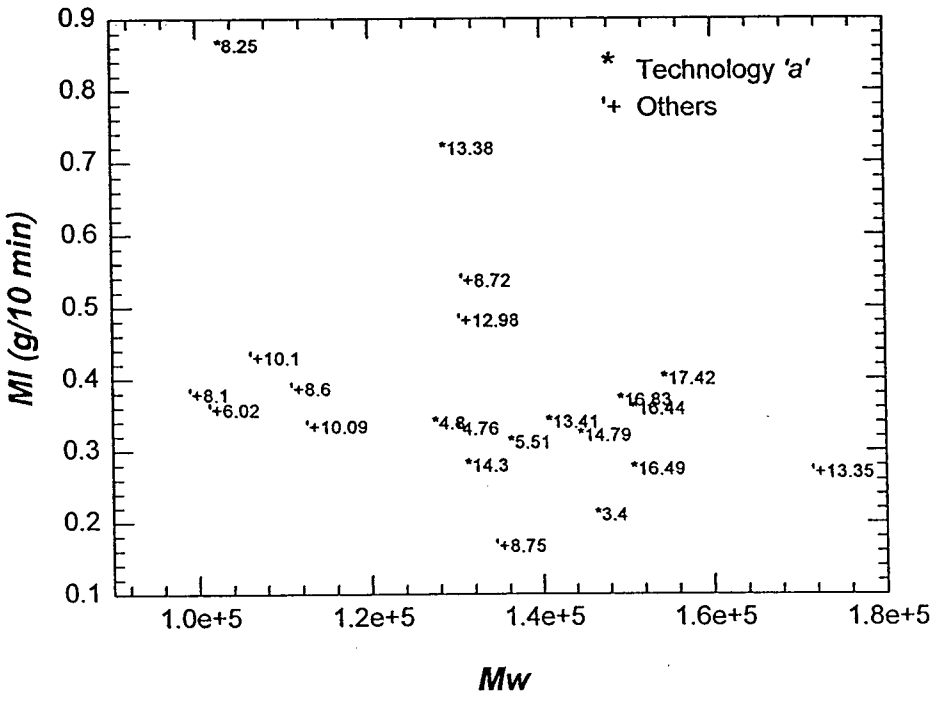

Figure 4.52 Correlating *MI* to M_w. Comparison should be made for resins with similar *PI*, or shear thinning properties.

show that increasing M_w decreases *MI*. Unfortunately, there are too few resins having similar *PI* that are produced using the same technology, making it difficult for a definite conclusion to be made.

MI is reported as the mass of a polymer that flows through a specific die under certain conditions over a period of ten minutes. Hence, higher *MI* values indicate faster flow and lower viscosity. By increasing M_w, *MI* decreases, and slower flow will result, indicating higher viscosity. This is consistent with the finding discussed earlier of the effect of M_w on shear viscosity. Therefore, *MI* can be used to predict viscosity. The effects of the molecular weight distribution and density should be reflected in the value of *MI*.

Figure 4.53 shows the implication of *MI* on shear viscosity. Since *MI* includes the effect of all molecular parameters, it is no longer necessary to differentiate between the resins according to their molecular weight distributions. The plot shows that increasing *MI* causes a decrease in shear viscosity, which is expected. A faster flowing polymer should have a higher *MI* and a lower viscosity. Considering the procedure followed to determine *MI*, however, it should be noted that *MI* should only be used to predict shear viscosity at a low deformation rates. Also, in comparing resins using *MI* values, the difference in *MI* should be large enough for a difference in shear viscosity curve to be observable. This problem has also been reported by Yoshikawa *et al.* (1990). Moreover, *MI* should only be used to compare resins manufactured using the same technology such as those shown in Figure 4.53. This is consistent with the previous analysis of the

viscosity profile. It is not possible to predict the shear flow behavior of resins from different technologies using *MI*.

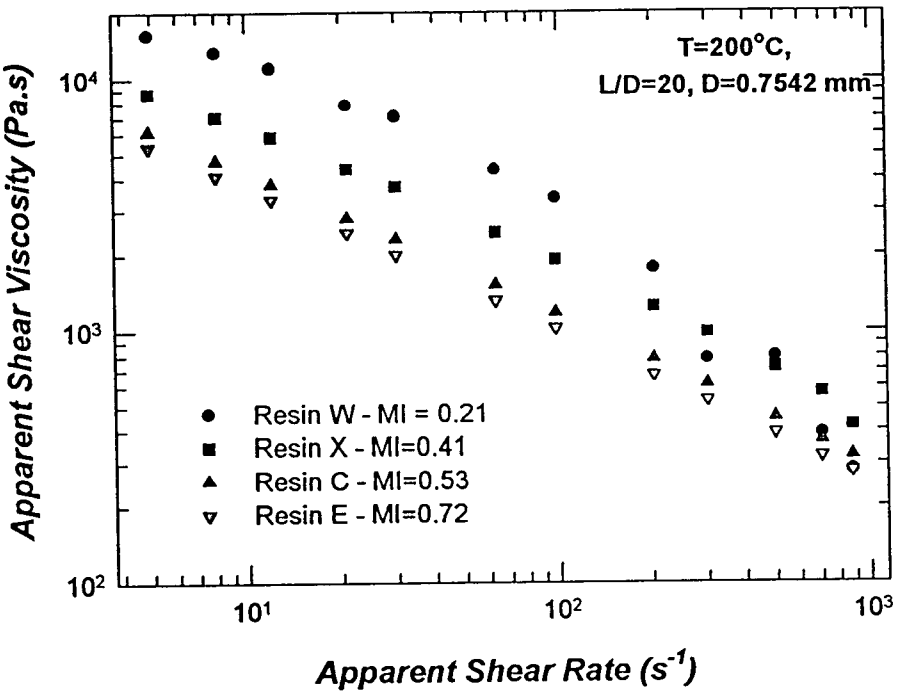

Figure 4.53 Implication of *MI* on shear viscosity curves.

It was also found that *MI* could be used to predict melt strength, as long as melt strength is defined and determined according to the procedure described in this work. Figure 4.54 shows the relationship between *MI* and melt strength. Again, differentiation has to be made with respect to the technology used to produce the resins. One can clearly see a general trend of decreasing melt strength with increasing *MI* from Figure 4.54. It is noted that the three polydispersity groups required in the analysis of melt strength are not reflected in this case. Also, it is interesting to note that resins produced using

technologies other than *'a'* have much higher melt strength. This can be attributed to the polydispersities of these resins, which fall mostly near the critical range of eight to ten.

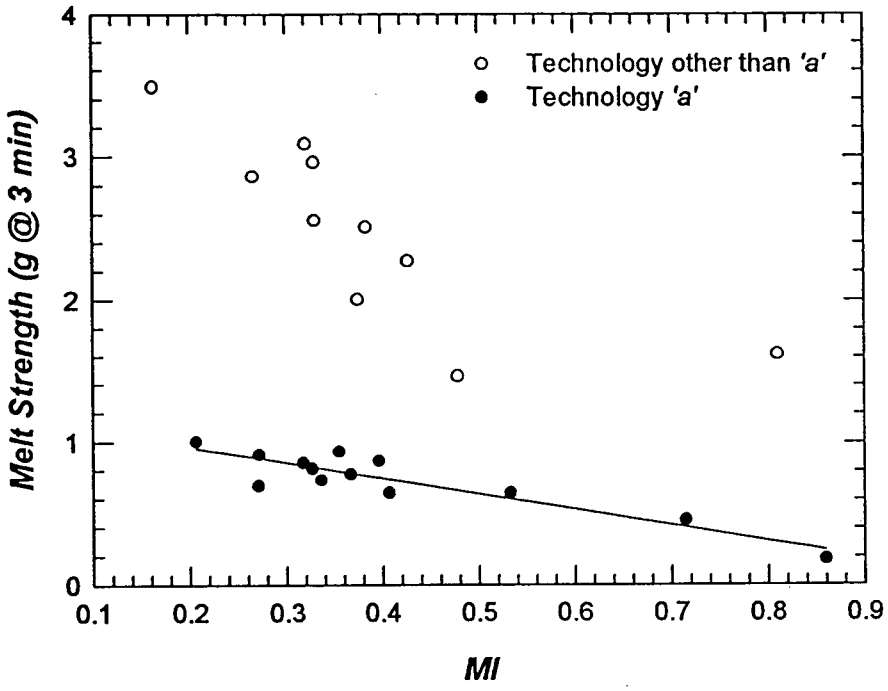

Figure 4.54 Correlation between melt strength and *MI*.

S.Ex. and *MFR* are both indicative of the shear thinning property of a resin. Considering the way the two parameters are calculated, it is apparent that *S.Ex.* and *MFR* show the differences in polymer flow under two different pressures. Hence, higher *S.Ex.* and *MFR* values indicate stronger shear thinning behavior in the shear viscosity curves. However, it is important to note that only comparisons of resins with similar *MI* are made, in order to show this. *S.Ex.* shows the shear thinning behavior in the narrow and smaller range of deformation, while *MFR* encompasses a larger range of deformation.

It was not possible to find a useful correlation between *S.Ex.* or *MFR* and the molecular parameters. However, knowing their significance, it is possible to use *S.Ex.* and *MFR* to predict the shear viscosity behavior of resins with similar *MI*. Figure 4.55 shows this observation. Increasing *S.Ex.* or *MFR* results in greater shear sensitivity of a polymer flow. Unfortunately, in this work, there are too few resins that are manufactured using the same technology and have similar *MI*.

In trying to relate *S.Ex.* or *MFR* to extrudate swell, no general trend was observed.

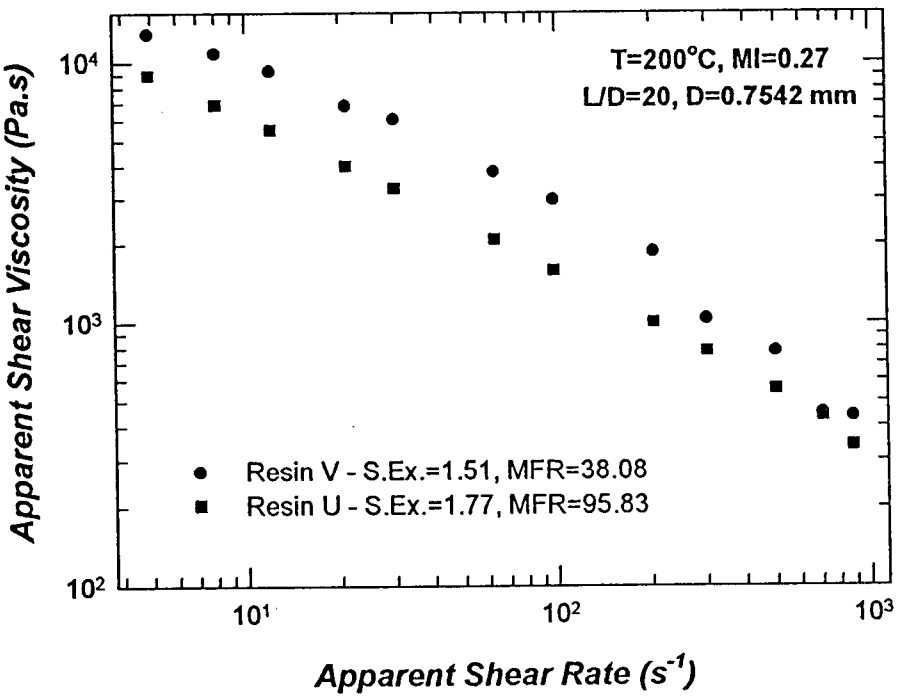

Figure 4.55 Implication of *S.Ex.* on shear viscosity profile.

Figure 4.56 shows a plot of *S.Ex.* versus *MFR*. It can be seen that generally, higher *S.Ex.* reflects higher *MFR*. This observation implies the redundancy of measuring *MFR* when *S.Ex.* data are available.

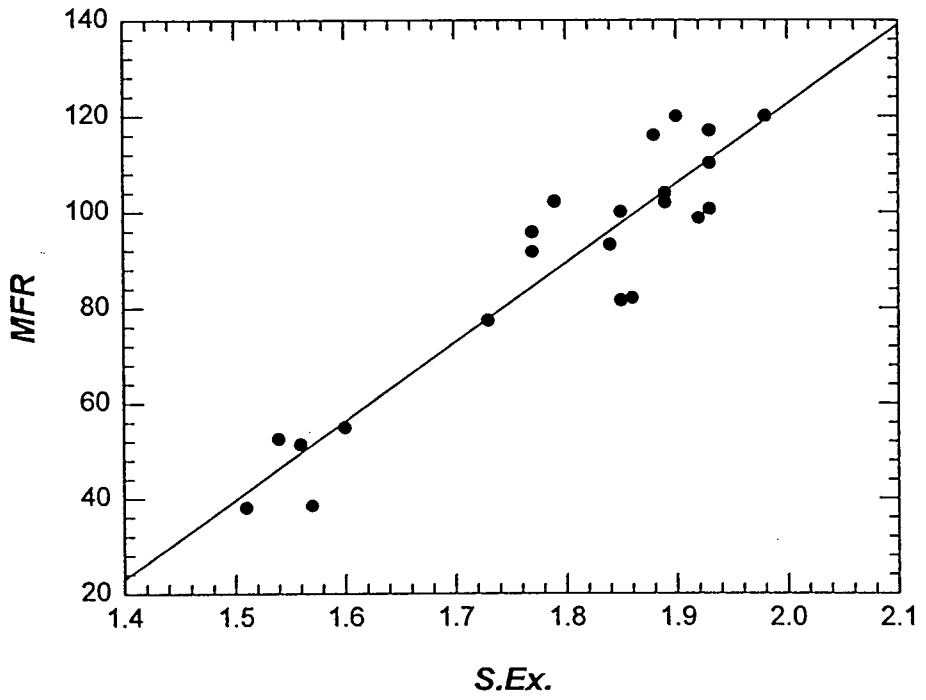

Figure 4.56 Correlation between *MFR* and *S.Ex.*

From this analysis, it can be concluded that *MI* and *S.Ex.* are useful for predicting shear flow behavior at low deformation rates. It is not possible to relate *MI* and *S.Ex.* to the extensional flow properties due to the different type of deformation involved. *MI* can also be used to predict melt strength. As far as extrudate swell is concerned, no useful

correlation was found. Moreover, *MI*, *S.Ex.* and *MFR* are only useful for comparing similar resins produced using the same technology.

4.5 IMPLICATIONS OF RHEOLOGICAL BEHAVIOUR ON PROCESSABILITY

As mentioned earlier, the process of blow molding is governed principally by the rheological behavior of the resin used. The molecular weight and its distribution, in turn, affect the way the resin behaves rheologically. It has been discussed how the molecular parameters affect the rheology of blow molding resins. It is now useful to consider the implications of rheology on processability.

The shear viscosity of a resin provides information about the ease of flow of the material. Hence, information on shear viscosity is particularly useful during the extrusion of the material through the die head. Higher shear viscosity implies that more power is required to extrude the polymer, if extrusion is to be done at a particular temperature. Otherwise, the temperature has to be raised to lower the material viscosity. However, by increasing the extrusion, and possibly, the blowing temperature, a longer cycle time will be required to cool the molded product.

The sensitivity of viscosity to temperature and shear rate is also important to maintain consistency in the manufacturing of blow molding products. It may be undesirable to use a polymer that is very sensitive to changes in temperature and shear. Although process variables, such as extrusion speed and barrel temperature, are normally well controlled, small variations due to process noise are inevitable. By using resins that are very sensitive to small changes in these variables, inconsistency in the final molded

product will result. On the other hand, if a resin exhibits large shear thinning behavior, it will have higher viscosity at low shear rates and lower viscosity at the processing shear rates. This is desirable since it means that the resin is easy to extrude through the die but at the same time does not flow as easily during subsequent parison formation when there is a very small rate of deformation (recall that the zero shear rate viscosity is related to the extensional viscosity). Hence, a trade off has to be made depending on the use and importance of the molded product.

During parison formation, it is important that the polymer melt has sufficient melt strength to counteract sagging. Considering the nature of sagging, the rheological properties applicable in this case would be the extensional flow properties of the resin. It has been shown that the Hencky strain correlates well with melt strength, at least qualitatively. This can again be seen in Figure 4.57, where the strain versus time curves were plotted for several resins having different melt strength values. Hence, it is desirable to use resins that show comparatively lower Hencky strains under creep conditions.

Extrudate swell is also important during parison formation. As discussed earlier, increasing extrudate swell indicates an increase in weight swell. For resins with large swell, this means that the downward force pulling on the melt during parison formation is greater, resulting in greater sag. Sagging is, of course, undesirable since it results in products with uneven wall thickness.

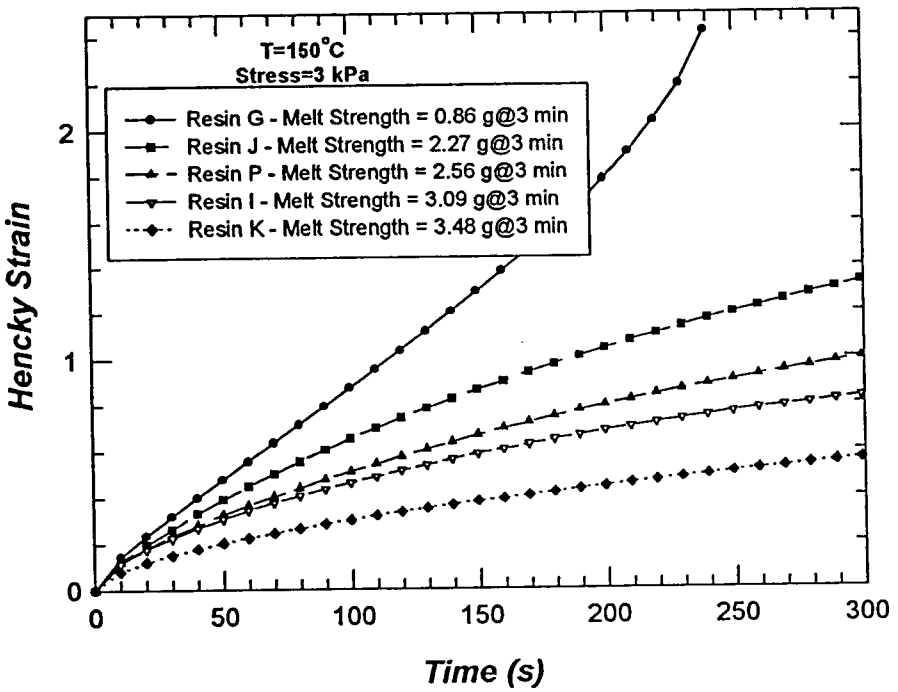

Figure 4.57 Implication of melt strength on Hencky strain.

The sensitivity of swell is probably a more important parameter to consider than the absolute magnitude of the swell. The magnitude of the swell determines the weight and the wall thickness of the final product, and this can be controlled by adjusting the position of the mandrel to an optimum one. Hence, it is useful to be able to predict the swell magnitude. Unfortunately, as has been shown in this work, this is difficult to do. The sensitivity of swell to small variations in process variables, however, is not as easy to control. Hence, it is important that the swell property of a blow molding resin is relatively insensitive to small changes in shear rate (or temperature). If a resin is very sensitive to changes in shear rate, for example, the final molded product will not have consistent weight, and this is of course undesirable.

In conclusion, the optimal design of the different parts of blow molding process require different resin properties. Considering the complex effect of molecular properties on both the rheology and processability of HDPE resins, one often has to make choices that involve some trade-off between two or more resin properties. The importance of each of these properties, on the other hand, is determined by the use of the final product. Hence, it is very difficult to say that a specific resin is the best for a particular application. In the design of a resin, consideration and careful weighing have to be made in regard to its application and economic implications.

From the results of this study, however, some useful recommendations can still be made in regard to resin design. Understanding the blow molding process and knowing the general processability requirements for blow molding resins, it can generally be said that, ideally, a blow molding resin should have:

- reasonable viscosity,
- a viscosity profile that is not very sensitive to temperature and shear rate variations,
- an extrudate swell profile that is not very sensitive to temperature and shear rate variations, and
- high melt strength.

Using the results of this study, one may conclude that one simple way to produce a blow molding resin with these requirements would be to optimize the concentration of medium

sized molecules, represented by M_w. Increasing M_w will increase the melt strength of the resin, while not affecting the sensitivity of shear viscosity to temperature variations significantly. By increasing M_z, melt strength will also increase, but the resin will become more sensitive to changes in temperature and this is, of course, undesirable. Increasing M_w will also increase the polydispersity. This may affect the sensitivity of shear viscosity to variations in shear rate. However, the effect will not be very significant compared to when polydispersity is increased by decreasing M_n (increasing the concentration of smaller molecules). Moreover, by increasing M_w, and hence, the polydispersity, the extrudate swell profile becomes less sensitive to shear rate variations in the processing range between 350 s^{-1} to 700 s^{-1}. Therefore, generally, it can be said that a resin with a comparatively high M_w value and low M_z value will process better. As far as M_n is concerned, it has to be optimized accordingly, depending on M_w and polydispersity.

5 CONCLUSIONS

Polymer science is still an inexact science, due to the many possible manifestations of molecular structure, resulting in interesting polymeric behavior. In this work, an attempt was made to correlate the rheology and processability of HDPE resins to molecular weight and its distribution through the study of twenty four commercial HDPE blow molding resins. The resins vary greatly in terms of molecular parameters, such as M_w, *PI*, and density. These are commercial resins produced from a number of different technologies, since it is not possible to produce resins with broad range of molecular parameters using a single polymerization technology. However, with this set of commercial resins produced from different technologies, it was not possible to systematically study the individual effects of specific molecular parameters. Hence, multiple regression was used as a tool for data analysis, wherever possible. In some cases, however, the molecular parameters are insufficient in describing the molecular weight distribution. In these cases, the actual qualitative comparisons of the distribution curves were performed.

The conclusions of this study are summarized as follows:

Shear Flow Properties:

- The expected effects of M_w and polydispersity on shear viscosity were confirmed. Increase of M_w and polydispersity increases the magnitude of shear viscosity and its tendency to shear thin, respectively. The effect of polydispersity has been found to be mainly due to the changes in the concentration of smaller molecules. Broadening the

molecular weight distribution by increasing the concentration of larger molecules does not seem to affect the shear thinning property of the resins as significantly.

- It was also found that it is only useful to compare the shear properties of resins produced using the same technology. Different reactors, solvents, catalysts and additives appear to cause the shear properties of the resins to be non-comparable.

- The activation energies of the HDPE flow curves were found to range from 20 kJ/mol to 28 kJ/mol.

- It was found that the resins have to be grouped according to their polydispersity index, into those with $PI<8$, $8<PI<10$, and $PI>10$ in order to obtain good correlations between the flow activation energy and molecular parameters. For narrowly distributed resins, there is no apparent correlation between molecular parameters to E_a. Above the polydispersity of eight, it was found that increasing polydispersity increases the temperature sensitivity of viscosity, with the effect mainly contributed by the increase in the concentration of smaller molecules. For PI greater than ten, however, the concentration of larger molecules becomes important and increasing it will increase both the polydispersity and E_a.

Extensional Flow Properties:

- Increasing M_w expectedly decreases the magnitude of Hencky strain and increases the extensional viscosity in creep experiments.

- Hencky strain can be related to melt strength in an inverse manner, i.e. lower Hencky strain at a constant time indicates higher melt strength.

- It was found that increasing polydispersity up to about nine decreases the Hencky strain. For *PI>9*, broadening the molecular weight distribution initially increases the Hencky strain. For broadly distributed resins (*PI>16*), the effect of polydispersity on Hencky strain becomes insignificant.

Extrudate swell:

- No correlation could be found to exist between the molecular weight averages and the shape of the molecular weight distribution to the magnitude of extrudate swell. This is probably due to the possibility of the effect of pre-shear history being more important than the effect of molecular weight distribution. Since the resins studied in this work may have been subjected to deformations in unknown and different ways, it is possible for resins with the same molecular weight distributions to show very different extrudate swell profiles.

- It is also thought that differences in polymerization technology may result in some variations in the degree of unsaturation, which may not be reflected in molecular weight distribution curves, but which may affect the elastic properties of the polymers significantly.

- The sensitivity of extrudate swell, however, was found to correlate well with M_z and polydispersity. Broadening the molecular weight distribution by increasing the concentration of larger molecules increases shear sensitivity at lower shear rates (5 s^{-1} to 350 s^{-1}) and decreases it at the higher shear rates (350 s^{-1} to 700 s^{-1}).

Melt Strength:

- Three polydispersity groups have to be identified in order to correlate melt strength to molecular parameters, i.e. resins with $PI<8$, $8<PI<10$, and $PI>10$.

- Increasing M_w was found to increase melt strength.

- Increasing polydispersity for resins with $PI \leq 8$ was found to increase melt strength. For resins with higher polydispersity $(PI>10)$, however, broadening molecular weight distribution decreases the melt strength.

- It was also found that density affects melt strength in an inverse manner, i.e. increasing density decreases melt strength.

Sagging and Weight Swell Characteristics:

- The individual effects of sagging and weight swell are difficult to differentiate in pillow mold experiments.

- Sagging and weight swell are reflected by melt strength and extrudate swell, respectively.

- Parison drop time has a significant effect on parison quality. For short parison drop times, the effect of weight swell dominates. For longer parison drop times, the effect of sagging becomes more important.

- Sagging and weight swell determine the total parison weight and length.

MI, S.Ex., and *MFR*:

- These parameters are only particularly useful for resin quality control (for the same technology).

- It may be possible to correlate *MI* to M_w for resins of the same technology and similar polydispersity, in which case *MI* is expected to be inversely proportional to M_w.

- *MI* can be used to predict shear viscosity at low shear rate as long as comparisons are made within the resins produced using the same technology.

- *MI* can also be used to predict melt strength of resins of the same technology.

- *S.Ex.* and *MFR* are indicative of the shear thinning behavior of a resin. Similarly, these parameters are technology dependent, and in addition, comparisons should only be made for resins with the same *MI*.

- *S.Ex.* and *MFR* are essentially useful for the same purpose.

In addition, it is possible to determine the molecular weight range that is critically affecting a certain polymer property by correlating the normalized area under the molecular weight distribution for each combination of molecular weight ranges to the desired property.

These conclusions are summarized in Table 5.1.

Table 5.1 Summary of conclusions.

Properties	Increasing Low MWD Tail *(Decreasing Mn)*	Increasing Medium MWD Portion *(Increasing Mw)*	Increasing High MWD Tail *(Increasing Mz)*	Increasing Density	Remarks
Rheology:					
Shear Viscosity	↓	↑	↑	-	Technology Dependent
Shear Thinning	↑	-	-	-	Technology Dependent
Ea	unknown	unknown	unknown	-	PI<8
	↑	↑	-	-	8<PI<10
	↕	-	↑	-	PI>10
Tensile Viscosity	-	↕	↕	-	
Hencky Strain	↓	↕	↕	unknown	PI<8
	-	↕	↕	↑	8<PI<10
	↑	↓	↓	↑	PI>10
Die Swell	unknown	unknown	unknown	-	Resins are non-comparable
Shear Sensitivity of Swell	-	-	↑	-	$5s^{-1}$ to $350s^{-1}$
	↓	-	-	-	$350s^{-1}$ to $700s^{-1}$
Processability:					
Melt Strength	-	↑	↑	-	PI<8
	-	↑	-	↓	8<PI<10
	↓	↑	-	↓	PI>10
Weight Swell	-	-	-	-	Increases with increasing die swell
Sagging	-	-	-	-	Increases with decreasing melt strength
					Increases with increasing weight/die swell
MI, S.Ex., MFR:	-	-	-	-	More useful to be compared to rheological properties and processability than to molecular parameters
					Technology Dependent

6 RECOMMENDATIONS

Based on the experience gained during this study, the following recommendations can be made for future work:

- The swell behavior and hence, the sagging and weight characteristics of a parison is governed by the elastic nature of the resins. By measuring the elastic recoil properties of a resin, one may be able to obtain a correlation suitable for predicting extrudate swell. A Melt Elasticity Indexer can be used for this purpose. If this proves to be possible, the unit can be implemented onsite in the plant as an easy and convenient way of predicting extrudate swell.

- Extrudate swell has been found to depend more strongly on the pre-shear history of the resin than on its molecular characteristics. Since it is important to be able to predict extrudate swell, a study should be conducted on resins produced using the same technology and having the same pre-shear history. By performing such study, correlation between extrudate swell and molecular parameters should become more apparent. A thorough molecular weight characterization will be very useful in such a study.

- It has been found that different polymerization technologies produce resins that may have the same molecular weight distributions but which may differ significantly in terms of rheology and processability. Possible reasons include the type of reactor used (dual or single reactor), the catalyst, the monomers used for polymerization, and various additives. A study should be conducted to investigate the differences in technology and how they affect the rheology and processability of a resin.

- Similar experiments may be conducted to investigate the effect of branching distribution, type of branching, and additives on the rheology and processability of HDPE resins. Also, the molecular effects on other physical properties of HDPE, such as environmental stress cracking resistance (ESCR) can be studied.

REFERENCES

Acierno, D., D. Curto, F. P. La Mantia, and A. Valenza, *Flow Properties of Low Density/Linear Low Density Polyethylenes*, Polym. Eng. Sci., **26** (1), 28 – 33 (1986)

Ajroldi, G., *Determination of Rheological Parameters from Parison Extrusion Experiments*, Polym. Eng. Sci., **18** (10), 742 – 9 (1978)

ASTM, *Standard Test Method for Flow Rates of Thermoplastics by Extrusion Plastometer*, D1238, 1995

Bagley, E. B., *End Corrections in the Capillary Flow of Polyethylene*, J. Appl. Phys., **28**, 624 (1957)

Bersted, B. H., *A Model Relating the Elastic Properties of High – Density Polyethylene Melts to the Molecular Weight Distribution*, J. Appl. Polym. Sci., **20** (10), 2705 – 14 (1976)

Bethea, R. M., B. S. Duran, and T. L. Boullion, Statistical Methods for Engineers and Scientists, 2nd ed., Marcel Dekker, Inc., NY, 1985

Bremner, T., *Personal Communication*, NOVA Research and Technology Center, 1998

Cannady, J. L., *Blow Molding – New Developments*, Seminar Presented by Program Division, Technomic Publishing Company Inc., PA, 1988

Carella, J. M., J. T. Gotro, and W. W. Graessley, *Thermorheological Effects of Long – Chain Branching in Entangled Polymer Melts*, Macromolec., **19**, 659 – 67 (1986)

Charrier, J. M., Polymeric Materials and Processing, Plastics, Elastomers, and Composites, Hanser, NY, 1990

CIL Inc., Polymers – Polyethylene, Technical Publication, Ont

Dealy, J. M., and K. F. Wissbrun, Melt Rheology and Its Role in Plastics Processing: Theory and Applications. Reinhold, NY, 1995

Dealy, J. M., Rheometers for Molten Plastics: A Practical Guide to Testing and Property Measurement, Van Nostrand Reinhold, NY, 1982

Goyal, S. K., *Influence of Polymer Structure on the Melt Strength Behavior of Polyethylene Resins*, ANTEC'94, 1232 – 8 (1994)

Goyal, S. K., *Personal Communication*, NOVA Research and Technology Center, 1998

Graessley, W. W., *Viscosity of Entangling Polydisperse Polymers*, J. Chem. Phys., **47**, 1942 – 53 (1967)

Han, C. D., and C. A. Villamizar, *Effects of Molecular Weight Distribution and Long-Chain Branching on the Viscoelastic Properties of High - and Low - Density Polyethylene Melts*, J. Appl. Polym. Sci., **22** (6), 1677 – 700 (1978)

Hatzikiriakos, S. G., and J. M. Dealy, *Wall Slip of Molten High Density Polyethylene. II. Capillary Rheometer Studies*, J. Rheol., **36** (4), 703-741 (1992)

Hatzikiriakos, S. G., *The Onset of Wall Slip and Sharkskin Melt Fracture in Capillary Flow*, Polym. Eng. Sci., **34** (19), 1441 – 9 (1994)

Henze, E. D., and W. C. L. Wu, *Variables Affecting Parison Diameter Swell and Their Correlation with Rheological Parameters*, Polym. Eng. Sci., **13** (2), 153 – 9 (1973)

Kamal, M. R., and K. T. Nguyen, *Analysis of the Blow Molding Process: Review and Recent Developments, in Polymer Rheology and Processing*, A. A. Collyer, and L. A. Utracki (eds.), Elsevier Applied Science, NY, 1990

Kaylon, D. M., and M. R., Kamal, *An Experimental Investigation of Capillary Extrudate Swell in Relation to Parison Swell Behavior in Blow Molding*, Polym. Eng. Sci., **26** (7), 508 – 16 (1986)

Kazatchkov, I. B., N. Bohnet, S. K. Goyal, and S. G. Hatzikiriakos, *Influence of Molecular Structure on the Rheological and Processing Behavior of Polyethylene Resins*, Polym. Eng. Sci., Accepted for Publication, Dec (1997)

Koopmans, R. J., *Die Swell – Molecular Structure Model for Linear Polyethylene*, J. Polym. Sci., Part A, **26**, 1157 (1988)

Koopmans, R. J., *Extrudate Swell of High Density Polyethylene. Part II: Time Dependency and Effects of Cooling and Sagging*, Polym. Eng. Sci., **32** (23), 1750 – 4 (1992a)

Koopmans, R. J., *Extrudate Swell of High Density Polyethylene. Part III: Extrusion Blow Molding Die Geometry Effects*, Polym. Eng. Sci., **32** (23), 1755 - 64 (1992b)

Koopmans, R. J., *Extrudate Swell of High Density Polyethylene. Part I: Aspects of Molecular Structure and Rheological Characterization Methods*, Polym. Eng. Sci., **32** (23), 1741 – 9 (1992c)

La Mantia, F. P., and D. Acierno, *Influence of the Molecular Structure on the Melt Strength and Extensibility of Polyethylenes*, Polym. Eng. Sci., **25** (5), 279 – 83 (1985)

La Mantia, F. P., and D. Acierno, *Melt Strength and Extensibility of High Density Polyethylene*, Plas. Rubber Process. Appl., 5 (2), 183 – 5 (1985)

Levy, S., and J. H. Du Bois, Plastics Product Design Engineering Handbook, Van Nostrand Reinhold, NY, 1977

Mavridis, H., and R. N. Shroff, *Temperature Dependence of Polyolefin Melt Rheology*, Polym. Eng. Sci., **32** (23), 1778 – 91 (1992)

Meissner, J., *Development of a Universal Extensional Rheometer for the Uniaxial Extension of Polymer Melts*, Trans. Soc. Rheol., **16** (3), 405 – 20 (1972)

Mendelson, R. A., and F. L. Finger, *High – Density Polyethylene Melt Elasticity: Anomalous Observations on the Effects of Molecular Structure*, J. Appl. Polym. Sci., **19** (4), 1061 – 78 (1975)

Michael, L. B. (ed.), Plastics of Engineering Handbook of the Society of the Plastic Industry, Inc., Van Nostrand Rheinhold, NY, 1991

Munstedt, H., and H. M. Laun, *Elongational Behavior of a Low – Density Polyethylene Melt. Transient Behavior in Constant Stretching Rate and Tensile Creep Experiments. Comparison with Shear Data. Temperature Dependence of the Elongational Properties*, Rheol. Acta., **18**, 492 (1979)

NOVACOR, *Density by Means of the Densimeter, Laboratory Test Procedures Manual*, 1993

NOVACOR, *Determination of the Melt Strength of Polyethylene Using a Rheometric RER-9000 Extensional Rheometer*, Laboratory Test Procedures Manual, 1994

Ogorkiewicz, R. M. (ed.), Engineering Properties of Themoplastics, A Collective Work Produced by Imperial Chemical Industries Limited, Plastics Division, Wiley-Interscience, NY, 1970

Progelhof, R.C., and J. L. Throne, Polymer Engineering Principles: Properties, Processes, Testing for Design, Hanser, NY, 1993

Ramamurthy, A. V., *Wall Slip in Viscous Fluids and Influence of Materials of Construction*, J. Rheol., **30** (2), 337 – 57 (1986)

Rauschenberger, V., and H. M. Laun, *A Recursive Model for Rheotens Tests*, SPE J. Rheol., **41** (3), 719 – 37 (1997)

Rosato, D. V., and D. V. Rosato (eds.), Blow Molding Handbook, Hanser, NY, 1989

Saini, D. R., and A. V. Shenoy, *Viscoelastic Properties of Linear Low Density Polyethylene Melts*, Eur. Polym J., **19** (9), 811 – 16 (1983)

Shenoy, A. V., S. Chattopadhyay, and V. M. Nadkarni, *From Melt Flow Index to Rheogram*, Rheol. Acta, **22**, 90 – 101 (1983)

Shroff, R. N., and S. Mitsuzo, *Effect of Molecular Weight and Molecular Weight Distribution on Elasticity of Polymer Melts*, Soc. Plast. Eng., Tech. Pap., **23**, 285 – 9 (1977)

Shroff, R., A. Prasad, and C. Lee, *Effect of Molecular Structure on Rheological and Crystallization Properties of Polyethylenes*, J. Polym. Sci., Part B, **34**, 2317 – 33 (1996)

Van Krevelen, D. W., Properties Of Polymers: Their Correlation with Chemical Structure; Their Numerical Extimation and Prediction from Additive Group Contributions, Elsevier, NY, 1990

Vetterling, W. T., W. H. Press, S. A. Teukolsky, and B. P. Flannery, Numerical Recipes: Example Book (FORTRAN), Cambridge University Press, NY, 1987

Wilson, N. R., M. E. Bentley, and B. T. Morgan, *How Extrusion Variables Affect Parison Swell*, SPE J., **26**, 34 – 40 (1970)

Winter, H. H., *A Collaborative Study on the Relation Between Film Blowing Performance and Rheological Properties of Two Low - Density and Two High – Density Polyethylene Samples*, Macromolec. Div., Commission on Polymer Characterization and Properties, IUPAC, Pure and Appl. Chem., 55 (6), 943 – 76 (1983)

Yoshikawa, K., N. Toneaki, Y. Moteki, M. Takahashi, and T Masuda, *Dynamic Viscoelasticity and Stress Relaxation of Column – Fractionated High Density Polyethylene Melts*, J. Soc. Rheol., Japan, **18**, 87 - 92 (1990)

Yoshikawa, K., N. Toneaki, Y. Moteki, M. Takahashi, and T. Masuda, *Dynamic Viscoelasticity, Stress Relaxation, and Elongational Flow Behavior of High Density Polyethylene Melts*, Nippon Reorogii Gaku Kaishi, **18**, 80 - 6 (1990)

NOTATION

a, b, c, d, e, f	Polymerization technology
A	Cross sectional area (m^2)
A_o	Cross sectional area before deformation (m^2)
a_T	Shift factor
b	Rabinowitsch correction
C^o_1, C^o_2	WLF constants
D	Diameter (m)
D_o	Diameter before deformation (m)
E	Tensile relaxation modulus (Pa)
E_a	Activation energy (kJ/mol)
F	Force (N)
G*	Complex modulus (Pa)
G	Shear relaxation modulus (Pa)
G'	Storage modulus (Pa)
G"	Loss modulus (Pa)
G_i	Discrete relaxation modulus (Pa)
h	Distance between two parallel plates (m)
I_2, I_6, I_{21}	Polymer flow rate under different conditions (g/10 minutes)
K	Power law constant ($Pa.s^n$)
L	Length (m)
L_o	Length before deformation (m)
M	Molecular weight of monodisperse polymer (kg/kmol)
M_i	Molecular weight of polymer chain *i* (kg/kmol)
M_n	Number average molecular weight (kg/kmol)
M_o	Location parameter in the 'log-normal' distribution curve ($kg/\{kmol.exp[\ln(kmol/kg)^{1/2}]\}$)
M_w	Weight average molecular weight (kg/kmol)
M_z	*Z*-average molecular weight (kg/kmol)
M_{z+1}	(*Z*+*1*)-average molecular weight (kg/kmol)

n	Power law exponent
n_i	Number average of polymer chain *i*
P	Pressure (Pa)
P_a	Ambient pressure (Pa)
P_d	Barrel driving pressure (Pa)
P_{end}	Pressure end correction (Pa)
Q	Volumetric flow rate (m^3/s)
R, r	Radius (m)
t	Time (s)
T	Temperature (K)
To	Reference temperature (K)
T_g	Glass transition temperature (K)
V	Velocity (m/s)
w	Weight fraction
w_i	Weight fraction of polymer chain *i*
X, x	Horizontal distance (m), or direction
β	Scale parameter in the 'log-normal' distribution curve
Δ	Quantity change
ε	Hencky strain
ε_o	Extensional Strain magnitude
$\dot{\gamma}_A$	Apparent wall shear rate (s^{-1})
$\dot{\gamma}_o$	Shear rate (s^{-1})
γ_o	Shear magnitude
$\dot{\gamma}_w$	True wall shear rate (s^{-1})
η	Shear viscosity (Pa.s)
η^*	Complex viscosity (Pa.s)
η_E	Extensional Viscosity (Pa.s)
η_o	Zero shear rate viscosity (Pa.s)
λ_i	Discrete relaxation time (s)

σ	Shear stress (Pa)
σ_E	Extensional stress (Pa)
σ_w	Wall shear stress (Pa)
ω	Frequency of oscillation (s^{-1})

APPENDIX A: Time Temperature Superposition Program Code

```
************************************************************************
*                                                                      *
*                          Alfonsius Budi Ariawan                      *
*                    Department of Chemical Engineering                *
*                    The University of British Columbia                *
*                             Vancouver, B.C.                          *
*                                                                      *
*                                                                      *
*     SUMMARY:                                                         *
*     The following program reads in sets of shear stress data as a function  *
*     of temperature and shear rate.  A master curve for the specific polymer  *
*     is then calculated corresponding to a specified reference temperature.   *
*     The shift factor is then correlated using either a simple thermally      *
*     activated model(Arrhenius), WLF model or both, depending on the desire   *
*     of the user.  An option is also provided to calculate the shear          *
*     viscosity of the polymer at a desired temperature and shear rate.        *
*                                                                      *
************************************************************************

      PROGRAM SHIFT
      IMPLICIT DOUBLE PRECISION (A-H,O-Z)
      DIMENSION TEMP(20),SRT(20,200),STRESS(20,200)
      DIMENSION SD(20,200),NDATA(20)
      DIMENSION ASRT(500),ASTRESS(500),AT(20)
      DIMENSION X(20),Y(20),A(2),AGUESS(2),SUMSQ(20)
      INTEGER CHOICE
      CHARACTER * 100 FNAME(20)
      CHARACTER * 100 COMMENT
      PARAMETER (TOL=2.D-5)
      COMMON/BLKA/Q(300),R(301),S(300)
      COMMON/BLKC/ALNSRT(300),ALNSTRS(300)
      COMMON/BLKD/REFSRT(300),REFSTRS(300)
      COMMON/BLKE/WT(300),MDATA,ITOTAL
      COMMON/BLKF/TREF
      EXTERNAL OBJ,AMODEL,DMODEL
      DATA AGUESS,T,IVIS,JVIS,W,II/-1.744D1,5.16D1,5*0.D0/
      DATA I1,IN,G1,GN/2*3,2*0/

C     Printing of available options and some information regarding the
C     program:

      PRINT 180
      PRINT 190

C     Prompting for input:

      PRINT 200
      READ *, CHOICE

      PRINT 210
      READ *, NSET

      PRINT 220
      READ *

      OPEN (7,FILE='DATA.TXT',STATUS='OLD')
```

```
      READ (7,*) (NDATA(I), I=1,NSET)
      READ (7,*) (TEMP(I), I=1,NSET)
      READ (7,'(A)') (FNAME(I), I=1,NSET)
      READ (7,'(A)') COMMENT

      CLOSE (7)

      PRINT 230
      READ *, ID

      DO 30 I=1,NSET

         OPEN (7,FILE=FNAME(I),STATUS='OLD')

         IF (ID.EQ.0) THEN
            DO 10 J=1,NDATA(I)
               READ (7,*) SRT(I,J),STRESS(I,J)
10          CONTINUE
         ELSE
            DO 20 J=1,NDATA(I)
               READ (7,*) SRT(I,J),STRESS(I,J),SD(I,J)
20          CONTINUE
         ENDIF

         CLOSE (7)

30    CONTINUE

C     Prompting for more information:

      PRINT 240, NSET
      READ *, NREF

      TREF=TEMP(NREF)
      ITOTAL=NDATA(NREF)

      PRINT 330
      READ *, NVIS

      IF (NVIS.EQ.1) THEN
         PRINT 340
         READ *, T
         PRINT 350
         READ *, W
      ENDIF

C     Initializing reference curve:

      DO 40 J=1,ITOTAL
         ASRT(J)=SRT(NREF,J)
         REFSRT(J)=DLOG(SRT(NREF,J))
         ASTRESS(J)=STRESS(NREF,J)
         REFSTRS(J)=DLOG(STRESS(NREF,J))

C     Defining the weight of each data point, if data are available:

         IF (ID.EQ.1) THEN
```

```
            WT(J)=1/SD(NREF,J)**2
         ELSE

C     Otherwise, the same weight of 1.D0 is applied to all points:

            WT(J)=1.D0
         ENDIF

40    CONTINUE

      DO 90 I=1,NSET

         IF ((NVIS.EQ.1).AND.(IVIS.EQ.0).AND.(T.EQ.TEMP(I))) THEN
            IVIS=I
            II=1
         ENDIF

C     Calculation of shift factor for each temperature, except the reference
C     temperature:

         IF (I.EQ.NREF) THEN
            AT(I)=1.D0
            SUMSQ(I)=0.D0
            GOTO 90
         ENDIF

         MDATA=NDATA(I)

         DO 50 J=1,MDATA

            IF ((II.EQ.1).AND.(SRT(I,J).EQ.W)) JVIS=J

C     Working in log scale:

            ALNSRT(J)=DLOG(SRT(I,J))
            ALNSTRS(J)=DLOG(STRESS(I,J))

50       CONTINUE

         II=0

         NM=NDATA(I)-1

C     Using cubic spline of fitted ends to allow interpolation between
C     points:

         CALL SPLINE(ALNSTRS,ALNSRT,MDATA,NM,Q,R,S,I1,IN,G1,GN)

         ICHECK=0
         AT0=1.D-6
         DAT=1.D-1

C     Determination of the interval which brackets the minimum value of
C     the objective function:

60       IF (OBJ(AT0+DAT).GT.OBJ(AT0)) THEN
            IF (ICHECK.EQ.1) THEN
```

```
            ATI=AT0-DAT
            ATF=AT0+DAT
            GOTO 70
         ENDIF
      ELSE
         ICHECK=1
      ENDIF

      AT0=AT0+DAT
      GOTO 60

C     Using the golden search method to minimize the objective function:

70       CALL GOLDEN (ATI,AT0,ATF,OBJ,TOL,AT(I),SUMSQ(I))

C     Shifting of curves and defining the shifted curve as part of the
C     new reference curve:

         DO 80 J=1,MDATA

            ASRT(ITOTAL+J)=SRT(I,J)*AT(I)
            REFSRT(ITOTAL+J)=DLOG(ASRT(ITOTAL+J))
            ASTRESS(ITOTAL+J)=STRESS(I,J)
            REFSTRS(ITOTAL+J)=DLOG(ASTRESS(ITOTAL+J))

C     Determining the weight of each point of the master curve:

            IF (ID.EQ.1) THEN
               WT(ITOTAL+J)=1/SD(I,J)**2
            ELSE
               WT(ITOTAL+J)=1.D0
            ENDIF

80       CONTINUE

         ITOTAL=ITOTAL+MDATA

90    CONTINUE

C     Sorting the master curve data points:

      CALL SORT(ITOTAL,ASRT,ASTRESS)

      OPEN (9,FILE='OUTPUT.TXT')
      WRITE (9,*) COMMENT
      WRITE (9,250)

C     Printing of output:

      DO 100 I=1,ITOTAL
         VISCOSITY=ASTRESS(I)/ASRT(I)
         WRITE (9,260) ASRT(I),ASTRESS(I),VISCOSITY
100   CONTINUE

      WRITE (9,270) TREF

      DO 110 I=1,NSET
```

```
         WRITE (9,280) TEMP(I),AT(I),SUMSQ(I)
110   CONTINUE

      M=NSET

      IF ((CHOICE.EQ.1).OR.(CHOICE.EQ.3)) THEN

         DO 120 I=1,NSET
            X(I)=1/(TEMP(I)+273.15)
            Y(I)=DLOG(AT(I))
120      CONTINUE

C     Linear regression if the first and the second models are both chosen:

         CALL LINREG(X,Y,NSET,CEPT,SLOPE,RSTAT)

         EA=SLOPE*8.314/1000

      ENDIF

C     If the simple thermally activated model is chosen, then the activation
C     energy of the polymer is returned:

      IF (CHOICE.EQ.1) THEN
         WRITE (9,290) EA,RSTAT
         GOTO 150
      ENDIF

C     If both the first and the second models are chosen, then use the
C     results obtained from the first model to obtain more data points
C     to be fitted for the second model:

      IF (CHOICE.EQ.3) THEN

         X(1)=TEMP(1)+273.15
         Y(1)=DLOG(AT(1))
         M=2*NSET-1

         DO 130 I=1,NSET-1
            X(2*I+1)=TEMP(I+1)+273.15
            Y(2*I+1)=DLOG(AT(I+1))
            X(2*I)=(TEMP(I)+TEMP(I+1))/2+273.15
            Y(2*I)=EA*1000/8.314*(1/X(2*I)-1/(TREF+273.15))
130      CONTINUE

      ELSEIF (CHOICE.EQ.2) THEN

C     If WLF (second) model is chosen, then prepare the data points
C     to be fitted:

         DO 140 I=1,NSET
            X(I)=TEMP(I)+273.15
            Y(I)=DLOG(AT(I))
140      CONTINUE

      ENDIF
```

```
C     Calling the subroutine GAUSSN to determine the best estimate of
C     unknown parameters:

      CALL GAUSSN(X,Y,AGUESS,M,TOL,AMODEL,DMODEL,A,SSQ)

C     Printing the second set of output:

      IF (CHOICE.EQ.2) WRITE (9,300) A(1),A(2),SSQ

      IF (CHOICE.EQ.3) THEN
         WRITE (9,310) EA,RSTAT,A(1),A(2)
         WRITE (9,320) SSQ
      ENDIF

C     Calculating the viscosity, if desired:

150   IF (NVIS.EQ.1) THEN

C     If viscosity at one of the experimentally found temperature and
C     shear rate (part of the input) is required, then calculate directly:

         IF ((IVIS.NE.0).AND.(JVIS.NE.0)) THEN
            VIS=STRESS(IVIS,JVIS)/W
              GOTO 170
         ENDIF

         IF (IVIS.NE.0) THEN
            AAT=AT(IVIS)
            GOTO 160
         ENDIF

C     Otherwise, fit cubic spline into the master curve:

         CALL
     +      SPLINE(REFSRT,REFSTRS,ITOTAL,ITOTAL-1,Q,R,S,I1,IN,G1,GN)

C     And calculate the shift factor corresponding to the temperature
C     using the chosen model:

         IF (CHOICE.EQ.1) THEN
            AAT=DEXP(EA/8.314*1000*(1/(T+273.15)-1/(TREF+273.15)))
         ELSE
            AAT=DEXP(A(1)*(T-TREF)/(A(2)+T-TREF))
         ENDIF

C     Calculate the shifted shear rate and from the master curve
C     obtain the corresponding G' and G" values:

160      WI=DLOG(W*AAT)

         VIS=(DEXP(F(REFSRT,REFSTRS,Q,R,S,ITOTAL,WI))/W)

170      WRITE (9,360) T,W,VIS

      ENDIF

C     Format statements:
```

```
180   FORMAT (1X'This program creates a master curve for a polymer ',
     +       'at a specified reference tem-'/1X,'perature.  The ',
     +       'viscosity of the polymer at a desired ',
     +       'temperature and shear rate'/1X,'may also be calculated.')
190   FORMAT (//,1X'Please choose one of the following options to ',
     +       'correlate shift factor to tem-'/1X,'perature:')
200   FORMAT (/1X,'1.  Simple Thermally Activated Model (a good ',
     +       'model for T > (Tg+100)K)'/1X,'2.  WLF model (a ',
     +       'good model for Tg < T < (Tg+100)K)'/1X,'3.  Both')
210   FORMAT (/1X'Please enter the number of available data sets:')
220   FORMAT (/1X,'Please copy the file: DATA.TXT into the appropriate ',
     +       'directory consisting of'/1X,'information on the number ',
     +       'of data available for each data set, the temperature'/1X,
     +       '(in Celsius) corresponding to each data set, and the ',
     +       'file names in which data'/1X,'of each set are stored. ',
     +       'These data should be stored in columns of 2 (or 3) in '
     +       /1X,'ascending orders of frequency (column 1).  The ',
     +       'second column of these data'/1X,'files should refer to ',
     +       'the shear stress. The third column may be added to'/1X,
     +       'correspond to the standard deviations (in %). ',
     +       'In cases where no standard'/1X,'deviation is available, ',
     +       'they are assumed to be zero.'//1X,'Please press enter ',
     +       'when ready...')
230   FORMAT (/1X'Is there third column on the file ',
     +       'c:\DATA.TXT?'/1X,'0 - no'/1X,'1 - yes')
240   FORMAT (/1X'Which data set do you want the master curve to be ',
     +       'referenced to? (1-',I2,')')
250   FORMAT (/'RESULTING MASTER CURVE DATA POINTS:'//3X,'Rate (1/s)',
     +       4X,'Stress (Pa)',4X,'Viscosity (Pa.s)'/'--------',
     +       '----------------------------------------')
260   FORMAT (F11.4,F14.0,F18.0)
270   FORMAT (//'SUMMARY OF RESULTS:'//'The master curve was ',
     +       'calculated based on the reference temperature of ',
     +       F6.1,' C'/)
280   FORMAT ('The shift factor corresponding to temperature of ',
     +       F6.1,' C is:',F7.4/'The corresponding value of the ',
     +       'objective function is:',F7.4)
290   FORMAT (/'Using simple thermally activated model, Ea= ',F8.4,
     +       ' kJ/mol'/'The corresponding regression correlation ',
     +       'coefficient is R= ',F6.4)
300   FORMAT (/'Using WLF model, C1=',F8.4,', C2=',F8.4/'The ',
     +       'associated sum of squares of differences is ',F6.4)
310   FORMAT (/'Using both simple thermally activated model and WLF ',
     +       'model,'/'EA= ',F8.4,' kJ/mol, R= ',F6.4,', C1= ',F8.4,
     +       ', C2= ',F8.4)
320   FORMAT (1X'The associated sum of squares of differences is ',F6.4)
330   FORMAT (/1X'Do you want to calculate viscosity?'/1X,'0 ',
     +       '- no'/1X,'1 - yes')
340   FORMAT (1X'At what temperature (in Celcius)?')
350   FORMAT (1X'At what shear rate (in rad/s)?')
360   FORMAT (/'The viscosity of the polymer at ',F6.1,' C and shear ',
     +       'rate of ',F6.2,' rad/s '/'is:',F10.4,' Pa.s')

      STOP
      END
```

```
C     The subroutine SPLINE fits a cubic polynomial into every
C     adjacent points of a given set of data to allow interpolation
C     between points.  The two end conditions used are those of spline
C     of fitted ends.

      SUBROUTINE SPLINE (X,Y,N,NM,Q,R,S,I1,IN,G1,GN)
      IMPLICIT DOUBLE PRECISION (A-H,O-Z)
      DIMENSION X(N),Y(N),Q(N),R(N+1),S(N)
      DIMENSION A(301),B(301),C(301),D(301)
      DIMENSION H(300)

      IF (I1.EQ.3) THEN
         AA=0.D0
         DO 20 I=1,4
            TERM=Y(I)
            DO 10 J=1,4
               IF (J.NE.I) TERM=TERM/(X(I)-X(J))
10          CONTINUE
            AA=AA+TERM
20       CONTINUE
      ENDIF

      IF (IN.EQ.3) THEN
         M=N-3
         BB=0.D0
         DO 40 I=M,N
            TERM=Y(I)
            DO 30 J=M,N
               IF (J.NE.I) TERM=TERM/(X(I)-X(J))
30          CONTINUE
            BB=BB+TERM
40       CONTINUE
      ENDIF

      DO 50 I=1,NM
         H(I)=X(I+1)-X(I)
50    CONTINUE

      A(1)=0.D0
      IF (I1.EQ.1) THEN
         B(1)=1.D0
         C(1)=0.D0
         D(1)=0.D0
      ELSEIF (I1.EQ.2) THEN
         B(1)=2.D0*H(1)
         C(1)=H(1)
         D(1)=3.D0*((Y(2)-Y(1))/H(1)-G1)
      ELSE
         B(1)=-H(1)
         C(1)=H(1)
         D(1)=3.D0*H(1)*H(1)*AA
      ENDIF

      DO 60 I=2,NM
         IM=I-1
         A(I)=H(IM)
         B(I)=2.D0*(H(IM)+H(I))
```

```
         C(I)=H(I)
         D(I)=3.D0*((Y(I+1)-Y(I))/H(I)-(Y(I)-Y(IM))/H(IM))
60     CONTINUE

       C(N)=0.D0
       IF (IN.EQ.1) THEN
          A(N)=0.D0
          B(N)=1.D0
          D(N)=0.D0
       ELSEIF (IN.EQ.2) THEN
          A(N)=H(NM)
          B(N)=2.D0*H(NM)
          D(N)=-3.D0*((Y(N)-Y(NM))/H(NM)-GN)
       ELSE
          A(N)=H(NM)
          B(N)=-H(NM)
          D(N)=-3.D0*H(NM)*H(NM)*BB
       ENDIF

       CALL TDMA (A,B,C,D,R,N,NM)

       DO 70 I=1,NM
          IP=I+1
          Q(I)=(Y(IP)-Y(I))/H(I)-H(I)*(2.D0*R(I)+R(IP))/3.D0
          S(I)=(R(IP)-R(I))/(3.D0*H(I))
70     CONTINUE

       RETURN
       END

C      The subroutine TDMA solves the tri-diagonal matrix using Thomas
C      algorithm.

       SUBROUTINE TDMA(A,B,C,D,X,N,NM)
       IMPLICIT DOUBLE PRECISION (A-H, O-Z)
       DIMENSION A(N),B(N),C(N),D(N),X(N),P(301),Q(301)

C      Argument list:
C      A,B,C,D      :  The coefficients of the tridiagonal set
C      X            :  Solution vector
C      N            :  Number of unknowns
C      NM           :  Number of interval between unknowns

       P(1)=-C(1)/B(1)
       Q(1)=D(1)/B(1)

       DO 10 I=2,N
          IM=I-1
          DEN=A(I)*P(IM)+B(I)
          P(I)=-C(I)/DEN
          Q(I)=(D(I)-A(I)*Q(IM))/DEN
10     CONTINUE

       X(N)=Q(N)

       DO 20 I=NM,1,-1
          X(I)=P(I)*X(I+1)+Q(I)
```

```
20    CONTINUE

      RETURN
      END

C     The subroutine GOLDEN uses the golden-search technique to find
C     the minimum value of a certain function, F.  The subroutine
C     returns the minimum value of the function and the value of the
C     independent variable at which it occurs.

      SUBROUTINE GOLDEN(AX,BX,CX,F,TOL,XMIN,FMIN)
      IMPLICIT DOUBLE PRECISION (A-H, O-Z)
      PARAMETER (R=0.61803399,C=1.D0-R)

C     Argument list:
C     AX    :  The lower limit of the interval at which the minimum occurs
C     BX    :  A point in the interval where the function evaluation is
C              lower than F(AX) and F(CX)
C     CX    :  The upper limit of the interval at which the minimum occurs
C     F     :  The function to be minimized
C     TOL   :  Pre-specified convergence tolerance
C     XMIN  :  The point where minimum occurs
C     FMIN  :  The minimum value of the function

      X0=AX
      X3=CX

      IF (DABS(CX-BX).GT.DABS(BX-AX)) THEN
         X1=BX
         X2=BX+C*(CX-BX)
      ELSE
         X2=BX
         X1=BX-C*(BX-AX)
      ENDIF

      F1=F(X1)
      F2=F(X2)

10    IF (DABS(X3-X0).GT.TOL*(DABS(X1)+DABS(X2))) THEN
         IF (F2.LT.F1) THEN
            X0=X1
            X1=X2
            X2=R*X1+C*X3
            F1=F2
            F2=F(X2)
         ELSE
            X3=X2
            X2=X1
            X1=R*X2+C*X0
            F2=F1
            F1=F(X1)
         ENDIF

         GOTO 10
      ENDIF

      IF (F1.LT.F2) THEN
```

```
         FMIN=F1
         XMIN=X1
      ELSE
         FMIN=F2
         XMIN=X2
      ENDIF

      RETURN
      END

C     The subroutine LINREG performs a linear regression of the form:
C
C                              Y = B * X + A
C
C     where A is the Y-intercept of the linearized equation and B is the
C     slope of the line.  In this subroutine, the correlation coefficient,
C     R, is also calculated.

      SUBROUTINE LINREG(X,Y,N,A,B,R)
      IMPLICIT DOUBLE PRECISION (A-H,O-Z)
      DIMENSION X(10),Y(10)

C     Argument list:
C     X     :  A vector of independent variable
C     Y     :  A vector of dependent variable
C     N     :  Number of data points
C     A     :  Y-intercept of the linear line
C     B     :  The slope of the line
C     R     :  The correlation coefficient of the linearized fit

      XBAR=0.D0
      YBAR=0.D0

      DO 10 I=1,N
         XBAR=XBAR+X(I)
         YBAR=YBAR+Y(I)
10    CONTINUE

      XBAR=XBAR/N
      YBAR=YBAR/N

      SX=0.D0
      SY=0.D0
      SUMXY=0.D0

      DO 20 I=1,N
         SX=SX+(X(I)-XBAR)**2
         SY=SY+(Y(I)-YBAR)**2
         SUMXY=SUMXY+(X(I)-XBAR)*(Y(I)-YBAR)
20    CONTINUE

      B=SUMXY/SX
      A=YBAR-B*XBAR

      SX=SQRT(SX/(N-1))
      SY=SQRT(SY/(N-1))
```

```
      PS=0.D0

      DO 30 I=1,N
         XI=(X(I)-XBAR)/SX
         YI=(Y(I)-YBAR)/SY
         PS=PS+XI*YI
30    CONTINUE

      R=PS/(N-1)

      RETURN
      END

C     The subroutine SORT sorts a set of data in increasing order of one
C     variable using the heap sort method.  This subroutine has been written
C     to sort sets of data of exactly three variables:

      SUBROUTINE SORT(N,RA,RB)
      IMPLICIT DOUBLE PRECISION (A-H,O-Z)
      DIMENSION RA(N), RB(N)

C     Argument list:
C     N     :  Number of data points to be sorted
C     RA    :  The first variable according to which data will be sorted
C     RB    :  The second variable of the data set

      L=N/2+1
      IR=N

10    IF(L.GT.1)THEN
         L=L-1
         RRA=RA(L)
         RRB=RB(L)
      ELSE
         RRA=RA(IR)
         RRB=RB(IR)
         RA(IR)=RA(1)
         RB(IR)=RB(1)
         IR=IR-1

         IF(IR.EQ.1)THEN
            RA(1)=RRA
            RB(1)=RRB
            GOTO 30
         ENDIF

      ENDIF
C
      I=L
      J=L+L

20    IF(J.LE.IR)THEN

         IF(J.LT.IR)THEN
            IF(RA(J).LT.RA(J+1))J=J+1
         ENDIF
```

```
            IF(RRA.LT.RA(J))THEN
               RA(I)=RA(J)
               RB(I)=RB(J)
               I=J
               J=J+J
            ELSE
               J=IR+1
            ENDIF

         GOTO 20

         ENDIF

         RA(I)=RRA
         RB(I)=RRB

         GOTO 10

30       RETURN
         END

C        The subroutine GAUSSJ solves a set of algebraic simulteneous equations
C        in the form of an augmented coefficient matrix using the Gauss-Jordan
C        elimination method:

         SUBROUTINE GAUSSJ (A, N, NDR, NDC, X, RNORM, IERROR)
         IMPLICIT DOUBLE PRECISION (A-H, O-Z)
         DIMENSION A(NDR,NDC), X(N), B(50,51)

C        Argument list:
C        A      :  An array of coefficients of augmented matrix
C        N      :  Number of equations (equivalent to the number of unknowns)
C        NDR    :  Number of rows for 'A'
C        NDC    :  Number of columns for 'A'
C        X      :  Output array in which the values of the solution vector
C                  are stored
C        RNORM  :  Measure of residual vector { [C] - [A] * [X] }
C        IERROR :  An indication of the success of solving the equations
C                  IERROR = 1 ==> successful
C                  IERROR = 2 ==> fails to find solution

C        Begin:

         NP = N + 1

C        Defining a new working matrix 'B':

         DO 20 I = 1, N
            DO 10 J = 1, NP
               B(I,J) = A(I,J)
10          CONTINUE
20       CONTINUE

C        Elimination steps to be done 'N' times:

         DO 80 K = 1, N
            KP = K + 1
```

```
         BIGS = 0.D0

C     When K = N, skip the search for pivot coefficient:

         IF (K .EQ. N) GOTO 55

C     For each row beginning from the 'K'th row where K is the elimination
C     step number,

         DO 40 I = K, N
            BIG = DABS (B(I,K))

C     Find the largest coefficients along the row:

            DO 30 J = KP, N
               BIG = DMAX1 (BIG, DABS(B(I,J)))
30          CONTINUE

C     Then find the scale factor, S, corresponding to each row (equation)
C     by dividing the (I,I)th coefficient by the largest coefficient
C     for that row:

            S = DABS (B(I,K) / BIG)

C     Among these equations (from the Kth to the Nth), find the biggest
C     Scale factor:

            BIGS = DMAX1 (BIGS,S)

C     The biggest scale factor should correspond to the pivot equation:

            IF (BIGS .EQ. S) IPIVOT = I

40       CONTINUE

C     If the pivot equation is not the same as the equation corresponding to
C     the elimination step number, then exchange row 'K' with the row
C     at which the pivot equation is located:

         IF (IPIVOT .NE. K) THEN

            DO 50 J = K, NP
               TEMP = B(IPIVOT,J)
               B(IPIVOT,J) = B(K,J)
               B(K,J) = TEMP
50          CONTINUE

         ENDIF

C     If at least one of the diagonal elements is zero, then return to main
C     program with 'fail' message:

55       IF (B(K,K) .EQ. 0.D0) THEN
            IERROR = 2
            RETURN
         ENDIF
```

```
C     Otherwise, start the elimination process, eliminating coefficients
C     above and below the diagonal elements simultaneously (see attached
C     explanations):

C     Start from the first row to the last

         DO 70 I = 1, N

C     But skipping the pivot row:

            IF (I .NE. K) THEN
               QUOT = B(I,K) / B(K,K)
               B(I,K) = 0.D0
               DO 60 J = KP, NP
                  B(I,J) = B(I,J) - QUOT * B(K,J)
60             CONTINUE
            ENDIF

70       CONTINUE
80    CONTINUE

C     Return with error message if the last diagonal element (after the
C     completion of all elimination steps) equals zero:

      IF (B(N,N) .EQ. 0.D0) THEN
         IERROR = 2
         RETURN
      ENDIF

C     Otherwise, start finding the solution vector by dividing the R.H.S.
C     coefficients by the corresponding elements of the diagonal matrix:

      DO 90 I = 1, N
         X(I) = B(I,NP) / B(I,I)
90    CONTINUE

C     Calculation of norm of residual vector:

      RSQ = 0.D0

      DO 110 I = 1, N
         SUM = 0.D0

         DO 100 J = 1, N
            SUM = SUM + A(I,J) * X(J)
100      CONTINUE

         RSQ = RSQ + (A(I,NP) - SUM) ** 2
110   CONTINUE

      RNORM = SQRT (RSQ)

C     If everything goes well, return with a 'success' message:

      IERROR = 1
      RETURN
      END
```

```
C     The subroutine GAUSSN returns the optimum value of the parameters of
C     a model using the Gauss-Newton method of optimization by minimizing
C     the sum of squares of differences (up to a specified tolerance):

C     Please note that in this case the subroutine has been modified to
C     solve for a model of only two parameters since the WLF model involves
C     only two parameters.  Also, this will allow the condition number to be
C     calculated more easily.

      SUBROUTINE GAUSSN(X,Y,AGUESS,M,TOL,AMODEL,DMODEL,A,SNEW)
      IMPLICIT DOUBLE PRECISION (A-H,O-Z)
      DIMENSION X(M),Y(M),A(2),DA(2),AA(2),AGUESS(2),ALPHA(2,3)
      EXTERNAL AMODEL,DMODEL
      DATA Z,N/1.D0,2/

C     Argument List:
C     X      :  A set of independent variables
C     Y      :  A set of dependent variables
C     AGUESS :  A vector of initial parameter values
C     M      :  The number of available data points
C     TOL    :  A specified convergence criteria
C     AMODEL :  The specific model which parameters are to be estimated
C     DMODEL :  A function that returns the derivative value of the model
c               with respect to the parameters
C     A      :  A vector of best estimated parameter values
C     SNEW   :  The corresponding sum of squares of differences as calculated
C               using the best estimated parameter values

C     Initialization of parameter values:

      DO 10 I=1,N
         A(I)=AGUESS(I)
10    CONTINUE

C     Calculation of the sum of squares of differences using the initial
C     values of A(I)

      SOLD=S(AMODEL,X,Y,M,A,N)

C     Setting up the augmented coefficient matrix, ALPHA, to be solved
C     for the increment in parameter values, DA(I):

20    DO 60 I=1,N

         DO 40 J=1,N

            ALPHA(I,J)=0.D0

            DO 30 K=1,M
               ALPHA(I,J)=ALPHA(I,J)+DMODEL(A,X(K),I)*DMODEL(A,X(K),J)
30          CONTINUE

            IF (J.NE.I) ALPHA(J,I)=ALPHA(I,J)

40       CONTINUE
```

```
         ALPHA (I,N+1)=0.D0

         DO 50 K=1,M
            ALPHA(I,N+1)=ALPHA(I,N+1)+
     +                   DMODEL(A,X(K),I)*(Y(K)-AMODEL(X(K),A))
50       CONTINUE

60     CONTINUE

C      Calculation of the Eigenvalues of the coefficient matrix, ALPHA:

       B=-(ALPHA(1,1)+ALPHA(2,2))
       C=ALPHA(1,1)*ALPHA(2,2)-ALPHA(1,2)*ALPHA(2,1)

       EIGEN1=(-B+SQRT(B**2-4*C))/2
       EIGEN2=(-B-SQRT(B**2-4*C))/2

C      Initializing the constant for Marquardt's modification:

       GAMMA=0.D0

C      Calculation of the condition number:

70     COND=DABS((DMAX1(EIGEN1,EIGEN2)+GAMMA)/
     +          (DMIN1(EIGEN1,EIGEN2)+GAMMA))

C      To perform Marquardt's modification if the condition number is large:

       IF (COND.GT.1.D3) THEN

          GAMMA=GAMMA+1.D1

          DO 80 I=1,N
             ALPHA(I,I)=ALPHA(I,I)+GAMMA
80        CONTINUE

          GOTO 70

       ENDIF

C      Calling the subroutine GAUSSJ to solve for DA(I):

       CALL GAUSSJ(ALPHA,N,N,N+1,DA,RNORM,IERROR)

C      Checking for singularity:

       IF (IERROR.EQ.2) THEN
          PRINT*,'WRN - Program fails to determine parameters!!'
          STOP
       ENDIF

       ERR=0.D0

C      Checking for convergence:

       DO 90 I=1,N
          ERR=DMAX1(ERR,DABS(DA(I)/A(I)))
```

```
90    CONTINUE

      IF (ERR.LE.TOL) GOTO 130

C     Updating the parameter values by Z * DA(I):

100   DO 110 I=1,N
         AA(I)=A(I)+(Z*DA(I))
110    CONTINUE

      SNEW=S(AMODEL,X,Y,M,AA,N)

C     Where Z is a real number that reduces the sum of squares of
C     differences:

      IF (SNEW.GT.SOLD) THEN
         Z=Z*5.D-1
         GOTO 100
      ELSE
         DO 120 I=1,N
            A(I)=AA(I)
120      CONTINUE
         SOLD=SNEW
         GOTO 20
      ENDIF

130   RETURN
      END

C     The following function returns the value of the sum of squares
C     of differences between the calculated data and the data obtained
C     from the model:

      DOUBLE PRECISION FUNCTION S(AMODEL,X,Y,M,A,N)
      IMPLICIT DOUBLE PRECISION (A-H,O-Z)
      DIMENSION X(M),Y(M),A(N)

      S=0.D0

      DO 10 K=1,M
         S=S+(Y(K)-AMODEL(X(K),A))**2
10    CONTINUE

      RETURN
      END

C     The following function returns the value of ln(AT(i)) as
C     calculated using the WLF model:

      DOUBLE PRECISION FUNCTION AMODEL(X,A)
      IMPLICIT DOUBLE PRECISION (A-H,O-Z)
      DIMENSION A(2)
      COMMON/BLKF/TREF

      DELT=X-(TREF+273.15)
      AMODEL=A(1)*DELT/(A(2)+DELT)
```

```
      RETURN
      END

C     The following is a function that calculates the derivative of the
C     WLF model with respect to the parameters A(1) or A(2):

      DOUBLE PRECISION FUNCTION DMODEL(A,X,I)
      IMPLICIT DOUBLE PRECISION (A-H,O-Z)
      DIMENSION A(2)
      COMMON/BLKF/TREF

      DELT=X-(TREF+273.15)

      GOTO (10,20), I

10    DMODEL=DELT/(A(2)+DELT)
      RETURN

20    DMODEL=-A(1)*DELT/((A(2)+DELT)**2)
      RETURN

      END

C     The following is a function that allows interpolation between points
C     to be done upon the availability of the parameters Q, R, S:

      DOUBLE PRECISION FUNCTION F(X,Y,Q,R,S,N,Z)
      IMPLICIT DOUBLE PRECISION (A-H,O-Z)
      DIMENSION X(300),Y(300),Q(300),R(301),S(300)

      IF (Z.LT.X(1)) THEN
         I=1
         WRITE (9,20) Z
      ELSEIF (Z.GT.X(N)) THEN
         I=N-1
         WRITE (9,20) Z
      ELSE

C     The bisection method is used to find the location of the point of
C     interest:

         I=1
         J=N
10       K=INT((I+J)/2)
         IF (Z.LT.X(K)) J=K
         IF (Z.GE.X(K)) I=K
         IF (J.GT.I+1) GOTO 10
      ENDIF

      DX=Z-X(I)
      F=Y(I)+DX*(Q(I)+DX*(R(I)+DX*S(I)))

20    FORMAT (/'Warning - ',D10.3,' is outside interpolation range'/)

      RETURN
      END
```

```
C     The following is the objective function that is to be minimized
C     to obtain the master curve:

      DOUBLE PRECISION FUNCTION OBJ(X)
      IMPLICIT DOUBLE PRECISION (A-H,O-Z)
      COMMON/BLKA/Q(300),R(301),S(300)
      COMMON/BLKC/ALNSRT(300),ALNSTRS(300)
      COMMON/BLKD/REFSRT(300),REFSTRS(300)
      COMMON/BLKE/WT(300),MDATA,ITOTAL

      OBJ=0.D0

      DO 10 I=1,ITOTAL

C     The objective function should only be calculated for a certain range
C     of shear rate values, for which there is a common stress value
C     between the reference curve and the curve that is to be shifted:

         IF ((REFSTRS(I).GE.ALNSTRS(1)).AND.
     +           (REFSTRS(I).LE.ALNSTRS(MDATA))) THEN

            OBJ=OBJ+(REFSRT(I)-
     +           F(ALNSTRS,ALNSRT,Q,R,S,MDATA,REFSTRS(I))
     +               -DLOG(X))**2*WT(I)
         ENDIF

10    CONTINUE

      RETURN
      END
```

****

Sample Input File:

Data.txt:

```
12
12
12
180
200
220
c:/fortran/program/project/data1.txt
c:/fortran/program/project/data2.txt
c:/fortran/program/project/data3.txt
Resin X, Lot# XX123-45600
```

Data1.txt:

```
4.8871      36248
8.0000      44980
12.000      53784
20.945      67761
30.000      79699
62.834      107734
97.741      129545
```

202.46	173244
300.21	202583
495.69	243410
698.15	274380
872.69	294949

Sample Output File:

Resin X, Lot# XX123-45600

RESULTING MASTER CURVE DATA POINTS:

Rate (1/s)	Stress (Pa)	Viscosity (Pa.s)
2.7900	31202	11184
3.5426	34618	9772
4.5671	38835	8503
4.8871	40129	8211
5.7990	43128	7437
6.8507	46379	6770
8.0000	49856	6232
8.6985	51552	5927
11.9573	58990	4933
12.0000	59517	4960
15.1826	65432	4310
17.1266	68688	4011
20.9450	75134	3587
21.7463	76319	3510
30.0000	87668	2922
35.8712	93375	2603
45.5470	103543	2273
55.7992	111925	2005
62.8340	117824	1875
70.8503	123646	1745
97.7410	140489	1437
115.5820	149881	1296
146.7588	164939	1123
171.3863	175495	1023
202.4600	186128	919
217.6156	191950	882
282.9835	212208	749
300.2100	215468	717
359.3148	231069	643
398.5655	241780	606
495.6900	258080	520
498.2083	263048	527
506.0736	261728	517
632.5938	283384	447
698.1500	289671	414
872.6900	309308	354

SUMMARY OF RESULTS:

```
The master curve was calculated based on the reference temperature of 180.0 C

The shift factor corresponding to temperature of 180.0 C is: 1.0000
The corresponding value of the objective function is:  .0000
The shift factor corresponding to temperature of 200.0 C is: 0.7249
The corresponding value of the objective function is:  .0019
The shift factor corresponding to temperature of 220.0 C is: 0.5709
The corresponding value of the objective function is:  .0113

Using simple thermally activated model, Ea=  26.0760 kJ/mol
The corresponding regression correlation coefficient is R=  .9982
```

APPENDIX B: GPC Analysis Program Code

```
*************************************************************************
*                                                                       *
*                      Alfonsius Budi Ariawan                           *
*                  Department of Chemical Engineering                   *
*                  The University of British Columbia                   *
*                           Vancouver, B.C.                             *
*                                                                       *
*                           April 15, 1998                              *
*                                                                       *
*     SUMMARY:                                                          *
*     This program inputs GPC profiles of several polymers and divides  *
*     each profile into a number of different MW groups.  Each profile  *
*     is then fitted to splines of fitted ends and the area             *
*     corresponding to each MW group is calculated using 4-panel        *
*     Newton-Cotes method.                                              *
*                                                                       *
*************************************************************************

      PROGRAM GPC
      IMPLICIT DOUBLE PRECISION (A-H, O-Z)
      DIMENSION ALOGMW(800), CONC(800)
      DIMENSION X(20), AREA(30,20,21)
      CHARACTER * 20 RESIN
      CHARACTER * 40 FNAME(30)
      EXTERNAL F
      DATA EPS / 1.D-6  /

C     Reading information from input file:

      OPEN (3, FILE='GPCDAT(all).TXT', STATUS='OLD')

      DO 10 I = 1, 30

         READ (3,'(A)', ERR=20) FNAME(I)
         NRESIN = I

10    CONTINUE

20    CLOSE (3)

C     Prompting for more information:

      PRINT 190
      READ *, ALOWER

      PRINT 200
      READ *, UPPER

      PRINT 210
      READ *, N

      NP = N + 1

C     Working in Log scale:

      X(1) = DLOG10 (ALOWER)
      X(NP) = DLOG10 (UPPER)
```

```
C     Calculating the width of each molecular weight range:
      DELTA = (X(NP) - X(1)) / N
C     Calculating the various molecular weight limits:
      DO 30 I = 2, N
         IM = I - 1
         X(I) = X(IM) + DELTA
30    CONTINUE
C     Initialization of area under each slice:
      DO 50 I = 1, NRESIN
         DO 40 J = 1, NP
            AREA(I,J,J) = 0.D0
40       CONTINUE
50    CONTINUE

C     Opening the output file:
      OPEN(5, FILE='GPC.TXT')
      WRITE (5,150)
      K=1
60    IF (K.LE.N) THEN
         KP=K+1
         WRITE (5,170)
         WRITE (5,160)
         DO 70 J = K, N
            WRITE (5,230) X(K)
70       CONTINUE
         WRITE (5,230)
         WRITE (5,160)
         DO 80 J = KP, NP
            WRITE (5,230) X(J)
80       CONTINUE
```

```
          WRITE (5,180)

          DO 130 J = 1, NRESIN

             OPEN (7, FILE=FNAME(J), STATUS='OLD')
             READ (7, *) RESIN

             DO 90 I = 1, 1000

                READ (7,*,ERR=100) ALOGMW(I), CONC(I)
                NDATA = I

90           CONTINUE

100          WRITE (5,230)
             WRITE (5,220) RESIN

             IF (K.EQ.1) THEN

                NDATAM = NDATA - 1

C       Fitting the MWD curve with spline:

                CALL SPLINE (ALOGMW, CONC, NDATA, NDATAM, 3, 3,
     +                       0.D0, 0.D0)

C       Integrating the fitted curve corresponding to the appropriate
C       molecular weight slice using 4-panel Newton-cotes method:

C       Total area:

                CALL ADNC (4, F, ALOGMW(1), ALOGMW(NDATA), EPS,
     +                     TOTAL, NPOINT)

C       Calculation of normalized area:

                DO 110 JJ = 2, NP

                   CALL ADNC(4,F,X(1),X(JJ),EPS,SUM,NPOINT)
                   AREA(J,1,JJ) = SUM / TOTAL
                   WRITE (5,230) AREA(J,1,JJ)

110             CONTINUE

             ELSE

C       Calculation of other intermediate slices:

                DO 120 JJ = KP, NP

                   AREA(J,K,JJ) = AREA(J,1,JJ) - AREA(J,1,K)
                   WRITE (5,230) AREA(J,K,JJ)

120             CONTINUE

             ENDIF
```

```
130       CONTINUE

          CLOSE (7)

          K = K + 1

          GOTO 60

        ENDIF

140     CLOSE (5)

C       FORMAT statements:

150     FORMAT (3X,'Resin',45X,'MW Limits (in Log)'\)
160     FORMAT (5X,'*',5X,\)
170     FORMAT (/F10.4\)
180     FORMAT (F10.4/)
190     FORMAT (1X,'Enter the absolute lower limit for integration: ',\)
200     FORMAT (/1X,'Enter the absolute upper limit for integration: ',\)
210     FORMAT (/1X,'Enter the number of MW groups desired: ',\)
220     FORMAT (1X,A10,\)
230     FORMAT (F10.4,\)


        STOP
        END

C       Subroutine SPLINE begins:

        SUBROUTINE SPLINE (X, Y, N, NM, I1, IN, G1, GN)
        IMPLICIT DOUBLE PRECISION (A-H,O-Z)
        COMMON /BLKB/ XX(801), YY(801), NN, NNM
        COMMON /BLKC/ Q(800), R(801), S(800)
        DIMENSION X(N), Y(N), H(800)
        DIMENSION A(801), B(801), C(801), D(801)

C       Argument List:
C       X      :  An array of independent variables
C       y      :  An array of dependent variables
C       N      :  Total number of available data points
C       NM     :  Number of intervals
C       I1     :  Boundary condition at X(1):
C                    1.  Natural
C                    2.  Clamped
C                    3.  Fitted
C       IN     :  Boundary condition at X(n)
C                    1.  Natural
C                    2.  Clamped
C                    3.  Fitted
C       G1, GN:   Derivative values at X(1) and X(n), respectively
C                 (needed only if 'clamped' spline is desired)

C       Assigning dummy variable values to be used in COMMON block:

        NN = N
        NNM = NM
```

```
      DO 5 I = 1, N
         XX(I) = X(I)
         YY(I) = Y(I)
5     CONTINUE

C     If 'fitted' spline is desired, then use Langrange
C     polynomial interpolation method to determine condition at the end
C     point(s):

      IF (I1 .EQ. 3) THEN

         AA = 0.D0

         DO 40 I = 1, 4
            TERM = Y(I)

            DO 30 J = 1, 4
               IF (J .NE. I) TERM = TERM / (X(I)-X(J))
30          CONTINUE

            AA = AA + TERM
40       CONTINUE

      ENDIF

      IF (IN .EQ. 3) THEN

         M = N - 3
         BB = 0.D0

         DO 60 I = M, N
            TERM = Y(I)

            DO 50 J = M, N
               IF (J.NE.I) TERM = TERM / (X(I)-X(J))
50          CONTINUE

            BB = BB + TERM
60       CONTINUE

      ENDIF

C     Calculating interval size:

      DO 70 I = 1, NM
         H(I) = X(I+1) - X(I)
70    CONTINUE

C     Calculating the coefficients for the tridiagonal set:

      A(1) = 0.D0

      IF (I1 .EQ. 1) THEN
         B(1) = 1.D0
         C(1) = 0.D0
         D(1) = 0.D0
```

```
      ELSEIF (I1 .EQ. 2) THEN
         B(1) = 2.D0 * H(1)
         C(1) = H(1)
         D(1) = 3.D0 * ((Y(2)-Y(1)) / H(1) - G1)
      ELSE
         B(1) = -H(1)
         C(1) = H(1)
         D(1) = 3.D0 * H(1) * H(1) * AA
      ENDIF

      DO 80 I = 2, NM
         IM = I - 1
         A(I) = H(IM)
         B(I) = 2.D0 * (H(IM)+H(I))
         C(I) = H(I)
         D(I) = 3.D0 * ((Y(I+1)-Y(I))/H(I) - (Y(I)-Y(IM))/H(IM))
80    CONTINUE

      C(N)=0.D0

      IF (IN .EQ. 1) THEN
         A(N) = 0.D0
         B(N) = 1.D0
         D(N) = 0.D0
      ELSEIF (IN .EQ. 2) THEN
         A(N) = H(NM)
         B(N) = 2.D0 * H(NM)
         D(N) = -3.D0 * ((Y(N)-Y(NM)) / H(NM) - GN)
      ELSE
         A(N) = H(NM)
         B(N) = -H(NM)
         D(N) = -3.D0 * H(NM) * H(NM) * BB
      ENDIF

C     Calling Thomas Algorithm to solve for the tridiagonal set:

      CALL TDMA (A, B, C, D, R, N, NM)

C     Determining the coefficients of the cubic polynomials
C     passing through each pair of data points:

      DO 90 I = 1, NM
         IP = I + 1
         Q(I) = (Y(IP)-Y(I)) / H(I) - H(I) *
     +          (2.D0 * R(I) + R(IP)) / 3.D0
         S(I) = (R(IP)-R(I)) / (3.D0 * H(I))
90    CONTINUE

      RETURN
      END

C     Subroutine TDMA begins:

C     This subroutine solves tridiagonal matrix using Thomas
C     Algorithm:

      SUBROUTINE TDMA (A,B,C,D,X,N,NM)
```

```
      IMPLICIT DOUBLE PRECISION (A-H, O-Z)
      DIMENSION A(N), B(N), C(N), D(N), X(N), P(801), Q(801)

      P(1) = -C(1) / B(1)
      Q(1) = D(1) / B(1)

      DO 10 I = 2, N
         IM = I - 1
         DEN = A(I) * P(IM) + B(I)
         P(I) = -C(I) / DEN
         Q(I) = (D(I) - A(I) * Q(IM)) / DEN
10    CONTINUE

      X(N) = Q(N)

      DO 20 I = NM, 1, -1
         X(I) = P(I) * X(I+1) + Q(I)
20    CONTINUE

      RETURN
      END

C     Subroutine ADNC begins:

      SUBROUTINE ADNC(N,F,A,B,EPS,AREA,NPOINT)
      IMPLICIT DOUBLE PRECISION (A-H, O-Z)
      DIMENSION H(20), TOL(20), SR(20), XR(20)
      DIMENSION FF(20,20), C(6), BB(6,7)

C     The following DATA statement defines the constants needed for the
C     various integration methods:

      DATA C,BB/5.D-1,0.333333333333333D0,3.75D-1,4.444444444444444D-2,
     +          1.73611111111111D-2,7.14285714285714D-3,3*1.D0,7.D0,
     +          1.9D1,4.1D1,1.D0,4.D0,3.D0,3.2D1,7.5D1,2.16D2,0.D0,
     +          1.D0,3.D0,1.2D1,5.0D1,2.7D1,2*0.D0,1.D0,3.2D1,5.0D1,
     +          2.72D2,3*0.D0,7.D0,7.5D1,2.7D1,4*0.D0,1.9D1,2.16D2,
     +          5*0.D0,4.1D1/

C     Defining the maximum adaptive level allowed:

      DATA MAXL /20/

C     Argument List:
C     N      :  'Panel' number (eg. N = 2 for adaptive Simpson
C               rule, etc.)
C     F      :  The function to be integrated
C     A      :  Lower limit of integration
C     B      :  Upper limit of integration
C     EPS    :  Convergence criteria
C     AREA   :  Result of integration
C     NPOINT :  Number of function evaluations

C     Initialization of variables:

      AREA = 0.D0
      S = 0.D0
```

```
C     Initial number of function evaluations:

      NPOINT = N + 1

C     Defining the original integration interval:

      X1 = A
      XR(1) = B

C     Defining the length of interval and the convergence criteria of
C     each adaptive level, up to the maximum level allowed:

      H(1) = (B-A) / N

      IF (MOD(N,2) .EQ. 0.D0) THEN
         NR = N + 2
      ELSE
         NR = N + 1
      ENDIF

      IF (MOD(INT(N/2.D0),2) .EQ. 0.D0) THEN
         RN = 2 ** NR - 4
      ELSE
         RN = 2 ** NR - 6
      ENDIF

      TOL(1) = RN * EPS

      DO 10 I = 2, MAXL
         IM = I - 1
         H(I) = H(IM) / 2.D0
         TOL(I) = TOL(IM) / 2.D0
10    CONTINUE

C     Calculation of area over the original integration interval:

      NP = N + 1
      J = -1.D0

      DO 20 I = 1, NP
         J = J + 2
      IF (I .NE. NP) THEN
         FF(1, J) = F(A + (I-1) * H(1))
      ELSE
      FF(1, J) = F(B)
      ENDIF
         S = S + BB(N,I) * FF(1,J)
20    CONTINUE

      S = S * C(N) * H(1)

C     Defining the first level:

      L = 1

C     Updating the number of function evaluations:
```

```
30    NPOINT = NPOINT + N

      DO 40 I = 1, N
         FF(L,2*I) = F(X1+(I*2-1)*H(L)/2.D0)
40    CONTINUE

C     Calculating the areas under the two new integration intervals
C     (each interval being half the size of the previous integration
C     interval):

      SL = 0.D0
      SR(L) = 0.D0

      DO 50 I = 1, NP
         SL = SL + BB(N,I) * FF(L,I)
         SR(L) = SR(L) + BB(N,I) * FF(L,I+N)
50    CONTINUE

      SL = SL * H(L) * C(N) / 2.D0
      SR(L) = SR(L) * H(L) * C(N) / 2.D0

C     If the sum of the areas are significantly different from the area
C     calculated for the previous interval size....

      IF (DABS(SL+SR(L)-S) .GT. TOL(L)) THEN

         LM = L
         L = L + 1

C     ...and the level is still smaller than the maximum possible level,

         IF (L .LE. MAXL) THEN

C     move to the left half of the integration interval, increase the
C     integration level and define a new integration interval:

            S = SL

            DO 60 I = 1, NP
               FF(L,2*I-1) = FF(LM,I)
60          CONTINUE

            XR(L) = X1 + N * H(L)
            GOTO 30

         ELSE

C     Otherwise, integration has failed:

            WRITE (5,90) X1
            RETURN

         ENDIF

      ELSE
```

```
C     If the sum of the areas are closed to the area calculated
C     for to the previous integral interval, then incorporate
C     the sum into the total area...

         AREA = AREA + SL + SR(L)
         X1 = X1 + N * H(L)

C     ..., move to the right and find the correct level to go to:

         DO 80 I = L, 1, -1

C     If the difference between X1 and XR(L) is closed to zero (or
C     smaller than half of the minimum interval size), then the correct
C     level has been found:

            IF (DABS(X1-XR(I)) .LT. H(MAXL)/2.D0) THEN

               L = I

C     If the first level is found, then integration is done:

               IF (L .EQ. 1) RETURN

               LM = L - 1
               S = SR(LM)

               DO 70 J = 1, NP
                  FF(L, 2*J-1) = FF(LM,J+N)
70             CONTINUE

C     Otherwise, continue...

               GOTO 30

            ENDIF

80       CONTINUE

      ENDIF

C     FORMAT statement:

90    FORMAT (/1X,'WARNING - Integration fails beyond x =',D10.3)

      RETURN
      END

C     The following function returns an interpolated value, knowing
C     the spline coefficients:

      DOUBLE PRECISION FUNCTION F(Z)
      IMPLICIT DOUBLE PRECISION (A-H,O-Z)
      COMMON /BLKB/ X(801), Y(801), N, NM
      COMMON /BLKC/ Q(800), R(801), S(800)

C     Print warning message if user tries to interpolate outside the
C     interpolation region:
```

```
      IF (Z .LT. X(1)) THEN
         I = 1
         PRINT 20, Z
      ELSEIF (Z. GT. X(N)) THEN
         I = NM
         PRINT 20, Z
      ELSE

C     Otherwise, use bisection method to determine the location of the
C     point of interest:

         I = 1
         J = N
10       K = INT ((I+J) / 2)
         IF (Z .LT. X(K)) J = K
         IF (Z .GE. X(K)) I = K
         IF (J .GT. I+1) GOTO 10
      ENDIF

C     Calculate the interpolated value using cubic spline coefficients:

      DX = Z - X(I)
      F = Y(I) + DX * (Q(I) + DX * (R(I) + DX * S(I)))

20    FORMAT (/'Warning - ',D10.3,' is outside interpolation range'/)

      RETURN
      END
```

****

Sample Input File:

GPCDAT(all).txt:

```
a.txt
b.txt
c.txt
  .
  .
  .
(Cont'd till x.txt)
```

a.txt:

```
Resin A
6.66289      0.00026
6.65412      0.00053
6.64537      0.00072
6.63665      0.00113
   .            .
   .            .
   .            .
(Cont'd till end)
```

Output File:

Resin	MW Limit(in Log)									
*	3.9542	3.9542	3.9542	3.9542	3.9542	3.9542	3.9542	3.9542	3.9542	3.9542
*	4.1542	4.3542	4.5542	4.7542	4.9542	5.1542	5.3542	5.5542	5.7542	5.9542
A	0.078	0.1763	0.2934	0.4127	0.5187	0.5998	0.6595	0.7075	0.7476	0.7804
B	0.0833	0.185	0.302	0.4185	0.519	0.5942	0.6482	0.6904	0.725	0.7548
C	0.082	0.1887	0.3167	0.4463	0.5592	0.6426	0.6998	0.7407	0.7709	0.7944
D	0.0813	0.1828	0.3016	0.4212	0.5271	0.6089	0.6685	0.7142	0.75	0.7786
E	0.0919	0.2042	0.3279	0.445	0.5442	0.6177	0.6723	0.7172	0.7536	0.781
F	0.0805	0.1856	0.3091	0.4312	0.5369	0.6178	0.6806	0.7347	0.7792	0.8128
G	0.0834	0.19	0.3124	0.4317	0.5343	0.6123	0.6712	0.7204	0.7617	0.7938
H	0.0798	0.1804	0.2996	0.4236	0.5429	0.6437	0.7211	0.7787	0.8152	0.8345
I	0.0789	0.1923	0.3318	0.4728	0.6009	0.7026	0.7784	0.832	0.8644	0.8817
J	0.0699	0.1657	0.2876	0.4219	0.5532	0.6605	0.7377	0.7896	0.8194	0.8356
K	0.0745	0.1716	0.2897	0.416	0.5371	0.6364	0.7119	0.7689	0.8082	0.8343
L	0.0795	0.1836	0.3082	0.4364	0.5552	0.6487	0.7167	0.7678	0.8042	0.8302
M	0.0931	0.2056	0.3284	0.4432	0.5402	0.6103	0.663	0.7068	0.7456	0.779
N	0.0796	0.1776	0.2885	0.3995	0.5011	0.5826	0.6467	0.7008	0.7465	0.7858
O	0.0823	0.1862	0.3084	0.4312	0.5448	0.6333	0.7031	0.7585	0.7973	0.8177
P	0.0685	0.1617	0.2801	0.4101	0.5383	0.6456	0.7261	0.783	0.8172	0.836
R	0.0866	0.1847	0.2892	0.3916	0.4886	0.5719	0.6413	0.6981	0.7398	0.7689
S	0.0701	0.1677	0.2922	0.4288	0.5627	0.6727	0.7521	0.8054	0.8358	0.852
T	0.0576	0.1491	0.279	0.4285	0.574	0.693	0.7822	0.8469	0.8908	0.9196
U	0.0717	0.159	0.2627	0.3753	0.4846	0.5767	0.6485	0.7056	0.7489	0.7812
V	0.0426	0.1126	0.2236	0.3723	0.5394	0.6856	0.7949	0.87	0.915	0.9381
W	0.0322	0.0912	0.194	0.3424	0.5185	0.6772	0.7981	0.8816	0.9336	0.9623
X	0.0578	0.1514	0.2855	0.4394	0.5837	0.6951	0.7755	0.8356	0.8798	0.9112
*	4.1542	4.1542	4.1542	4.1542	4.1542	4.1542	4.1542	4.1542	4.1542	
*	4.3542	4.5542	4.7542	4.9542	5.1542	5.3542	5.5542	5.7542	5.9542	
A	0.0984	0.2154	0.3348	0.4407	0.5218	0.5816	0.6296	0.6697	0.7024	
B	0.1017	0.2188	0.3352	0.4357	0.5109	0.5649	0.6071	0.6417	0.6715	
C	0.1068	0.2347	0.3644	0.4773	0.5606	0.6178	0.6588	0.689	0.7124	
D	0.1015	0.2203	0.3399	0.4458	0.5276	0.5872	0.6329	0.6687	0.6973	
E	0.1122	0.2359	0.3531	0.4522	0.5258	0.5804	0.6253	0.6617	0.689	
F	0.1051	0.2286	0.3507	0.4564	0.5373	0.6001	0.6542	0.6988	0.7324	
G	0.1067	0.229	0.3484	0.4509	0.5289	0.5879	0.6371	0.6783	0.7105	
H	0.1006	0.2198	0.3438	0.4631	0.5639	0.6413	0.6989	0.7355	0.7547	
I	0.1134	0.2528	0.3939	0.5219	0.6236	0.6995	0.753	0.7855	0.8028	
J	0.0958	0.2177	0.352	0.4833	0.5906	0.6678	0.7197	0.7495	0.7657	
K	0.0971	0.2152	0.3416	0.4626	0.562	0.6374	0.6944	0.7337	0.7598	
L	0.1041	0.2287	0.3569	0.4756	0.5692	0.6372	0.6883	0.7247	0.7507	
M	0.1125	0.2353	0.3501	0.447	0.5172	0.5698	0.6137	0.6524	0.6859	
N	0.098	0.2089	0.32	0.4215	0.503	0.5671	0.6212	0.6669	0.7063	
O	0.1039	0.2261	0.3489	0.4625	0.551	0.6208	0.6762	0.715	0.7354	
P	0.0932	0.2117	0.3416	0.4698	0.5771	0.6576	0.7145	0.7487	0.7675	
R	0.0981	0.2026	0.305	0.402	0.4854	0.5547	0.6116	0.6533	0.6823	
S	0.0976	0.222	0.3586	0.4926	0.6026	0.682	0.7353	0.7657	0.7819	
T	0.0915	0.2214	0.3709	0.5164	0.6354	0.7246	0.7893	0.8332	0.862	
U	0.0873	0.191	0.3036	0.4129	0.505	0.5769	0.634	0.6772	0.7095	
V	0.0701	0.181	0.3298	0.4968	0.643	0.7524	0.8275	0.8724	0.8956	
W	0.059	0.1618	0.3102	0.4863	0.645	0.7659	0.8495	0.9015	0.9301	
X	0.0936	0.2277	0.3815	0.5259	0.6373	0.7177	0.7778	0.822	0.8534	
*	4.3542	4.3542	4.3542	4.3542	4.3542	4.3542	4.3542	4.3542		
*	4.5542	4.7542	4.9542	5.1542	5.3542	5.5542	5.7542	5.9542		
A	0.117	0.2364	0.3424	0.4234	0.4832	0.5312	0.5713	0.604		
B	0.1171	0.2336	0.334	0.4092	0.4633	0.5054	0.5401	0.5698		
C	0.1279	0.2576	0.3705	0.4539	0.511	0.552	0.5822	0.6057		
D	0.1189	0.2384	0.3443	0.4261	0.4857	0.5314	0.5672	0.5959		
E	0.1237	0.2409	0.34	0.4136	0.4682	0.5131	0.5494	0.5768		
F	0.1235	0.2456	0.3513	0.4322	0.495	0.5491	0.5937	0.6272		
G	0.1224	0.2417	0.3442	0.4223	0.4812	0.5304	0.5717	0.6038		
H	0.1191	0.2432	0.3625	0.4633	0.5407	0.5983	0.6348	0.6541		
I	0.1394	0.2804	0.4085	0.5102	0.5861	0.6396	0.6721	0.6894		
J	0.1219	0.2562	0.3875	0.4949	0.5721	0.624	0.6538	0.67		

K	0.118	0.2444	0.3655	0.4648	0.5403	0.5973	0.6366	0.6627
L	0.1245	0.2527	0.3715	0.465	0.5331	0.5842	0.6206	0.6465
M	0.1228	0.2376	0.3345	0.4047	0.4573	0.5012	0.5399	0.5734
N	0.1109	0.2219	0.3235	0.4049	0.4691	0.5232	0.5689	0.6082
O	0.1222	0.245	0.3586	0.4471	0.5169	0.5723	0.6111	0.6315
P	0.1185	0.2484	0.3766	0.4839	0.5644	0.6213	0.6555	0.6743
R	0.1045	0.2069	0.3039	0.3872	0.4566	0.5134	0.5551	0.5842
S	0.1244	0.2611	0.395	0.505	0.5844	0.6377	0.6681	0.6843
T	0.13	0.2794	0.425	0.5439	0.6331	0.6978	0.7417	0.7705
U	0.1038	0.2163	0.3256	0.4178	0.4896	0.5467	0.59	0.6222
V	0.111	0.2597	0.4267	0.573	0.6823	0.7574	0.8024	0.8255
W	0.1028	0.2512	0.4273	0.586	0.7069	0.7904	0.8424	0.8711
X	0.1342	0.288	0.4324	0.5438	0.6241	0.6842	0.7284	0.7598
*	4.5542	4.5542	4.5542	4.5542	4.5542	4.5542	4.5542	
*	4.7542	4.9542	5.1542	5.3542	5.5542	5.7542	5.9542	
A	0.1193	0.2253	0.3064	0.3661	0.4142	0.4543	0.487	
B	0.1165	0.2169	0.2922	0.3462	0.3883	0.423	0.4528	
C	0.1297	0.2426	0.3259	0.3831	0.4241	0.4543	0.4777	
D	0.1195	0.2254	0.3072	0.3669	0.4125	0.4484	0.477	
E	0.1172	0.2163	0.2899	0.3445	0.3894	0.4257	0.4531	
F	0.1221	0.2278	0.3087	0.3715	0.4256	0.4702	0.5037	
G	0.1193	0.2219	0.2999	0.3588	0.408	0.4493	0.4814	
H	0.124	0.2434	0.3441	0.4216	0.4792	0.5157	0.535	
I	0.141	0.2691	0.3708	0.4467	0.5002	0.5327	0.55	
J	0.1343	0.2656	0.373	0.4502	0.502	0.5319	0.5481	
K	0.1264	0.2474	0.3468	0.4222	0.4792	0.5185	0.5446	
L	0.1282	0.247	0.3405	0.4085	0.4597	0.496	0.522	
M	0.1148	0.2117	0.2819	0.3345	0.3784	0.4171	0.4506	
N	0.1111	0.2126	0.2941	0.3582	0.4123	0.458	0.4973	
O	0.1228	0.2364	0.3248	0.3946	0.45	0.4888	0.5092	
P	0.1299	0.2581	0.3654	0.4459	0.5029	0.537	0.5558	
R	0.1024	0.1994	0.2828	0.3521	0.4089	0.4507	0.4797	
S	0.1366	0.2706	0.3806	0.46	0.5133	0.5437	0.5599	
T	0.1495	0.295	0.414	0.5032	0.5678	0.6118	0.6406	
U	0.1126	0.2219	0.314	0.3858	0.4429	0.4862	0.5185	
V	0.1487	0.3158	0.462	0.5713	0.6465	0.6914	0.7145	
W	0.1484	0.3245	0.4832	0.6041	0.6877	0.7396	0.7683	
X	0.1538	0.2982	0.4096	0.49	0.55	0.5942	0.6256	
*	4.7542	4.7542	4.7542	4.7542	4.7542	4.7542		
*	4.9542	5.1542	5.3542	5.5542	5.7542	5.9542		
A	0.106	0.1871	0.2468	0.2948	0.3349	0.3676		
B	0.1004	0.1757	0.2297	0.2718	0.3065	0.3363		
C	0.1129	0.1963	0.2534	0.2944	0.3246	0.3481		
D	0.1059	0.1877	0.2473	0.293	0.3288	0.3575		
E	0.0991	0.1727	0.2273	0.2722	0.3086	0.336		
F	0.1057	0.1866	0.2494	0.3035	0.348	0.3816		
G	0.1025	0.1806	0.2395	0.2887	0.33	0.3621		
H	0.1194	0.2201	0.2975	0.3551	0.3917	0.4109		
I	0.1281	0.2298	0.3056	0.3592	0.3916	0.4089		
J	0.1313	0.2386	0.3158	0.3677	0.3975	0.4137		
K	0.1211	0.2204	0.2958	0.3529	0.3921	0.4183		
L	0.1188	0.2123	0.2803	0.3315	0.3678	0.3938		
M	0.0969	0.1671	0.2197	0.2636	0.3023	0.3358		
N	0.1016	0.183	0.2472	0.3013	0.347	0.3863		
O	0.1136	0.202	0.2718	0.3272	0.366	0.3864		
P	0.1282	0.2355	0.316	0.3729	0.4071	0.4259		
R	0.097	0.1804	0.2497	0.3065	0.3482	0.3773		
S	0.134	0.244	0.3234	0.3767	0.407	0.4232		
T	0.1455	0.2645	0.3537	0.4184	0.4623	0.4911		
U	0.1093	0.2014	0.2732	0.3303	0.3736	0.4059		
V	0.1671	0.3133	0.4226	0.4977	0.5427	0.5658		
W	0.1761	0.3348	0.4557	0.5393	0.5912	0.6199		
X	0.1444	0.2558	0.3361	0.3962	0.4404	0.4718		
*	4.9542	4.9542	4.9542	4.9542	4.9542			
*	5.1542	5.3542	5.5542	5.7542	5.9542			

A	0.0811	0.1408	0.1888	0.2289	0.2616
B	0.0752	0.1293	0.1714	0.2061	0.2358
C	0.0834	0.1405	0.1815	0.2117	0.2352
D	0.0818	0.1414	0.1871	0.2229	0.2516
E	0.0736	0.1282	0.1731	0.2094	0.2368
F	0.0809	0.1437	0.1978	0.2423	0.2759
G	0.078	0.137	0.1862	0.2274	0.2596
H	0.1007	0.1782	0.2358	0.2723	0.2916
I	0.1017	0.1776	0.2311	0.2636	0.2809
J	0.1073	0.1845	0.2364	0.2662	0.2824
K	0.0993	0.1748	0.2318	0.2711	0.2972
L	0.0935	0.1616	0.2127	0.249	0.275
M	0.0702	0.1228	0.1666	0.2054	0.2389
N	0.0815	0.1456	0.1997	0.2454	0.2847
O	0.0885	0.1582	0.2137	0.2524	0.2728
P	0.1073	0.1878	0.2447	0.2789	0.2977
R	0.0833	0.1527	0.2095	0.2512	0.2803
S	0.11	0.1894	0.2427	0.2731	0.2893
T	0.1189	0.2082	0.2728	0.3168	0.3456
U	0.0921	0.1639	0.221	0.2643	0.2966
V	0.1462	0.2555	0.3307	0.3756	0.3988
W	0.1587	0.2796	0.3632	0.4151	0.4438
X	0.1114	0.1918	0.2518	0.296	0.3275
*	5.1542	5.1542	5.1542	5.1542	
*	5.3542	5.5542	5.7542	5.9542	
A	0.0597	0.1078	0.1479	0.1806	
B	0.054	0.0961	0.1308	0.1606	
C	0.0572	0.0981	0.1283	0.1518	
D	0.0596	0.1053	0.1411	0.1697	
E	0.0546	0.0995	0.1359	0.1633	
F	0.0627	0.1169	0.1614	0.195	
G	0.0589	0.1081	0.1494	0.1815	
H	0.0774	0.135	0.1716	0.1908	
I	0.0759	0.1294	0.1619	0.1792	
J	0.0772	0.1291	0.1589	0.1751	
K	0.0755	0.1325	0.1717	0.1979	
L	0.0681	0.1192	0.1555	0.1815	
M	0.0526	0.0965	0.1352	0.1687	
N	0.0642	0.1182	0.1639	0.2033	
O	0.0698	0.1252	0.164	0.1844	
P	0.0805	0.1374	0.1716	0.1904	
R	0.0693	0.1262	0.1679	0.1969	
S	0.0794	0.1327	0.1631	0.1793	
T	0.0892	0.1539	0.1978	0.2266	
U	0.0718	0.1289	0.1722	0.2045	
V	0.1093	0.1845	0.2294	0.2525	
W	0.1209	0.2045	0.2564	0.2851	
X	0.0804	0.1404	0.1846	0.2161	
*	5.3542	5.3542	5.3542		
*	5.5542	5.7542	5.9542		
A	0.048	0.0881	0.1208		
B	0.0421	0.0768	0.1066		
C	0.041	0.0712	0.0946		
D	0.0457	0.0815	0.1101		
E	0.0449	0.0813	0.1086		
F	0.0541	0.0987	0.1323		
G	0.0492	0.0905	0.1226		
H	0.0576	0.0941	0.1134		
I	0.0536	0.086	0.1033		
J	0.0519	0.0817	0.0979		
K	0.057	0.0963	0.1224		
L	0.0511	0.0875	0.1135		
M	0.0438	0.0826	0.1161		
N	0.0541	0.0998	0.1391		
O	0.0554	0.0942	0.1146		
P	0.0569	0.0911	0.1099		
R	0.0568	0.0986	0.1276		

```
S          0.0533  0.0837  0.0999
T          0.0646  0.1086  0.1374
U          0.0571  0.1004  0.1327
V          0.0751  0.1201  0.1432
W          0.0836  0.1355  0.1642
X          0.0601  0.1043  0.1357

*          5.5542  5.5542
*          5.7542  5.9542

A          0.0401  0.0728
B          0.0347  0.0645
C          0.0302  0.0537
D          0.0358  0.0644
E          0.0364  0.0637
F          0.0446  0.0781
G          0.0413  0.0734
H          0.0365  0.0558
I          0.0325  0.0498
J          0.0298   0.046
K          0.0393  0.0654
L          0.0364  0.0623
M          0.0388  0.0722
N          0.0457   0.085
O          0.0388  0.0592
P          0.0342   0.053
R          0.0417  0.0707
S          0.0304  0.0466
T          0.0439  0.0727
U          0.0433  0.0756
V          0.0449  0.0681
W           0.052  0.0806
X          0.0442  0.0756

*          5.7542
*          5.9542

A          0.0327
B          0.0298
C          0.0235
D          0.0286
E          0.0274
F          0.0336
G          0.0321
H          0.0193
I          0.0173
J          0.0162
K          0.0261
L           0.026
M          0.0335
N          0.0393
O          0.0204
P          0.0188
R           0.029
S          0.0162
T          0.0288
U          0.0323
V          0.0231
W          0.0286
X          0.0314
```